AD NUMBER

AD861428

NEW LIMITATION CHANGE

TO
Approved for public release, distribution
unlimited

FROM
Distribution authorized to U.S. Gov't.
agencies and their contractors; Critical
Technology; JUN 1969. Other requests shall
be referred to Air Force Space and Missile
Systems Organization, Los Angeles AFB, CA.

AUTHORITY

SAMSO ltr, 30 Jun 1981

SAMSO-TR-69-259

ESSA RESEARCH LABORATORIES
Institute for Telecommunication Sciences
Boulder, Colorado
June 1969

Samso Phase C – Final Report

Noise Data and Analysis

A. D. SPAULDING
R. T. DISNEY
L. R. ESPELAND

. ⁻: 18 1969

Technical Memorandum ERLTM-ITS 184

U.S. DEPARTMENT OF COMMERCE / ENVIRONMENTAL SCIENCE SERVICES ADMINISTRATION

/23

ESSA RESEARCH LABORATORIES

INSTITUTE FOR TELECOMMUNICATION SCIENCES

Ionospheric Telecommunications Laboratory

Tropospheric Telecommunications Laboratory

ENVIRONMENTAL SCIENCE SERVICES ADMINISTRATION

BOULDER, COLORADO

SAMSO-TR-69-259

U.S. DEPARTMENT OF COMMERCE
Environmental Science Services Administration
Research Laboratories

ESSA Technical Memorandum ERLTM-ITS 184

SAMSO PHASE C - FINAL REPORT
NOISE DATA AND ANALYSIS

A. D. Spaulding
R. T. Disney
L. R. Espeland

Spectrum Utilization and Satellite Systems Group

THIS DOCUMENT IS SUBJECT TO SPECIAL EXPORT CONTROLS AND
EACH TRANSMITTAL TO FOREIGN GOVERNMENTS OR FOREIGN NATIONALS
MAY BE MADE ONLY WITH PRIOR APPROVAL OF SPACE AND MISSILE
SYSTEMS ORGANIZATION (SAMSO), LOS ANGELES AIR FORCE STATION,
CALIFORNIA.

Institute for Telecommunication Sciences
Boulder, Colorado
June 1969

FOREWORD

This document, the final report for Task 2.10e and f is submitted by the Institute for Telecommunication Sciences, Boulder, Colorado, in accordance with contract F04701-68-F-0072. The Air Force Project Officer was Captain M. Marin of Headquarters Space and Missile Systems Organization, SMQHN, Air Force Systems Command, Norton Air Force Base, California. The study was initiated on 20 January 1969 and completed on 30 June 1969.

This document is subject to special export controls, and each transmittal to foreign governments or foreign nationals may be made only with prior approval of SAMSO (SMSD).

Information in this report is embargoed under the Department of State International Traffic in Arms Regulations. This report may be released to foreign governments by departments or agencies of the U.S. Government subject to approval of Space and Missile Systems Organization (SMSD), Los Angeles AFS, California, or higher authority with the Department of the Air Force.

Publication of this report does not constitute Air Force approval of the report's findings or conclusions. It is published only for the exchange and stimulation of ideas.

SAMSO-TR-69-259

ABSTRACT

Atmospheric radio-noise samples were recorded near
Boulder, Colorado, and analyzed to obtain amplitude and time
statistics of MF and HF noise. Amplitude and time statistics
derived from the HALL model were compared with the corresponding
measured statistics for atmospheric noise. The measured dis-
tributions of noise samples previously used in error-rate tests
were compared with distributions derived from the HALL model
and from standard atmospheric radio-noise distributions. Per-
formance curves were computed for a CPSK system and for an
optimum receiver operating under the same conditions. Atmos-
pheric radio-noise predictions for 20 CONUS locations were
furnished.

TABLE OF CONTENTS

LIST OF FIGURES

LIST OF FIGURES (Continued)

LIST OF FIGURES (continued)

LIST OF FIGURES (Continued)

LIST OF TABLES

LIST OF TABLES (Continued)

SAMSO PHASE C - FINAL REPORT
NOISE DATA AND ANALYSIS

A. D. Spaulding, R. T. Disney, and L. R. Espeland

Atmospheric radio-noise samples were recorded near Boulder, Colorado, and analyzed to obtain amplitude and time statistics of MF and HF noise. Amplitude and time statistics derived from the Hall model were compared with the corresponding measured statistics for atmospheric noise. The measured distributions of noise samples used in previous error-rate tests were compared with distributions derived from the Hall model and from standard atmospheric radio-noise distributions. Performance curves were computed for a CPSK system and for an optimum receiver operating under the same conditions. Atmospheric radio-noise predictions for 20 CONUS locations were furnished.

1. INTRODUCTION

The work covered by this report consists of that performed in compliance with task 2.10e and f of Addendum No. 2 (Phase C) to Contract F04701-68-F-0072, Communications Field Test FY-68, Project 672A in support of HRSD Program 125B. Task 2.10e was to record atmospheric radio noise at suitable times near Boulder, Colorado, at frequencies of 495 kHz and 2.5 MHz and analyze the recorded noise samples to obtain the amplitude probability distributions (APD) and pulse duration distributions (PDD), pulse spacing (interval between pulses) distributions (PSD), and average crossing rates at various levels. The recording system used made additional recordings possible at a negligible increase in cost. Because three frequencies at a time can be recorded on a single seven-track tape, recordings were also made at 250 kHz and 5 MHz. The requirements of Task 2.10f were to (1) determine the applicability of the Hall model for impulsive phenomena to HF atmospheric radio noise, (2) analytically develop an optimum (minimum probability of bit error) receiver for HF atmospheric radio noise,

(3) Compute the error rate for the optimum receiver and for a matched filter linear receiver for NCFSK and DCPSK systems operating in the same noise environment, and (4) compute the error rate for a CPSK, 8 bps, 4 kHz bandwidth system and the optimum receiver performance for the atmospheric radio noise samples used in earlier Minuteman tests, comparing the results with the earlier results. Much of the original work on the definition and specification of the mathematical modeling of the noise was performed on a different project (Disney and Spaulding, 1968). Part of that project report dealing with the Hall model for impulsive phenomena and its applicability to atmospheric and man-made noise and the derivation and analysis of performance of the optimum receiving system is appended to this report for clarity and background information.

In addition to these requirements, additional analysis of the atmospheric radio noise tapes recorded under Task 2.10e provided other statistics of the noise. The spectrum and autocovariance were computed for several 200 ms random segments of the recordings.

Predictions of atmospheric radio noise were provided in terms of time-block medians, decile deviations from the medians, and standard deviations of these values within the time block for 20 possible installation locations in the continental United States.

The results obtained and the methods used in the above tasks are presented in the following sections.

2. ATMOSPHERIC RADIO-NOISE RECORDINGS AND ANALYSIS

Estimates of the amplitude statistics of atmospheric radio noise are given in a report by CCIR (1964), which does not contain a description of the time statistics at various amplitudes; nor are adequate estimates of these statistics of the noise envelope available elsewhere.

Time and amplitude statistics of atmospheric radio noise in the MF and lower HF portions of the spectrum are needed to verify the

-2-

accuracy of the mathematical model of the noise. This information was needed also for theoretical prediction of system operation when such noise is the predominant type. Because of time limitations, noise recordings from which the statistics could be obtained had to be made during a season of the year when daytime atmospheric noise was low at the frequencies of interest. The recordings, therefore, had to be made at night when atmospheric radio noise was higher than other types of noise. To obtain some variation of the statistics, they were made on four separate nights. One tape with three simultaneous frequencies was recorded each night. The 500 kHz and 2.5 MHz channels were recorded on each of the four nights, the 250 kHz channel was recorded on three nights, and the 5.0 MHz channel on one night. The recordings were all made at a site remote from power and telephone lines and from highways, and all were recorded shortly after midnight. The tape recording system described in the Phase B final report (Disney and Spaulding, 1968) was used. The noise envelope was obtained from the analog tapes and digitized for computer analysis. The A to D conversion was done at a 10 kHz sampling rate. Seven levels and 11 time intervals were used in the computer analysis. The time intervals throughout were 0.2, 0.6, 2, 6, 20, 60, 200, 600, 2000, 6000, and 20000 ms. The levels were limited by the dynamic range of the A to D converter. A 60 dB dynamic range was available, and only the top 60 dB of the 90 dB recorded on the analog tape was used. Six levels 10 dB apart (50 dB) and one step of 8 dB at the top were used. The table 1 calibration sheet gives the levels in terms of dB above kT_ob for each of the following 12 computer print-outs. Tables 2 through 13 are the computer printouts, all in the same format. Tables 2, 3, 4, and 5 are the results of the analysis of the 2.5 MHz recordings for March 29 and April 3, 4, and 5, respectively; tables 6, 7, 8, and 9 are from the 500 kHz channel for the same respective days; tables 10, 11, and 12 are from the 250 kHz recordings on

-3-

March 29, April 3, and April 5, and table 13 shows the results of the analysis of the 5 MHz recording made on April 4.

The APD's are given at the top of the page. The top line is the percent of the time that level 1 is exceeded, the second line is the percent level 2 is exceeded, etc., through level 7 on line seven.

The cumulative PSD's are given in the next group of figures. The first column is the distribution for level 1, the second column for level 2, etc., through the seventh column for level 7. The first line is the percentage of the intervals between pulses that are 0.2 ms or more in duration. The other lines in order are the percentage of intervals that equal or exceed 0.6, 2, 6, 20, 60, 200, 600, 2000, 6000, and 20000 ms.

The next group of numbers gives the percentage of pulse durations that equal or exceed the various lengths of time in the same order as the intervals are given. That is, the first column gives the percentage of pulse durations that equal or exceed 0.2, 0.6, 2, 6, etc., ms at level 1.

The bottom line on the printout is the average crossing rate at each of the levels. The number of positive crossings per second at level 1 through 7 are given from left to right.

Computer printouts of the same information for man-made radio noise have been furnished in an earlier report (ESSA, 1968).

Sample plots of the data given in the tables are shown on figures 1 through 12. Figures 1 through 4 are the plots of the data given in table 2 for atmospheric radio noise at 2.5 MHz. Figure 1 is a plot of the amplitude probability distribution, figure 2 presents the curves of the PSD's, figure 3 shows the PDD's, and figure 4 is a plot of average crossing rates. These values were recorded on March 29. The same sets of values for 500 kHz recorded on April 3 and tabulated in table 7 are shown on figures 5 through 8, and the data for 250 kHz recorded on April 5 (table 12) are presented in figures 9 through 12.

-4-

Each tape was further analyzed to obtain the autocovariance function. From each tape, three intervals of 2048 samples each were chosen at random. The 2048 data points correspond to a time interval of essentially 0.2 s (10000 kHz sampling rate). For each set of data, the d-c term was removed, and the conditioned data were fast-Fourier-transformed to obtain an estimate of the spectrum. Each data point is considered to be complex, and the resulting spectrum is used to compute the power spectrum. The power spectrum (properly scaled) is inverse fast-Fourier-transformed to obtain the autocovariance. This procedure is, by far, faster for obtaining the autocovariance than the standard, average-lagged products method.

Figures 13 through 18 show two such sets of calculations for 500 kHz recorded on April 3. Figures 19 through 21 show a set for 500 kHz recorded on April 4, and figures 22 through 24 show a set for 2.5 MHz recorded on April 4. Each set of three figures first shows the input (digitized) data, then the amplitude spectrum, and third, the resulting autocovariance. All levels given are in millivolts and can be converted to absolute levels using table 1. While all possible (1024) Fourier coefficients are computed in the above, only the first 50 are given in the figures. Each point shown on the spectrum corresponds to harmonics spaced about five cycles apart, and each harmonic has its corresponding negative frequency component. That is, the result is a two-sided spectrum, of which only the first 50 harmonics of the positive half are shown.

Because the desired result is the autocovariance, the above procedure does not give a particularly good estimate of the spectrum itself, since no conditioning (windowing) of the data was used. The spectral estimates obtained above can be converted to a reasonable estimate of the true spectrum by standard conditioning (Hamming, for example) of these estimates.

Each of the above samples is taken from within a burst of noise. Two low-level and two relatively high-level bursts are shown. Figure 22 also shows the start of a short burst at 2.5 MHz. Between such bursts are periods of much lower-level background noise.

3. COMPARISON OF MEASUREMENTS WITH THE HALL MODEL

In this section we will compare the measured statistics (APD, average crossing rates, PDD's, and PSD's) obtained for atmospheric radio noise with the corresponding statistics calculated from the Hall model. The model has been specified in a previous report to SAMSO (Disney and Spaulding, 1968), and the portion of that report concerning the Hall model and optimum receiver performance is included here for completeness as appendix A. While measured APD's and average crossing rates have been compared before for LF atmospherics (Hall, 1966), the above four statistics have never been obtained for the same sample of noise and, of course, never compared with any model.

The computations of the envelope and phase probability distributions are given in appendix B. Note that the phase is uniformly distributed and independent of the envelope, as one would intuitively expect. The APD used in the comparisons is given by (B-15).

The computations of the average rate of envelope-level crossings is given in appendix C. Some of the calculations in appendices B and C were performed earlier under a different contract (USAFSS Memorandum of Agreement TT-67-334). As shown, the average crossing rate is dependent on the spectral moments of the measurement receiver bandpass characteristic and the autocovariance function of the noise process. For typical receiver characteristics, these parameters can be included in the rms bandwidth, B_c, as defined in (C-13). Our measurements were made in a bandwidth of 4 kHz, which corresponds for typical bandpass shapes to an rms bandwidth, B_c, somewhere between 800 and 1500 Hz.

We will use 1000 Hz for B_c in the following comparisons so that the average number of crossings by the envelope of the level V_o, $N(V_o)$ is given by (C-14). Since we obtained only the positive going crossings from the tape recordings of the noise, we require $N(V_o)/2$.

The determination of the distribution of envelope-level crossings (PDD's and PSD's) for a random process is, in general, a classical unsolved problem--even for Gaussian processes. Since we are dealing with a bandlimited envelope, a useful representation of the envelope can be given in terms of $2T_oB$ samples, along with a set of appropriate orthonormal basis functions (see, for example, Hannock and Wintz, 1966, App. II), where 2B is the bandwidth and T_o is the time interval of interest. That is, the envelope for the time interval is given by

$$V(t) = \sum_{i=1}^{2T_oB} V(t_i) \, \phi_i(t) \, , \qquad (1)$$

where $V(t_i)$ denotes the value of the envelope at time t_i and $\phi_i(t)$ denotes the basis function. Of course, each $V(t_i)$ is a random variable. Since the expected shape of the received atmospherics is determined by the bandpass of the receiver, $\phi_i(t)$ should be related to this bandpass charac-teristic. Although generally the best approximation comes from using prolate spheroidal-wave functions for $\phi_i(t)$, we will follow Hall's (1966) example and use pulse-basis functions. The ith-basis functions will be a rectangle pulse of width Δt from $t_i - \Delta t/2$ to $t_i + \Delta t/2$ and a height $1/\sqrt{\Delta t}$, Δt denoting the time interval between samples. Letting the number of samples $2T_oB$ be denoted by N, and from (C-2), we have the envelope given by

$$V(t) = \sum_{i=0}^{N} |a(t_i)| \, E(t_i) \, \phi_i(t) \, \sqrt{\Delta t} \, . \qquad (2)$$

where, as in appendix C, $E(t)$ is the envelope of the narrow-band Gaussian process, $n(t)$.

We can now proceed to compute the distribution of the pulse spacings at the envelope level V_o. Let Prob $[T > T_o]$ denote the probability that the time between a down crossing of level V_o to the next up crossing, T, is greater than T_o. Then

$$\text{Prob } [T > T_o] = \text{Prob } \{\text{no up crossing of } V_o \text{ in } [t, \ t + T_o] \mid$$
$$\text{a down crossing at time } t \} \ . \tag{3}$$

The vertical line in (3) denotes a conditional probability, i.e., (3) is the probability the first statement is true, given that the second is true, and is, therefore, given by

$$\text{Prob } [T > T_o] = \frac{\text{Prob } \{\text{no up crossing of } V_o \text{ in } [t, \ t + T_o], \text{ and a downcrossing at } t \}}{\text{Prob } \{\text{down crossing at } t \}} \ . \tag{4}$$

In the range $[t, \ t + T_o]$ we have N samples, where $N = 2T_o B$ (i.e., smallest integer $\geq 2T_o B$). Thus (4) becomes, in terms of these samples,

$$\text{Prob}[T > T_o] = \frac{\text{Prob}[V(t_o) > V_o, \ V(t_1) \leq V_o, \ V(t_2) \leq V_o, \ \dots, \ V(t_N) \leq V_o]}{\text{Prob}[V(t_o) > V_o, \ V(t_1) \leq V_o]} \ . \tag{5}$$

If atmospheric noise were composed of independently occurring events (e.g., events occurring according to a Poisson distribution), the pulse spacings would be essentially exponentially distributed, especially at the higher envelope levels. Some slight deviation might be expected due to the receiver response characteristic. The measurements given indicate that we are not dealing with independently occurring events, since an exponential distribution plots as a straight line of slope -1 on the coordinates used for plotting the PSD's and PDD's (Rayleigh paper).

-8-

We see from the measured statistics (figs. 2, 6, and 10) that for time intervals on the order of 20 ms or less the PSD's are reasonably close to being exponentially distributed. These time intervals correspond to events within a burst of noise, and we have seen that the autocovariance function generally shows only low correlation for these short time periods (figs. 15 and 24). However, a great deal of correlation exists at longer time periods (time between bursts, for example), as reflected by the much greater steepness of the PSD's at the longer time intervals and higher envelope levels.

We will calculate (5) and the corresponding expression for PDD's for two cases. In the first case we will assume independent samples, and in the second we will introduce some correlation between samples.

If the samples are independent, then (5) becomes

$$Prob\,[\,T > T_o\,] = \frac{Prob\,[\,V(t) > V_o\,]\,\{Prob\,[\,V(t) \le V_o\,]\}^N}{Prob\,[\,V(t) > V_o\,]\,Prob\,[\,V(t) \le V_o\,]} \,, \qquad (6)$$

so that

$$Prob\,[\,T > T_o\,] = \{Prob\,[\,V(t) \le V_o\,]\}^{N-1} \,, \qquad (7)$$

and, from the expression for the envelope distribution (B-15),

$$Prob\,[\,T > T_o\,] = \left\{1 - \frac{\left(\gamma/V_o\right)^m}{\left[1 + \left(\gamma/V_o\right)^2\right]^{m/2}}\right\}^{N-1} \,. \qquad (8)$$

The result (8) corresponds to one previously obtained by Hall (1966). Similarly, if we let U_o denote the time interval of interest, then for the

pulse durations, i.e., the time between an up-going crossing and the
next down-going crossing of level V_o, we have

$$\text{Prob}[U > U_o] = \frac{\text{Prob}[V(t_o) < V_o, V(t_1) \geq V_o, V(t_2) \geq V_o, \ldots, V(t_N) \geq V_o]}{\text{Prob}[V(t_o) < V_o, V(t_1) \geq V_o]} ,$$

(9)

which reduces, for independent samples, to

$$\text{Prob}[U > U_o] = \{\text{Prob}[V(t) \geq V_o]\}^{N-1} ,$$

(10)

so that

$$\text{Prob}[U > U_o] = \left\{\frac{(\gamma/V_o)^m}{[1+(\gamma/V_o)^2]^{m/2}}\right\}^{N-1}$$

(11)

We next introduce some correlation into the noise process.
This means that a covariance function must be specified for the process $a(t)$.
(The independence assumption above corresponds to specifying a delta
function covariance.) We will let $a(t)$ remain constant over the time
interval of interest (T_o or U_o), so that $a(t)$ is now a random variable
rather than a random process.

Let $P_N(V_o)$ denote the numerator of (5),

$$\text{Prob}[V(t_o) > V_o, V(t_1) \leq V_o, V(t_2) \leq V_o, \ldots, V(t_N) \leq V_o] .$$

We now have

$$P_N(V_o) = \int_{V_o}^{\infty} dV_o \int_{0}^{V_o} dV_1 \ldots \int_{0}^{V_N} dV_N \, P_{\underline{V}}(\underline{V}) ,$$

(12)

-10-

where V_i denotes $V(t_i)$, and $\underline{V}$ denotes the vector of samples $\{V_0, V_1, \ldots, V_N\}$. To maintain notation consistent with previous work, we now have an ambiguity. Although V_o is the particular envelope level of interest, in (12) V_o is also used for the sample $V(t_o)$. The context is such, however, that no confusion will arise.

Since our envelope $V(t)$ over the time interval T_o is now given by (see app. C)

$$V(t) = |a| \, E(t) \, , \tag{13}$$

where $E(t)$ is the envelope of the narrow-band Gaussian process $n(t)$,

$$p_{\underline{V}}(\underline{V}) = \int_0^\infty \frac{dx}{x^{N+1}} \, p_{|a|}(x) \, p_{\underline{E}}\left(\frac{\underline{V}}{x}\right) \, , \tag{14}$$

where $\underline{E}$ denotes the vector $\{E_i\}$ of N samples corresponding to the vector $\{V_i\}$. Now $p_{|a|}(x)$ is given by (C-7) and, since E is the envelope of a Gaussian process, each E_i is Rayleigh distributed and independent so that (see app. A)

$$p_{\underline{E}}(\underline{E}) = \prod_{i=0}^{N} \left[\frac{E_i}{\sigma_1^2} \exp\left(-\frac{E_i^2}{2\sigma_1^2}\right) \right] . \tag{15}$$

The integral (14) can now be evaluated, giving

$$p_{\underline{V}}(\underline{V}) = 2^{N+1} \gamma^m \, \frac{\Gamma\left(\frac{2N+m+2}{2}\right)}{\Gamma\left(\frac{m}{2}\right)} \, \frac{\prod\limits_{i=0}^{N} V_i}{\left[\sum\limits_{i=1}^{N} V_i^2 + \gamma^2\right]^{\frac{2N+m+2}{2}}} \, . \tag{16}$$

-11-

Substituting (16) into (12) and evaluating the N + 1 dimensional integral, we have

$$P_N(V_o) = \gamma^m \sum_{k=0}^{N} \frac{(-1)^k \binom{N}{k}}{\left[(k+1) V_o^2 + \gamma^2\right]^{m/2}} \quad . \tag{17}$$

Likewise, for pulse durations (time interval U_o), $P_N(V_o)$ is now given by

$$P_N(V_o) = \int_0^{V_o} dV_o \int_{V_o}^{\infty} dV_1 \cdots \int_{V_o}^{\infty} dV_N \, P_V(\underline{V}) \quad , \tag{18}$$

which gives

$$P_N(V_o) = \frac{1}{\left[(N+1) V_o^2 + \gamma^2\right]^{m/2}} - \frac{1}{\left[(N+2) V_o^2 + \gamma^2\right]^{m/2}} \quad . \tag{19}$$

Finally then, for this case of dependent samples, (5) gives

$$\text{Prob}[\, T > T_o\,] = \frac{\displaystyle\sum_{k=0}^{N} \frac{(-1)^k \binom{N}{k}}{\left[k+1 + (\gamma/V_o)^2\right]^{m/2}}}{\displaystyle\sum_{k=0}^{1} \frac{(-1)^k}{\left[k+1 + (\gamma/V_o)^2\right]^{m/2}}} \quad , \tag{20}$$

and (9) gives

$$\text{Prob}[\, U > U_o\,] = \frac{\dfrac{1}{\left[(N+1)(V_o/\gamma)^2 + 1\right]^{m/2}} - \dfrac{1}{\left[(N+2)(V_o/\gamma)^2 + 1\right]^{m/2}}}{\dfrac{1}{\left[(V_o/\gamma)^2 + 1\right]^{m/2}} - \dfrac{1}{\left[2(V_o/\gamma)^2 + 1\right]^{m/2}}} \quad . \tag{21}$$

-12-

Figures 25 through 34 show the comparison of the measured envelope distributions and average crossing rates with those calculated (B-15) and (C-14) for the Hall model for five of the atmospheric-noise tapes analyzed, two at 500 kHz, two at 2.5 MHz, and one at 250 kHz. The levels are given relative to the parameter γ, since the theoretical results are in terms of V_o/γ. They can be converted easily to absolute values (dB $>$ kT$_o$b), as explained earlier. The comparison shows good agreement, and for the average crossing rates could be made even better by specifying the proper spectral moments (app. C), rather than the "loose" parameter B$_c$.

Figures 35 and 36 show the comparison of the measured PSD's and PDD's with those derived from the Hall model, considering independent samples ((8) and (11)). The comparison is shown only for the 250 kHz case. We see that the derived distributions are essentially exponential especially at the low probabilities, and do not match the measured distributions for the larger time intervals.

Figures 37 and 38 show the comparison for considering dependent samples ((20) and (21)). which indicates too much dependence at the larger time intervals as characterized by the derived distributions becoming too steep and grouping together more rapidly than the measured distributions at the higher envelope levels.

While the amplitude statistics and the average time statistics (average number of crossings per second) match quite well, the PDD's and PSD's do not match as well. The two cases given (independent samples and some degree of correlation) bracket the real situation. It is apparent that a proper covariance function can be specified for a(t), so that these time statistics also can be closely matched.

Note that (2) is quite difficult to evaluate if N is at all large because of the alternating series, coupled with the binomial coefficients,

$\binom{N}{k}$. For example, in our 4 kHz bandwidth, a time interval of 2000 ms corresponds to an N of 8000 Techniques have been developed to evaluate (20) and computer programs written to implement them.

Consider also the special case $\Theta = 3(m = 2)$, where (20) can be evaluated easily, since

$$\sum_{k=0}^{N} \frac{(-1)^k \binom{N}{k}}{\left[k + 1 + (\gamma/V_0)^2\right]} = \int_0^1 z^{(\gamma/V_0)^2} (1 - z)^N \, dz \, , \qquad (22)$$

and the integral can be readily evaluated numerically.

4. CALCULATION OF PERFORMANCE OF OPTIMUM RECEIVER FOR CURRENT MINUTEMAN SYSTEM

The current Minuteman receiver uses limiting of the noise in a 4 kHz bandwidth, followed by an effective bandwidth reduction to 8 Hz. The receiver is a standard DCPSK receiver operating at 8 bps. We will apply the results of appendix A to the above situation to obtain the performance of the optimum receiver.

Many tests of the effect of limiting and hole punching on the performance of the above standard receiver have been conducted (Sisco, 1964, Sylvania, 1963), and the object here is to determine how much better the optimum receiver would perform. Since atmospheric-noise tapes were used in the tests cited, we must first specify the parameters of the Hall model that match the statistics of the noise used. The noise had essentially the values of V_d(app. A) of 26.0 dB, 12.0 dB, and 7.0 dB.

Figure 39 is a comparison of the measured distribution and the distribution from the Hall model for $m = 1.0$ ($V_d = 26.0$ dB) for tracks 5 and 7, reel 1, of the Canal Zone tape. Figure 40 shows the standard atmospheric-noise distribution for $V_d = 7.0$ dB , with the distribution

-14-

from the Hall model for m = 2.5. Figure 41 is a comparison of the measured distribution from tracks 1 and 3, reel 2, of a Canal Zone tape, along with distributions for V_d = 12.0 dB and m = 1.7. Figure 42 shows the measured distribution from tracks 1 and 3, reel 1, Canal Zone tape along with the distribution for m = 1.0. The value V_d = 26.0 dB would correspond here also. The frequency throughout is 450 kHz, and since the bandwidth is 4 kHz we require the performance of the optimum receiving system for m = 1.0, 1.7, and 2.5.

The tests reported by Sisco (1964) and Sylvania (1963) were generally conducted with the receiver operating in a CPSK mode rather than DCPSK. We will therefore compute performance for CPSK signals.

First, for comparison, we will give the performance of the standard CPSK receiver operating at 8 bps. The 4 kHz noise distributions of V_d's of 26.0, 12.0, and 7.0 dB reduce in an 8 Hz bandwidth to distributions with V_d's of 3.7, 1.83, and 1.55 dB (Spaulding et al., 1962). The performance for these three values of V_d is shown in figure 43 and were computed by Halton and Spaulding (1966) and Spaulding. Also shown is the performance curve for the standard (linear, matched filter CPSK receiver in Gaussian noise.

Now it remains to compute the performance of the optimum receiving system for the corresponding situations. As shown in (A-35), performance (probability of error, p_e) is given by

$$p_e = \text{Prob}\left\{\sum_{i=1}^{2TB} \ln z_i \geq 0\right\},\tag{23}$$

where 2B is the bandwidth, T is the time duration of the signal, and the random variables z_i are functions of the complex envelopes of the noise

and signal, as given in (A-36). In our situation then, 2TB is 500. In appendix A, performance was calculated for 2TB equal 10 and 20, and was given by the appropriate Chernoff upper bound (A-46). Here the high value of 2TB results in this upper bound not, in itself, being a very good estimate, which must be modified according to (A-41). That is, the factor $1/\sqrt{2\pi s^2 \, \ddot{\rho}\,(s)}$ must be calculated. While this factor was of little significance in the previous calculation, it now becomes highly significant, as can be seen from (A-52), which gives $\ddot{\rho}\,(s)$ for the special case m = 2. Numerical techniques were developed to evaluate $\ddot{\rho}\,(s)$ for the values of m of interest here. Even so, since we are dealing with low signal-to-noise ratios, the resulting estimate (A-41) is valid only for quite low p_e.

To complete the performance estimates, we now will obtain a lower bound that is quite good for low signal-to-noise ratios and high p_e.

Using the inequality, as suggested by Hall (1966),

$$\ell n \, z_i \geq 1 - \frac{1}{z_i} \; , \tag{24}$$

we have

$$p_e \geq \text{Prob} \left\{ \sum_{i=1}^{2TB} (1 - \frac{1}{z_i}) \geq 0 \right\} . \tag{25}$$

Since 2TB is 500, we now apply the central limit theorem to (25), that is, we require the mean and variance of the random variables $1 - 1/z_i$.

-16-

From appendix A, we have

$$1 - \frac{1}{z_i} = \frac{|\eta_i|^2 - |\eta_i - \mu_i|^2}{|\eta_i|^2 + \xi^2} , \qquad (26)$$

where η_i is the ith sample of the complex noise envelope, μ_i is the ith sample of the complex signal envelope, and ξ^2 is $m\sigma_1^2 \Delta t / 2\sigma^2$ (app. A). With $\eta_i = \eta_{ic} + j \eta_{is}$ and $\mu_i = \mu_{ic} + j \mu_{is}$ (that is, η_{ic} and η_{is} are the real and imaginary parts of the complex random variable η_i), we have

$$E\left[1 - \frac{1}{z_i}\right] = \int_{-\infty}^{\infty} d\eta_{ic} \int_{-\infty}^{\infty} d\eta_{is} \left[\frac{|\eta_i|^2 + |\eta_i - \mu_i|^2}{|\eta_i|^2 + \xi^2}\right] P_{\eta_{ic}, \eta_{is}}\left(\eta_{ic}, \eta_{is}\right),$$
$$(27)$$

where (Hall, 1966)

$$P_{\eta_{ic}, \eta_{is}}\left(\eta_{ic}, \eta_{is}\right) = \frac{m \xi^m}{2\pi} \frac{1}{\left[|\eta_i|^2 + \xi^2\right]^{\frac{m+2}{2}}} , \qquad (28)$$

and E denotes the expectation operation (mean value operation).

Evaluating (27), we obtain

$$E\left[1 - \frac{i}{z_i}\right] = - \frac{m|\mu_i|^2}{(m+2)\xi^2} , \qquad (29)$$

so

$$E\left[\sum_{i=1}^{2TB} \left(1 - \frac{1}{z_i}\right)\right] = - \frac{m}{m+2} \sum_{i=1}^{2TB} \frac{|\mu_i|^2}{\xi^2} . \qquad (30)$$

Similarly,

$$E\left[1 - \frac{1}{z_i}\right]^2 = \frac{4m|\mu_i|^2}{(m+2)(m+4)\xi^2} + \frac{m|\mu_i|^4}{(m+4)\xi^4} . \qquad (31)$$

-17-

The variance of the variable $1 - 1/z_i$ is then given by

$$\text{Var}\left[1 - \frac{1}{z_i}\right] = \frac{4m}{(m+2)(m+4)} \left|\frac{\mu_i}{\xi}\right|^2 + \left(\frac{m}{m+4} - \frac{m^2}{(m+2)^2}\right) \left|\frac{\mu_i}{\xi}\right|^4 . \tag{32}$$

Finally, with

$$\mu_z = -\frac{m}{m+2} \sum_{i=1}^{2TB} \left|\frac{\mu_i}{\xi}\right|^2 \tag{33}$$

and

$$\sigma_z^2 = \frac{4m}{(m+4)(m+2)} \sum_{i=1}^{2TB} \left|\frac{\mu_i}{\xi}\right|^2 + \left(\frac{m}{m+4} - \frac{m^2}{(m+2)^2}\right) \sum_{i=1}^{2TB} \left|\frac{\mu_i}{\xi}\right|^4 , \tag{34}$$

we obtain an estimate of the lower bound given by (25)

$$P_e \gtrsim \text{erfc}\left(\frac{-\mu_z}{\sigma_z}\right) , \tag{35}$$

Here

$$\text{erfc}(x) = \frac{1}{\sqrt{2\pi}} \int_x^\infty \exp(-y^2/2)\,dy . \tag{36}$$

By using both the upper bound (A-41) and the lower bound (35), the performance curves for $m = 1.0$, 1.7, and 2.5, given in figure 43, were obtained. Note that the above calculations are for signals with zero crosscorrelation (app. A), so that the curves of figure 43 also incorporate the standard 3 dB improvement one expects in going to signals with -1 crosscorrelation (as in the case of CPSK signals).

While the results of the limiter tests (Sisco, 1964; Sylvania, 1963) are not included in figure 43, they generally group about the Gaussian characteristic, indicating that even in this rather extreme case of limiting and bandwidth reduction, the optimum receiver still performs substantially better.

5. REFERENCES

Akima, H. (1967), Speeding up of HF radio-transmissions and broadcasts
  (World Weather Watch Study T. 21), ESSA Tech. Memo. IERTM-ITSA 42.

Beckmann, P. (1964), Amplitude probability distribution of atmospheric
  radio noise, Radio Sci. 68D, No. 6, 723-736.

Bello, P.A. (1965), Error probabilities due to atmospheric noise and
  flat fading in HF ionospheric communications systems, IEEE
  Trans. Commun. Technol. COM-13, No. 3, 266-279.

Bowen, B. A. (1963), Some analytical techniques for a class of non-
  Gaussian processes, Research Report No. 63-3, Queens University,

CCIR (1964), World distribution and characteristics of atmospheric radio
  noise, Report 322, ITU, Geneva.

Conda, A. M. (1965), The effects of atmospheric noise on the probability
  of error for an NC FSK system, IEEE Trans. Commun. Technol.
  COM-13, No. 3, 280-283.

Crichlow, W. Q., A. D. Spaulding, C. J. Roubique, and R. T. Disney
  (1960), Amplitude Probability Distributions for Atmospheric
  Radio Noise, NBS Monograph 23 (U.S. Government Printing Office,
  Washington, D.C.).

Disney, R. T. and A. D. Spaulding (1968), Interference measurements and
  analysis, Final Rept. to Space and Missile Systems Organization, VI,
  prepared by the Environmental Science Services Administration under
  Contract No. F04701-69-F-0072, Project 672A.

ESSA (1967), Communications Task - Project 672A, Final Rept. to Space
  and Missile Systems Organization, prepared by the Environmental
  Science Services Administration under Contract AFD/0 (04-591)-67-3.

ESSA (1968), Interference field tests, Interim Evaluation Rept., prepared
  by the Environmental Science Services Administration under
  Contract No. F04701-68-F-0072, Project 672A.

Furutsu, K., and T. Ishida (1960), On the theory of amplitude distributions
  of impulsive random noise and its application to atmospheric
  noise, Japan Radio Res. Labs. J. 7, No. 32, 279-307.

Galejs, J. (1966), Amplitude distributions of radio noise at ELF and
VLF, J. Geophys. Res. 71, 201-216.

Hall, H. M. (1966), A new model for "impulsive" phenomena: application
to atmospheric-noise communication channels, Tech. Rept.
No. 3412-8 and 7050-7, Stanford Electronic Laboratories,
Stanford, California.

Halton, J. H., and A. D. Spaulding (1966), Error rates in differentially
coherent phase systems in non-Gaussian noise, IEEE Trans.
Commun. Technol. COM-14, No. 5, 594-601.

Hannock, J. C. and P. A. Wintz (1966), Signal Detection Theory,
(McGraw-Hill Book Co., Inc., New York).

Helstron, C. W. (1960), Statistical Theory of Signal Detection (Pergamon
Press, Oxford, England).

Ibukun, O. (1966), Structural aspects of atmospheric radio noise in the
tropics, Proc. IEEE 54, 361-367.

Lindenalub, J. C., and K. A. Chen (1965), Performance of matched
filter receivers in non-Gaussian noise environments, IEEE Trans.
Communi. Technol. 13, No. 4, 545-547.

Linfield, R. F. (1965), High performance reliable VLF component of
the Naval Advanced Communication System - VLF system design
specification and evaluation process, Final Report No. 34-F,
prepared by DECO Electronics, Inc. for U.S. Navy Bureau of Ships.

Mandelbrot, B. (1964), Self-similar turbulence and non-Wienerian
conditional spectra (unpublished IBM research paper).

Middleton, D. (1961), Introduction to Statistical Communication Theory
(McGraw-Hill Book Co., Inc., New York).

Shchukin, A. N. (1946), On a method of combating impulse interference
in radio reception, Bull. Academy of Sci. USSR, Phys. Series 10,
No. 1, 49-56.

Shepelavey, B. (1963), Non-Gaussian noise in binary data phase coherent

Sisco, W. B. (1964), Bit and message error rate in atmospheric noise
with and without peak limiting, Report No. 7070-6323-RU-000,
TRW Space Technology Laboratories, Redondo Beach, California.

Spaulding, A. D., C. J. Roubique, and W. Q. Crichlow (1962),
Conversion of the amplitude probability distribution function for
atmospheric radio noise from one bandwidth to another, J. Res.
NBS 66D, 713-720.

Spaulding, A. D. (1964), Determination of error rates for narrowband
communication of binary-coded messages in atmospheric radio
noise. Proc. IEEE 52, No. 2, 220-221.

Spaulding, A. D. (1966), The characteristics of atmospheric radio
noise and its effects on digital communications systems,
IEEE Intern. Commun. Conf., Paper No. CP 1126.

Sylvania (1963), Design review report for project 124-221 (Contained
in report on hole puncher performance investigation of radio
subsystems of Minuteman Ground Electronic Systems), Sylvania
Electronics, Waltham, Mass.

Van Trees, H. L. (1968), Detection, Estimation, and Modulation Theory,
Part 1 (John Wiley and Sons, Inc., New York).

Table 1. Calibration Sheet

Absolute levels corresponding to levels 1 through 7 on computer printouts. Levels given to nearest dB.

Level	$dB > kT_o b$	$dB > kT_o b$	$dB > kT_o b$	$dB > kT_o b$
	Table 2	Table 3	Table 4	Table 5
1	42	41	53	57
2	52	51	63	67
3	62	61	73	77
4	72	71	83	87
5	82	81	93	97
6	92	91	103	107
7	100	99	111	115
	Table 6	Table 7	Table 8	Table 9
1	63	42	67	77
2	73	52	77	87
3	83	62	87	97
4	93	72	97	107
5	103	82	107	117
6	113	92	117	127
7	121	100	125	135
	Table 10	Table 11	Table 12	Table 13
1	83	62	91	67
2	93	72	101	77
3	103	82	111	87
4	113	92	121	97
5	123	102	131	107
6	133	112	141	117
7	141	120	149	125

Table 2. Distributions of atmospheric radio noise. Eggleston Reservoir
No. 4, Boulder, Colorado, March 29, 1969, 0000-0400 hrs.
Frequency: 2.5 MHz.   Impulse bandwidth: 4 kHz.

AMPLITUDE-PROBABILITY DISTRIBUTIONS

34.36854	57.28767	91.6071429				
0.80391	10.25463	61.9876543				
0.00000	0.18725	5.2490146				
0.00000	0.00000	1.7341270				
0.00000	0.00000	0.1045132				
0.00000	0.00000	0.0055666				
0.00000	0.00000	0.0007165				
0.00000	0.00000					
0.00000	0.00000					
0.00000	0.00000					
0.00000	0.00000					

CUMULATIVE PULSE INTERVAL DISTRIBUTIONS IN PERCENT

81.67226	68.26578	80.67485	78.78788	100.00000		
60.84774	28.48897	51.12474	54.54545	100.00000		
41.94137	9.94100	27.40286	37.87879	100.00000		
29.14743	4.78450	17.17791	31.81818	100.00000		
3.31794	2.47563	11.55419	25.75758	100.00000		
0.05100	1.45208	6.33947	19.69697	100.00000		
0.00000	1.09030	4.08998	18.18182	100.00000		
0.00000	0.76963	3.57873	16.66667	100.00000		
0.00000	0.37199	2.45309	16.66667	100.00000		
0.00000	0.08979	1.02249	13.63636	100.00000		
0.00000	0.00000	0.00000	6.06061	100.00000		

CUMULATIVE PULSE DURATION DISTRIBUTIONS IN PERCENT

86.85707	74.43456	46.60958	60.83889	41.82004	26.78788	100.00000
46.51329	21.75118	7.23514	11.05695	3.16973	1.51515	50.00000
14.65703	2.01029	1.11135	0.53874	0.20450	0.00000	0.00000
10.75562	0.14715	0.09395	0.05131	0.10225	0.00000	0.00000
0.09068	0.01246	0.00268	0.00000	0.00000	0.00000	0.00000
0.02343	0.00000	0.00000	0.00000	0.00000	0.00000	0.00000
0.00000	0.00000	0.00000	0.00000	0.00000	0.00000	0.00000
0.00000	0.00000	0.00000	0.00000	0.00000	0.00000	0.00000
0.00000	0.00000	0.00000	0.00000	0.00000	0.00000	0.00000
0.00000	0.00000	0.00000	0.00000	0.00000	0.00000	0.00000
0.00000	0.00000	0.00000	0.00000	0.00000	0.00000	0.00000

POSITIVE CROSSING RATES FROM LEVEL 1 TO LEVEL 7(.0VOLT)

540.923	1415.779	205.313	42.967	5.390	0.364	0.011

Table 3. Distributions of atmospheric radio noise. Eggleston Reservoir
No. 4, Boulder, Colorado, April 3, 1969, 0000-0400 hrs.
Frequency: 2.5 MHz.   Impulse bandwidth: 4 kHz.

AMPLITUDE-PROBABILITY DISTRIBUTIONS

98.2188051
89.8755614
40.1622509
7.6426984
0.4750331
0.0054563
0.0003307

CUMULATIVE PULSE INTERVAL DISTRIBUTIONS IN PERCENT

22.0646.7	64.07620	72.50096	84.97747	92.95775	100.00000
0.23741	29.53791	34.44894	55.40511	91.69014	100.00000
0.00000	1.94964	17.64467	25.42446	72.23944	100.00000
0.00000	0.02235	5.91137	13.13131	44.78873	100.00000
0.00000	0.00000	2.25068	7.17814	60.56338	100.00000
0.00000	0.00000	0.88432	4.26830	56.70423	100.00000
0.00000	0.00000	0.24626	2.40705	40.84507	100.00000
0.00000	0.00000	0.06046	1.37544	32.80282	100.00000
0.00000	0.00000	0.00000	0.40430	28.16901	
0.00000	0.00000	0.00000	0.04447	12.67606	
0.00000	0.00000	0.00000	0.00000	2.81690	

CUMULATIVE PULSE DURATION DISTRIBUTIONS IN PERCENT

94.34773	43.40656	54.41811	44.74533	28.16901	100.00000
76.74137	9.55826	9.77071	2.72942	1.40845	100.00000
14.37944	1.01477	0.54528	0.00000	0.00000	0.00000
3.01727	0.08932	0.01156	0.00000	0.00000	0.00000
0.44413	0.00147	0.00000	0.00000	0.00000	0.00000
0.04787	0.02070	0.00000	0.00000	0.00000	0.00000
0.00000	0.00000	0.00000	0.00000	0.00000	0.00000
0.00000	0.00000	0.00000	0.00000	0.00000	0.00000
0.00000	0.00000	0.00000	0.00000	0.00000	0.00000
0.00000	0.00000	0.00000	0.00000	0.00000	0.00000

POSITIVE CROSSING RATES FROM LEVEL 1 TO LEVEL 7 (BVOLT)

141.145	771.925	1503.919	286.045	25.645	0.391	0.006

-24-

Table 4.   Distributions of atmospheric radio noise.   Eggleston Reservoir
No. 4, Boulder, Colorado, April 4, 1969, 0000-0400 hrs.
Frequency: 2.5 MHz.   Impulse bandwidth: 4 kHz.

AMPLITUDE-PROBABILITY DISTRIBUTIONS

90.2279541
66.9798280
18.1013029
4.6175595
0.4526565
0.0282346
0.0006063

CUMULATIVE PULSE INTERVAL DISTRIBUTIONS IN PERCENT

54.28295	75.63740	81.07460	83.64023	87.55556	100.00000
19.82349	38.84937	44.42217	52.05382	57.77778	85.71429
3.25492	14.91739	19.54419	26.55807	33.77778	85.71429
0.07316	5.89711	10.72425	16.39518	24.00000	85.71429
0.00000	1.47535	5.11156	9.95042	18.66667	85.71429
0.00000	0.63755	2.10412	6.55099	16.00000	85.71429
0.00000	0.07555	0.71902	4.10765	16.00000	85.71429
0.00000	0.02428	0.19174	2.26629	10.66667	71.42857
0.00000	0.00000	0.00436	1.09773	9.33333	57.14286
0.00000	0.00000	0.00000	0.07082	5.33333	57.14286
0.00000	0.00000	0.00000	0.00000	0.44444	28.57143

CUMULATIVE PULSE DURATION DISTRIBUTIONS IN PERCENT

88.24009	79.66986	73.91471	63.63314	45.33333	28.57143
46.10608	21.34743	15.25187	16.83569	4.88889	0.00000
17.54746	2.67490	1.29859	0.56657	0.00000	0.00000
13.70313	0.29792	0.10894	0.03541	0.00000	0.00000
0.56802	0.01140	0.00436	0.00000	0.00000	0.00000
0.09105	0.00285	0.00000	0.00000	0.00000	0.00000
0.00564	0.00000	0.00000	0.00000	0.00000	0.00000
0.00000	0.00000	0.00000	0.00000	0.00000	0.00000
0.00000	0.00000	0.00000	0.00000	0.00000	0.00000
0.00000	0.00000	0.00000	0.00000	0.00000	0.00000
0.00000	0.00000	0.00000	0.00000	0.00000	0.00000

POSITIVE CROSSING RATES FROM LEVEL 1 TO LEVEL 7 (.8VOLT)

605.589	783.504	388.646	126.477	15.564	1.240	0.039

Table 5. Distributions of atmospheric radio noise. Eggleston Reservoir
No. 4, Boulder, Colorado, April 5, 1969, 0000-0400 hrs.
Frequency: 2.5 MHz.   Impulse bandwidth: 4 kHz.

AMPLITUDE-PROBABILITY DISTRIBUTIONS

A1 1461640		0.00000
38.7945877		0.00000
3.0827822		0.00000
0.2419533		0.00000
0.0034722		0.00000
0.0000000		0.00000
0.0000000		0.00000

CUMULATIVE PULSE INTERVAL DISTRIBUTIONS IN PERCENT

82.16695	87.64756	94.11765	0.00000
47.97469	61.52815	76.47059	0.00000
21.47184	38.04071	70.54824	0.00000
10.48007	24.72029	47.64706	0.00000
3.91803	17.82942	58.82353	0.00000
1.55518	10.27703	44.11765	0.00000
0.53701	5.74408	35.29412	0.00000
0.27025	2.99374	35.29412	0.00000
0.02148	1.11707	32.35294	0.00000
0.00000	0.04668	23.52941	0.00000
0.00000	0.00000	8.82353	0.00000

CUMULATIVE PULSE DURATION DISTRIBUTIONS IN PERCENT

72.13200	49.64254	52.94118	0.00000
19.47475	7.21716	2.94118	0.00000
4.36510	0.04468	0.00000	0.00000
0.21914	0.00000	0.00000	0.00000
0.00218	0.00000	0.00000	0.00000
0.00000	0.00000	0.00000	0.00000
0.00000	0.00000	0.00000	0.00000
0.00000	0.00000	0.00000	0.00000
0.00000	0.00000	0.00000	0.00000
0.00000	0.00000	0.00000	0.00000
0.00000	0.00000	0.00000	0.00000

POSITIVE CROSSING RATES FROM LEVEL 1 TO LEVEL 7 (.8VOLT)

551.636	739.557	128.290	12.335	0.187	0.000

-26-

Table 6.   Distributions of atmospheric radio noise. Eggleston Reservoir
No. 4, Boulder, Colorado, March 29, 1969, 0000-0400 hrs.
Frequency: 500 MHz.   Impulse bandwidth: 4 kHz.

AMPLITUDE-PROBABILITY DISTRIBUTIONS

70.5099206
25.7118056
1.8863536
0.4308862
0.0402337
0.0047006
0.0007165

CUMULATIVE PULSE INTERVAL DISTRIBUTIONS IN PERCENT

72.83700	75.92093	83.05604	83.07350	81.59722	95.23810	100.00000
20.93766	32.61665	56.35780	56.64439	59.72222	85.71429	100.00000
4.90440	13.41831	26.92436	32.62806	47.56944	85.71429	100.00000
0.00000	6.65366	18.35031	21.67780	43.05556	80.95238	100.00000
0.00000	0.00000	11.30667	14.29102	36.11111	76.19048	100.00000
0.00000	0.00000	5.92626	8.12918	24.65278	71.42857	100.00000
0.00000	0.00000	2.29564	4.50891	15.27778	61.90476	100.00000
0.00000	0.00000	0.57040	2.22717	11.80556	57.14286	100.00000
0.00000	0.00000	0.04456	1.11359	8.33333	54.38095	100.00000
0.00000	0.00000	0.00000	0.14848	3.12500	38.09524	100.00000
0.00000	0.00000	0.00000	0.00000	0.34722	14.28571	50.00000
0.00000	0.00000	0.00000	0.00000	0.00000		

CUMULATIVE PULSE DURATION DISTRIBUTIONS IN PERCENT

71.64316	73.04222	67.14718	67.29770	58.33333	54.38095	100.00000
19.13264	17.09811	15.60867	9.94803	6.25000	4.76190	50.00000
10.74782	1.50384	2.61484	0.55679	0.34722	0.00000	0.00000
0.17040	0.05088	0.16075	0.00000	0.00000	0.00000	0.00000
0.03049	0.00000	0.00499	0.00000	0.00000	0.00000	0.00000
0.00350	0.00000	0.00000	0.00000	0.00000	0.00000	0.00000
0.00000	0.00000	0.00000	0.00000	0.00000	0.00000	0.00000
0.00000	0.00000	0.00000	0.00000	0.00000	0.00000	0.00000
0.00000	0.00000	0.00000	0.00000	0.00000	0.00000	0.00000
0.00000	0.00000	0.00000	0.00000	0.00000	0.00000	0.00000
0.00000	0.00000	0.00000	0.00000	0.00000	0.00000	0.00000

POSITIVE CROSSING RATES FROM LEVEL 1 TO LEVEL 7 (.8VOLT)

| 614.594 | 630.859 | 49.476 | 14.848 | 1.587 | 0.116 | 0.011 |

Table 7. Distributions of atmospheric radio noise. Eggleston Reservoir
No. 4, Boulder, Colorado, April 3, 1969, 0000-0400.
Frequency: 500 kHz.   Impulse bandwidth: 4 kHz.

AMPLITUDE-PROBABILITY DISTRIBUTIONS

99.6331570
98.2083333
84.2741402
37.2428351
5.4413029
0.8957099
0.0984899

CUMULATIVE PULSE INTERVAL DISTRIBUTIONS IN PERCENT

2.78422	5.95336	29.02153	73.44815	79.42783	41.86170	79.55056
0.00000	0.00000	0.59318	31.53815	54.52146	64.24506	65.84270
0.00000	0.00000	0.00000	3.19095	29.22831	49.14394	60.11236
0.00000	0.00000	0.00000	0.01370	13.54130	37.11668	53.25843
0.00000	0.00000	0.00000	0.00000	4.59206	16.99429	43.48315
0.00000	0.00000	0.00000	0.00000	1.42734	6.86430	28.42697
0.00000	0.00000	0.00000	0.00000	0.33151	2.63158	12.58427
0.00000	0.00000	0.00000	0.00000	0.03990	0.99873	7.86517
0.00000	0.00000	0.00000	0.00000	0.00000	0.09512	2.69663
0.00000	0.00000	0.00000	0.00000	0.00000	0.00000	0.44944
0.00000	0.00000	0.00000	0.00000	0.00000	0.00000	0.00000

CUMULATIVE PULSE DURATION DISTRIBUTIONS IN PERCENT

98.56126	96.81493	84.16526	64.58657	65.11449	54.96366	41.57303
94.13676	85.85252	44.69637	11.82595	12.13089	7.50818	4.38202
83.40037	59.67657	7.50569	0.88579	0.50648	0.28135	0.00000
73.49938	32.61149	0.60086	0.09025	0.02149	0.00000	0.00000
38.86139	3.58525	0.02406	0.00137	0.00000	0.00000	0.00000
11.33973	0.29194	0.00000	0.00000	0.00000	0.00000	0.00000
0.80446	0.00656	0.00000	0.00000	0.00000	0.00000	0.00000
0.01547	0.00000	0.00000	0.00000	0.00000	0.00000	0.00000
0.00000	0.00000	0.00000	0.00000	0.00000	0.00000	0.00000
0.00000	0.00000	0.00000	0.00000	0.00000	0.00000	0.00000
0.00000	0.00000	0.00000	0.00000	0.00000	0.00000	0.00000

POSITIVE CROSSING RATES FROM LEVEL 1 TO LEVEL 7(.AVOLT)

35.632	168.028	1076.863	1206.459	179.552	36.766	4.905

Table 8. Distributions of atmospheric radio noise. Eggleston Reservoir
No. 4, Boulder, Colorado, April 4, 1969, 0000-0400 hrs.
Frequency: 500 kHz.   Impulse bandwidth: 4 kHz.

AMPLITUDE-PROBABILITY DISTRIBUTIONS

```
30.0934465
11.4128086
24.6571869
 9.1070326
 1.2497138
 0.0063404
 0.0048501
```

CUMULATIVE PULSE INTERVAL DISTRIBUTIONS IN PERCENT

50.92858	64.78094	76.91123	83.31055	94.51178	92.10526
6.72634	28.21040	44.92694	63.63445	71.15600	86.84211
0.12562	10.55136	22.82586	49.50047	66.10550	86.84211
0.03000	3.55503	8.74843	34.29383	62.28956	86.84211
0.00000	0.92077	1.97182	15.86608	52.63749	84.21053
0.00000	0.26497	0.61825	4.97423	37.93490	78.94737
0.00000	0.07297	0.24447	1.46332	24.20202	68.42105
0.00000	0.00994	0.05135	0.57840	11.11111	60.52632
0.00000	0.00000	0.00000	0.02103	1.68350	34.21053
0.00000	0.00000	0.00000	0.00000	0.00000	0.00000
0.00000	0.00000				

CUMULATIVE PULSE DURATION DISTRIBUTIONS IN PERCENT

84.74276	78.12421	72.61636	60.90485	47.47475	28.94737
42.90879	24.92078	14.24747	6.74943	2.58137	10.52632
18.71647	3.22164	0.71889	0.09423	0.11223	2.63158
13.54622	0.14463	0.00411	0.00000	0.00000	0.00000
0.95929	0.00110	0.00000	0.00000	0.00000	0.00000
0.14131	0.00000	0.00000	0.00000	0.00000	0.00000
0.00143	0.00000	0.00000	0.00000	0.00000	0.00000
0.00000	0.00000	0.00000	0.00000	0.00000	0.00000
0.00000	0.00000	0.00000	0.00000	0.00000	0.00000
0.00000	0.00000	0.00000	0.00000	0.00000	0.00000

POSITIVE CROSSING RATES FROM LEVEL 1 TO LEVEL 7 (LEVELS)

386.095	789.648	499.704	248.331	52.409	116.9	0.209

Table 9. Distributions of atmospheric radio noise. Eggleston Reservoir
No. 4, Boulder, Colorado, April 5, 1969, 0000-0400 hrs.
Frequency: 500 kHz.   Impulse bandwidth: 4 kHz.

AMPLITUDE-PROBABILITY DISTRIBUTIONS

```
86.5164446
55.1634700
17.7712191
 4.7692041
 0.7211508
 0.0459456
 0.0014881
```

CUMULATIVE PULSE INTERVAL DISTRIBUTIONS IN PERCENT

```
65.62717   67.03270   78.45930   84.60022   84.65121   85.71429
23.173-5   31.76742   47.39389   65.5-735   69.75717   78.57143
 6.45747   14.06167   25.37817   51.34250   45.78366   78.57143
 1.23721    5.95924   12.01291   37.02044   40.92715   78.57143
 0.00000    1.52816    3.90362   18.94944   54.76614   78.57143
 0.00000    0.38562    1.24411    8.04948   42.60486   71.42857
 0.00000    0.10178    0.37230    2.92219   24.28256   57.14286
 0.00000    0.01720    0.09928    1.3-664   13.68653   50.00000
 0.00000    0.00000    0.00310    0.07171    7.72627   35.71429
 0.00000    0.00000    0.00000    0.00000    0.44150   21.42857
 0.00000    0.00000    0.00000    0.00000    0.00000
 0.00000    0.00000    0.00000    0.00000    0.00000
```

CUMULATIVE PULSE DURATION DISTRIBUTIONS IN PERCENT

```
74.92226   74.77189   71.70736   61.07226   41.94260   42.85714
26.90177   22.90124   13.02163    5.57647    1.54525    0.00000
 9.03273    2.75102    0.54778    0.07172    0.00000    0.00000
 1.463 4    0.10322    0.00310    0.00000    0.00000    0.00000
 0.05370    0.00143    0.00000    0.00000    0.00000    0.00000
 0.00147    0.00000    0.00000    0.00000    0.00000    0.00000
 0.00000    0.00000    0.00000    0.00000    0.00000    0.00000
 0.00000    0.00000    0.00000    0.00000    0.00000    0.00000
 0.00000    0.00000    0.00000    0.00000    0.00000    0.00000
 0.00000    0.00000    0.00000    0.00000    0.00000    0.00000
 0.00000    0.00000    0.00000    0.00000    0.00000    0.00000
```

POSITIVE CROSSING RATES FROM LEVEL 1 TO LEVEL 7(.8VOLT)

```
461.899   749.2-9   344.663   177.646   30.743   2.497   0.077
```

Table 10. Distributions of atmospheric radio noise. Eggleston Reservoir
No. 4, Boulder, Colorado, March 29, 1969, 0000-0400 hrs.
Frequency: 250 kHz.   Impulse bandwidth: 4 kHz.

AMPLITUDE-PROBABILITY DISTRIBUTIONS

95.5609921	
72.2008377	
0.7173170	
0.1038911	
0.0153770	
0.0019290	
0.0006063	

28.77679	60.51591
0.33707	6.50538
0.00165	0.52827
0.00000	0.00458
0.00000	0.00000
0.00000	0.00000
0.00000	0.00000
0.00000	0.00000
0.00000	0.00000
0.00000	0.00000
0.00000	0.00000

CUMULATIVE PULSE INTERVAL DISTRIBUTIONS IN PERCENT

86.54463	91.51019	92.17391	100.00000
67.34694	68.27807	80.86957	100.00000
48.97959	43.10827	71.30435	100.00000
37.07483	31.54215	63.47826	100.00000
27.72109	23.29205	56.52174	100.00000
14.96599	13.54380	45.21739	93.33333
8.61354	4.65441	31.30435	93.33333
5.95238	0.77907	23.47826	86.66667
4.09163	0.02993	20.86957	73.33333
1.53061	0.00000	8.69565	53.33333
0.00000	0.00000	0.00000	33.33333

CUMULATIVE PULSE DURATION DISTRIBUTIONS IN PERCENT

96.41937	83.87999	50.49940	70.91837	59.13043	60.00000	100.00000
45.33377	20.70460	10.06742	14.11565	6.95652	6.66667	50.00000
18.89458	5.17009	0.59928	0.17007	0.00000	0.00000	0.00000
15.62293	2.10209	0.00000	0.00000	0.00000	0.00000	0.00000
2.41573	0.00137	0.00000	0.00000	0.00000	0.00000	0.00000
0.00165	0.00000	0.00000	0.00000	0.00000	0.00000	0.00000
0.00000	0.00000	0.00000	0.00000	0.00000	0.00000	0.00000
0.00000	0.00000	0.00000	0.00000	0.00000	0.00000	0.00000
0.00000	0.00000	0.00000	0.00000	0.00000	0.00000	0.00000
0.00000	0.00000	0.00000	0.00000	0.00000	0.00000	0.00000
0.00000	0.00000	0.00000	0.00000	0.00000	0.00000	0.00000

POSITIVE CROSSING RATES FROM LEVEL 1 TO LEVEL 7 (.8VOLT)

333.559	1203.979	277.590	3.241	0.634	0.183	0.013

Table 11. Distributions of atmospheric radio noise. Eggleston Reservoir No. 4, Boulder, Colorado, April 3, 1969, 0000-0400 hrs.
Frequency: 250 kHz.   Impulse bandwidth: 4 kHz.

AMPLITUDE-PROBABILITY DISTRIBUTIONS

99.1141424
93.8740664
45.0309744
2.5417769
0.1724190
0.0202271
0.0032518

CUMULATIVE PULSE INTERVAL DISTRIBUTIONS IN PERCENT

9.873644	76.75738	93.64386	91.77680	92.85714	89.47368
0.00000	23.87600	78.79421	79.51542	85.71429	84.21053
0.00000	1.12495	53.84648	68.04167	74.37363	84.21053
0.00000	0.01769	29.38943	59.17768	71.42857	84.21053
0.00000	0.00000	10.03541	47.57709	45.93407	84.21053
0.00000	0.00000	1.55310	32.23201	54.59341	84.21053
0.00000	0.00000	0.04267	15.63877	47.80220	73.68421
0.00000	0.00000	0.00000	5.43319	34.61538	68.42105
0.00000	0.00000	0.00000	0.80764	15.38462	47.36842
0.00000	0.00000	0.00000	0.00000	1.64835	15.78947
0.00000	0.00000	0.00000	0.00000	0.00000	

CUMULATIVE PULSE DURATION DISTRIBUTIONS IN PERCENT

96.48522	70.34651	43.97054	54.99266	44.15385	52.63158
86.34857	17.23054	4.21556	5.87372	3.29670	10.52632
65.43295	0.57190	0.08960	0.07342	0.00000	0.00000
51.01505	0.00844	0.00000	0.00000	0.00000	0.00000
16.95208	0.00000	0.00000	0.00000	0.00000	0.00000
2.14749	0.00000	0.00000	0.00000	0.00000	0.00000
0.00641	0.00000	0.00000	0.00000	0.00000	0.00000
0.00000	0.00000	0.00000	0.00000	0.00000	0.00000
0.00000	0.00000	0.00000	0.00000	0.00000	0.00000
0.00000	0.00000	0.00000	0.00000	0.00000	0.00000

POSITIVE CROSSING RATES FROM LEVEL 1 TO LEVEL 7(.8VOLT)

79.823	449.966	1308.730	129.172	7.507	1.003	0.105

Table 12:   Distributions of atmospheric radio noise. Eggleston Reservoir
            No. 4, Boulder, Colorado, April 5, 1969, 0000-0400 hrs.
            Frequency: 250 kHz.   Impulse bandwidth: 4 kHz.

AMPLITUDE-PROBABILITY DISTRIBUTIONS

77.7373236	
38.1494709	
3.7900132	
0.6492504	
0.0454211	
0.0053461	
0.0005511	

63.15387	
10.10895	
1.29421	
2.90201	
0.00000	
0.00000	
0.00000	
0.00000	
0.00000	
0.00000	
0.00000	

CUMULATIVE PULSE INTERVAL DISTRIBUTIONS IN PERCENT

88.42745	90.81928	94.10609	92.30769	100.00000
63.17698	75.90361	85.84662	84.53846	100.00000
37.50515	59.92771	76.62083	84.53846	100.00000
19.53833	45.59036	71.90570	84.53846	100.00000
4.56430	28.36145	64.87301	84.53846	100.00000
1.91158	12.55422	50.68762	84.61538	100.00000
0.71105	3.68675	32.02358	74.00000	100.00000
0.19680	1.56627	16.30648	57.69231	100.00000
0.01031	0.14458	4.32220	42.30769	100.00000
0.00000	0.00000	0.19644	19.23077	100.00000
0.00000	0.00000	0.00000	1.92308	100.00000

CUMULATIVE PULSE DURATION DISTRIBUTIONS IN PERCENT

72.50862	75.45857	68.16867	61.49312	48.07692	100.00000
19.43938	16.25618	10.00000	5.10806	1.92308	100.00000
4.42434	0.63376	0.14458	0.00000	0.00000	0.00000
0.18235	0.03607	0.00000	0.00000	0.00000	0.00000
0.00200	0.00000	0.00000	0.00000	0.00000	0.00000
0.00074	0.00000	0.00000	0.00000	0.00000	0.00000
0.00000	0.00000	0.00000	0.00000	0.00000	0.00000
0.00000	0.00000	0.00000	0.00000	0.00000	0.00000
0.00000	0.00000	0.00000	0.00000	0.00000	0.00000
0.00000	0.00000	0.00000	0.00000	0.00000	0.00000
0.00000	0.00000	0.00000	0.00000	0.00000	0.00000

POSITIVE CROSSING RATES FROM LEVEL 1 TO LEVEL 7 (/AVOLT)

743.116	828.169	106.966	22.873	2.805	0.287	0.006

-33-

Table 13. Distributions of atmospheric radio noise. Eggleston Reservoir
No. 4, Boulder, Colorado, April 4, 1969, 0000-0400 hrs.
Frequency: 5 MHz.   Impulse bandwidth: 4 kHz.

AMPLITUDE-PROBABILITY DISTRIBUTIONS

48.52424	47.1432571
7.16360	87.3492615
0.84726	22.7222222
0.00000	0.2547399
0.00000	0.0075507
0.00000	0.0020944
0.00000	0.0017637
0.00000	
0.00000	
0.00000	
0.00000	

CUMULATIVE PULSE INTERVAL DISTRIBUTIONS IN PERCENT

74.07944	90.82452	90.32258	100.00000	100.00000
34.75560	69.55603	77.41935	87.50000	100.00000
15.74550	48.37209	69.35484	87.50000	100.00000
4.93062	35.24427	67.74194	87.50000	100.00000
0.87366	24.16144	61.29032	87.50000	100.00000
0.29080	14.29175	53.22581	87.50000	100.00000
0.07172	4.72304	46.77419	87.50000	100.00000
0.00130	0.59197	45.16129	87.50000	100.00000
0.00000	0.00000	37.09677	87.50000	100.00000
0.00000	0.00000	12.90323	87.50000	100.00000
0.00000	0.00000	1.61290	37.50000	20.00000

CUMULATIVE PULSE DURATION DISTRIBUTIONS IN PERCENT

88.74238	64.29520	49.06634	54.83871	100.00000
56.82597	13.56852	3.50951	6.45161	60.00000
33.04695	4.71444	2.04228	0.00000	0.00000
26.07102	0.71721	0.71721	0.00000	0.00000
1.83625	0.02099	0.02099	0.00000	0.00000
1.73267	0.00522	0.00522	0.00000	0.00000
0.58073	0.00000	0.00000	0.00000	0.00000
0.10472	0.00000	0.00000	0.00000	0.00000
0.00474	0.00000	0.00000	0.00000	0.00000
0.00000	0.00000	0.00000	0.00000	0.00000
0.00000	0.00000	0.00000	0.00000	0.00000

POSITIVE CROSSING RATES FROM LEVEL 1 TO LEVEL 7 (ABOVE)

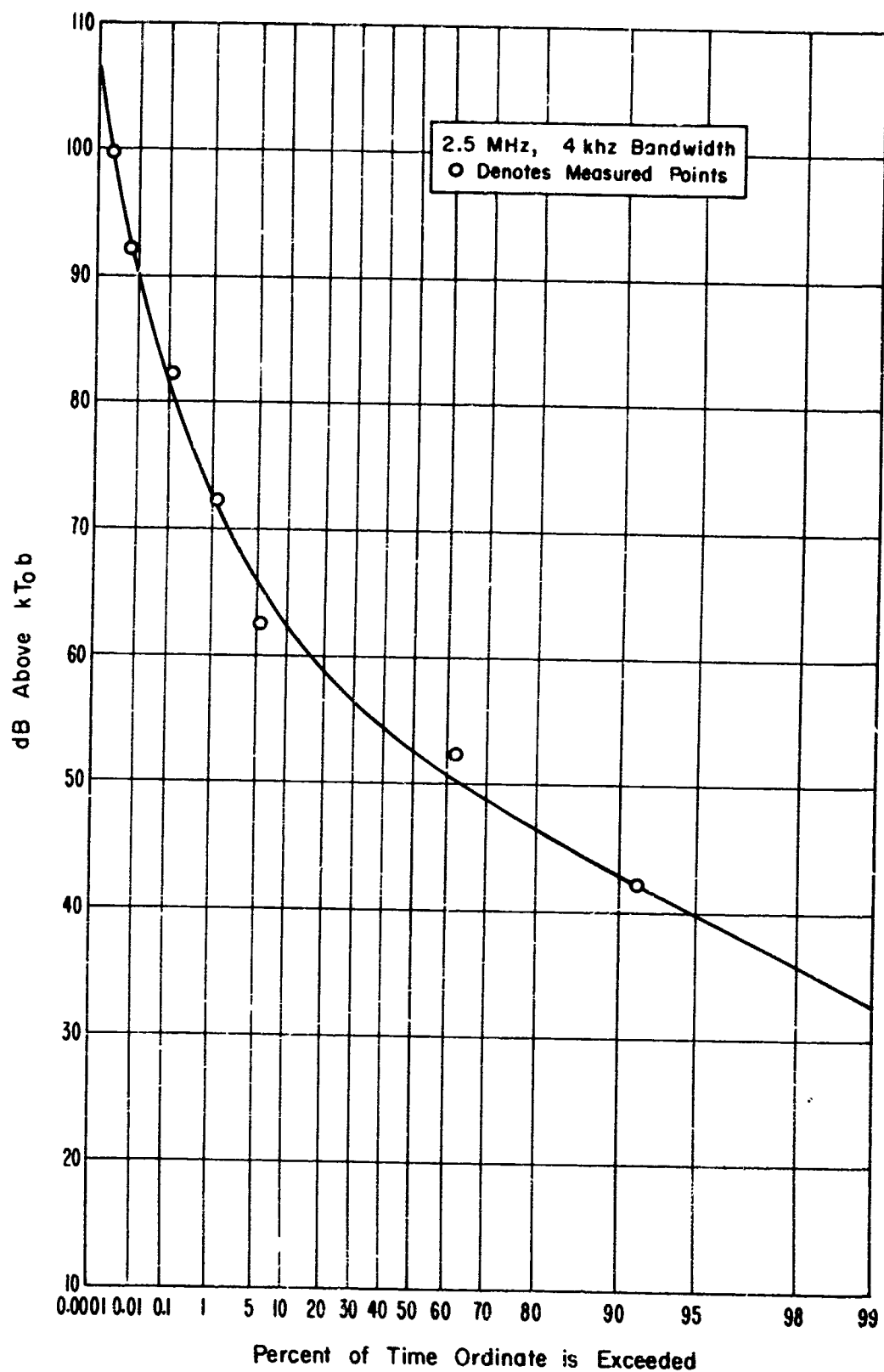|						
115.790	331.733	422.652	13.035	0.342	0.044	0.028

-34-

Figure 1.   Amplitude probability distribution of atmospheric radio noise
recorded at Eggleston Reservoir No. 4, Boulder, Colorado.
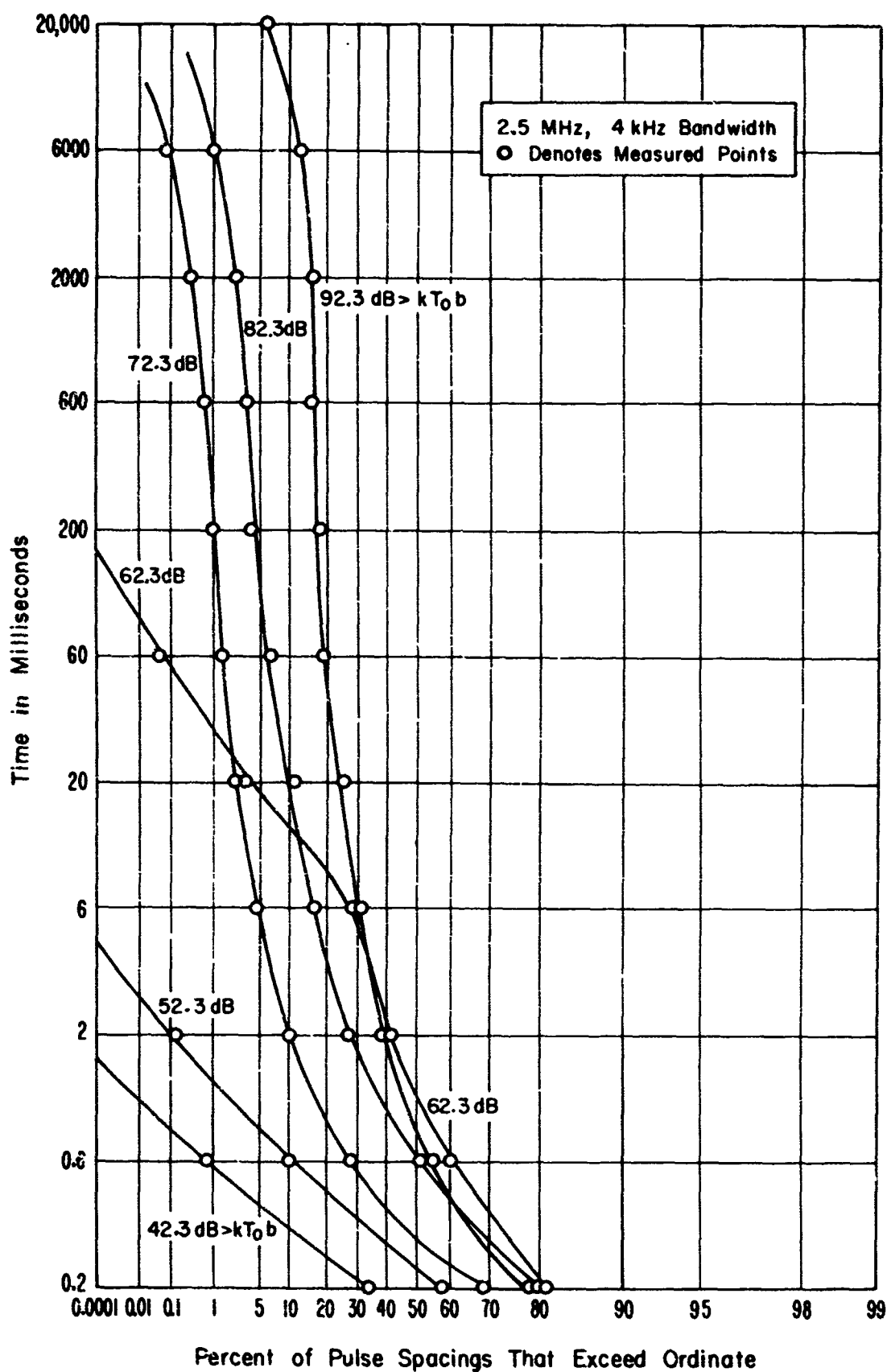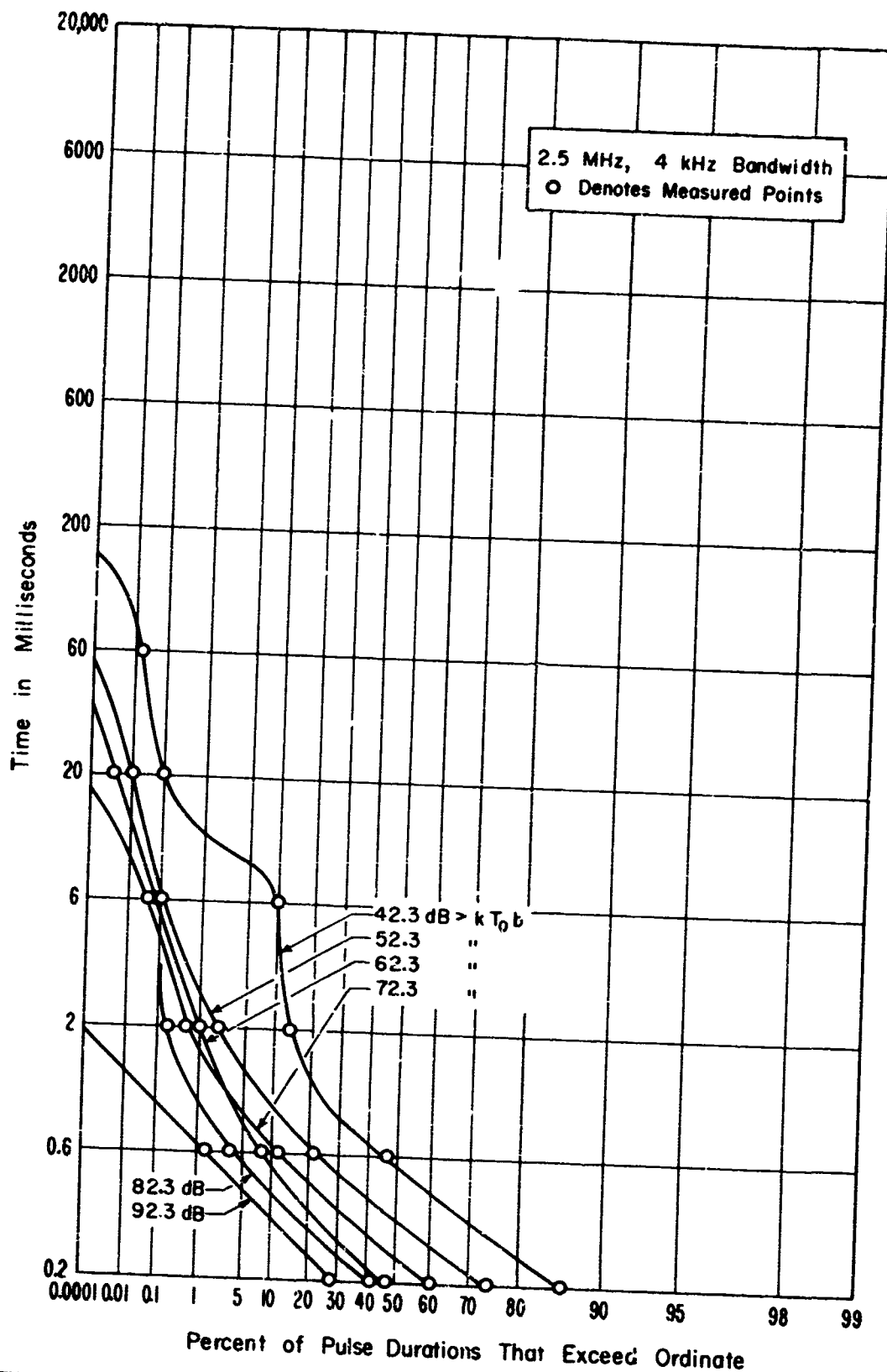$F = 2.5$ MHz, $B_i = 4$ kHz, March 29, 1969, 0000-0400 hrs.

Figure 2. Pulse spacing distributions of atmospheric radio noise recorded at Eggleston Reservoir No. 4, Boulder, Colorado.
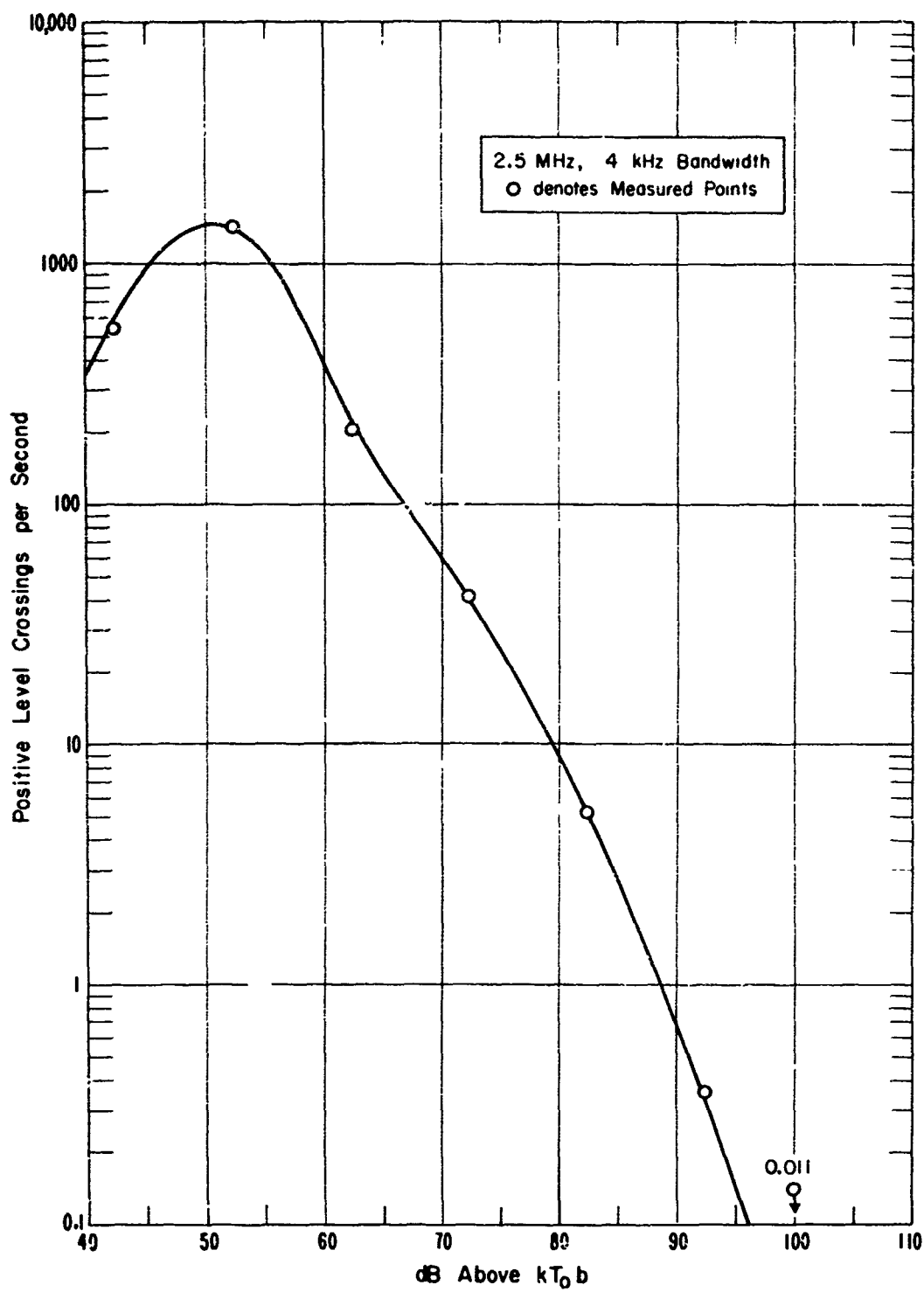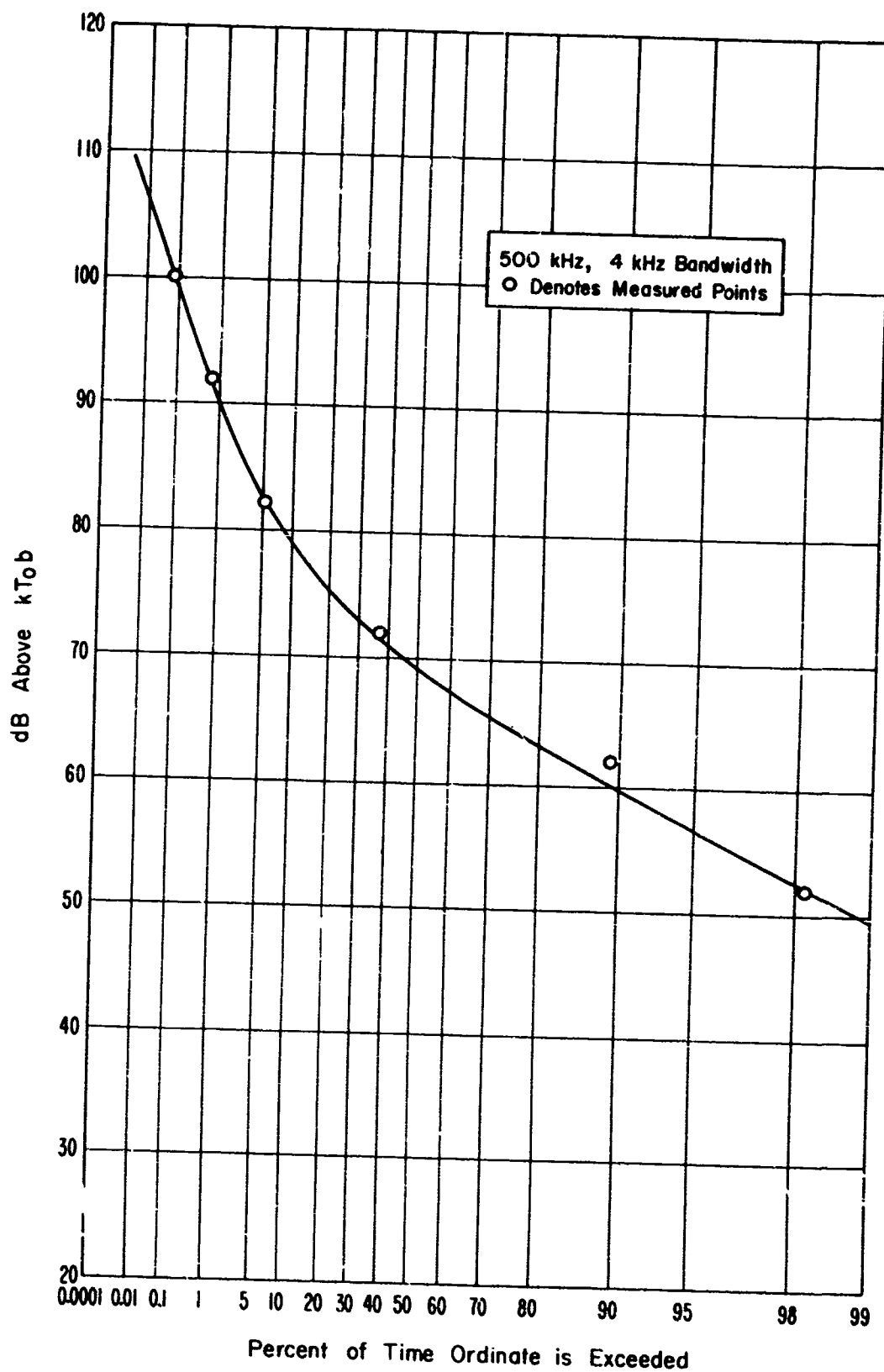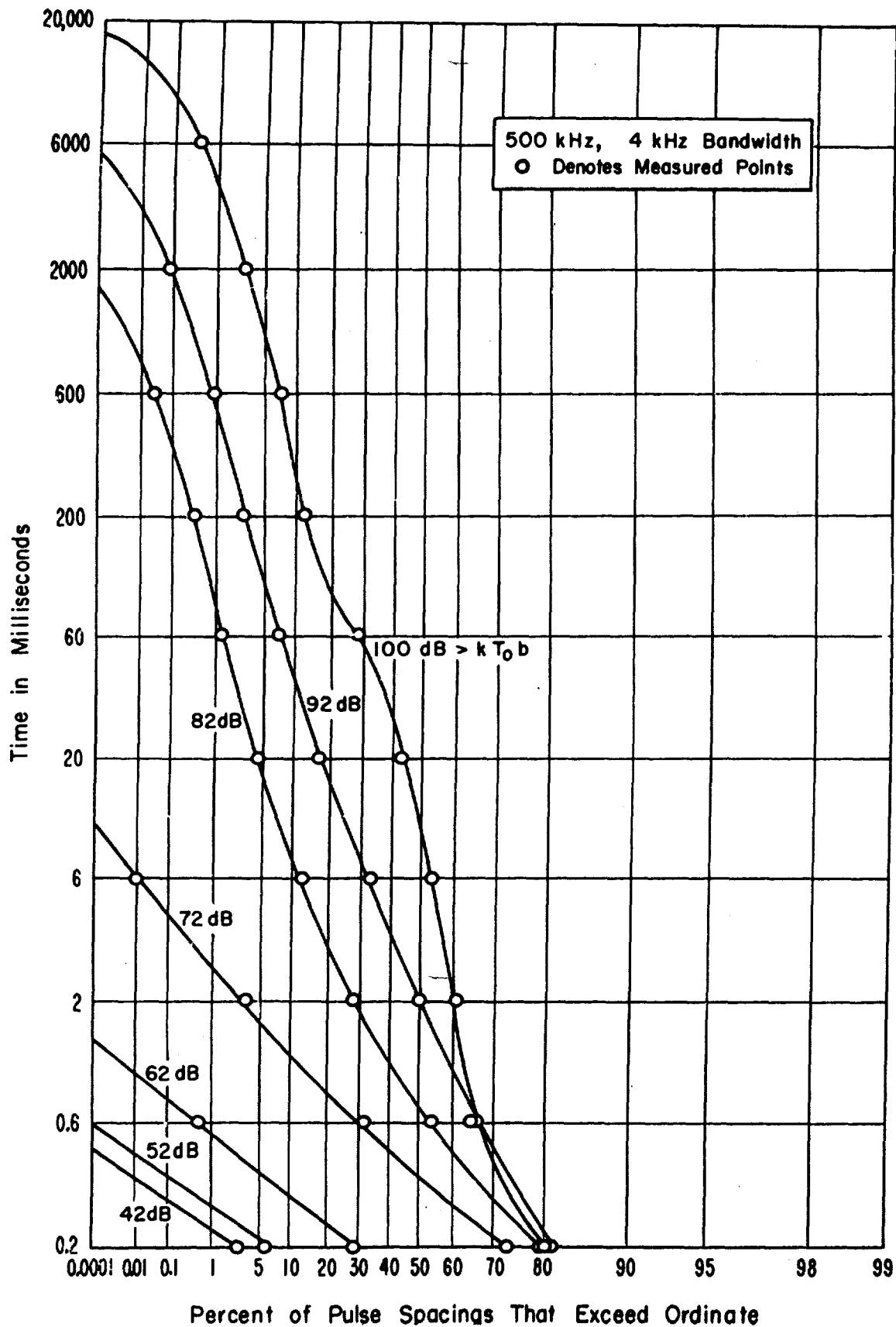F = 2.5 MHz, B_i = 4 kHz, March 29, 1969, 0000-0400 hrs.
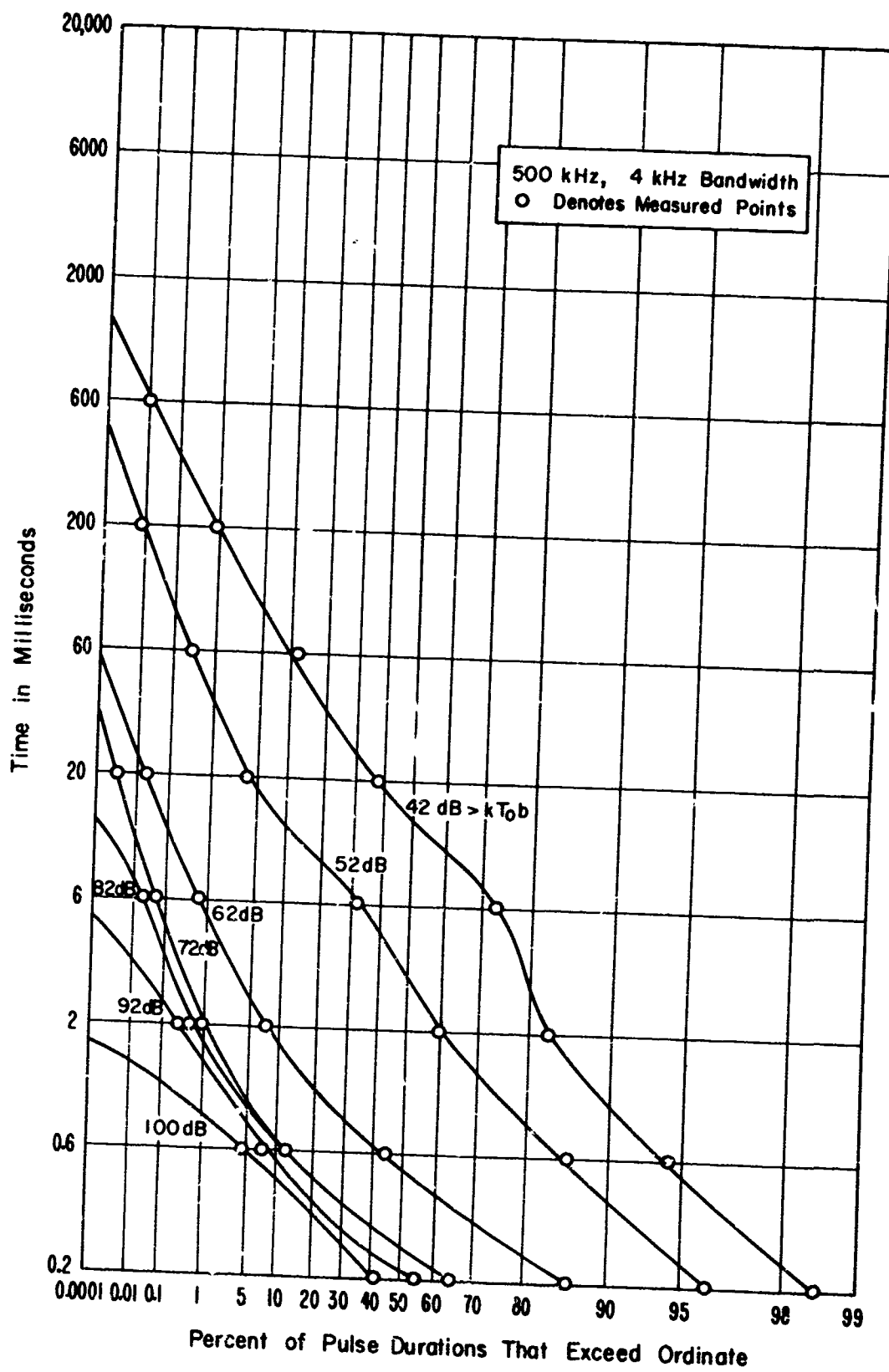
Figure 3. Pulse duration distributions of atmospheric radio noise recorded at Eggleston Reservoir No. 4, Boulder, Colorado. $F = 2.5$ MHz, $B_i = 4$ kHz, March 29, 1969, 0000-0400 hrs
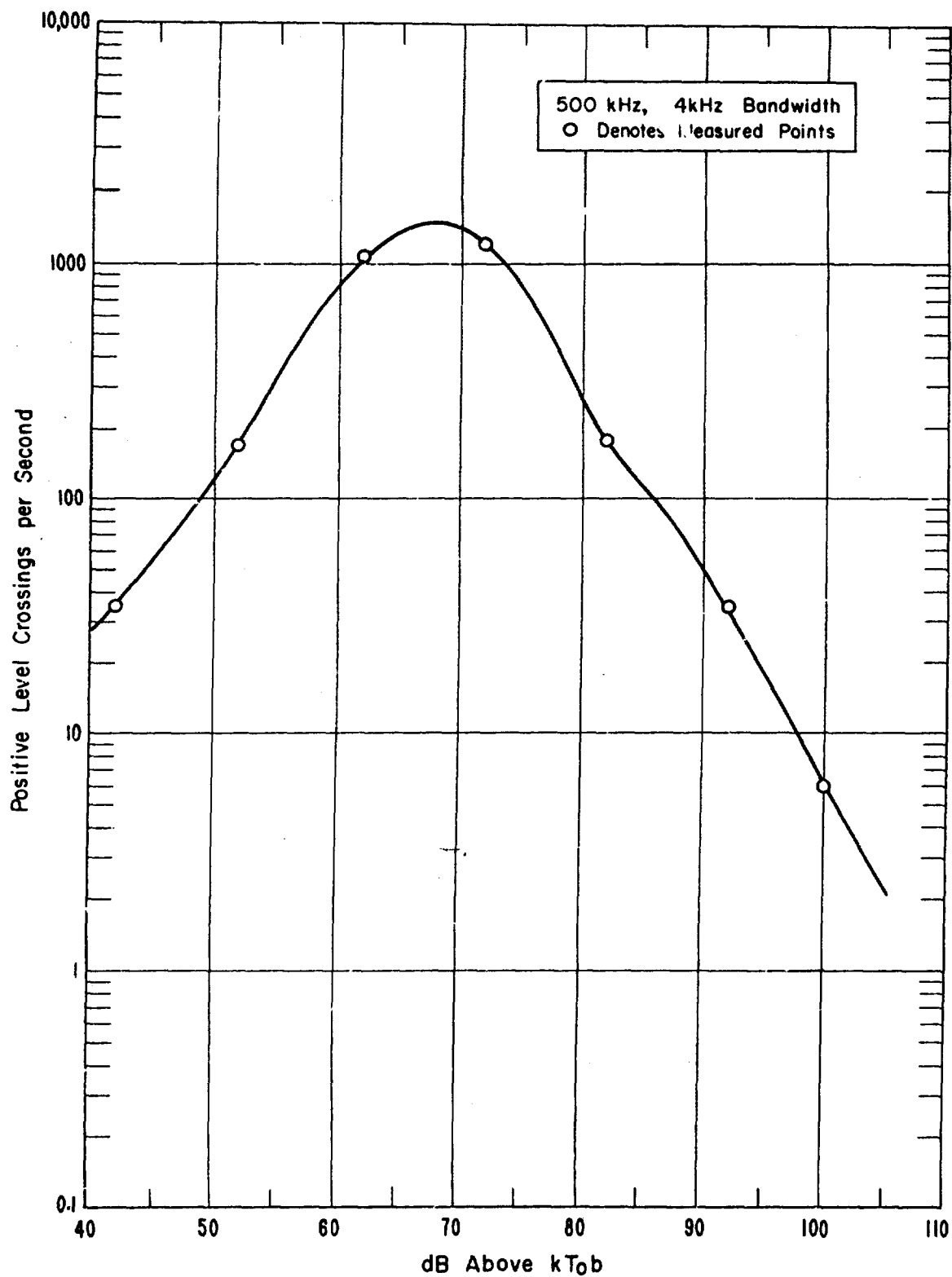
Figure 4. Average crossing rates of atmospheric radio noise recorded at Eggleston Reservoir No. 4, Boulder, Colorado. $F = 2.5$ MHz, $B_i = 4$ kHz, March 29, 1969, 0000-0400 hrs.
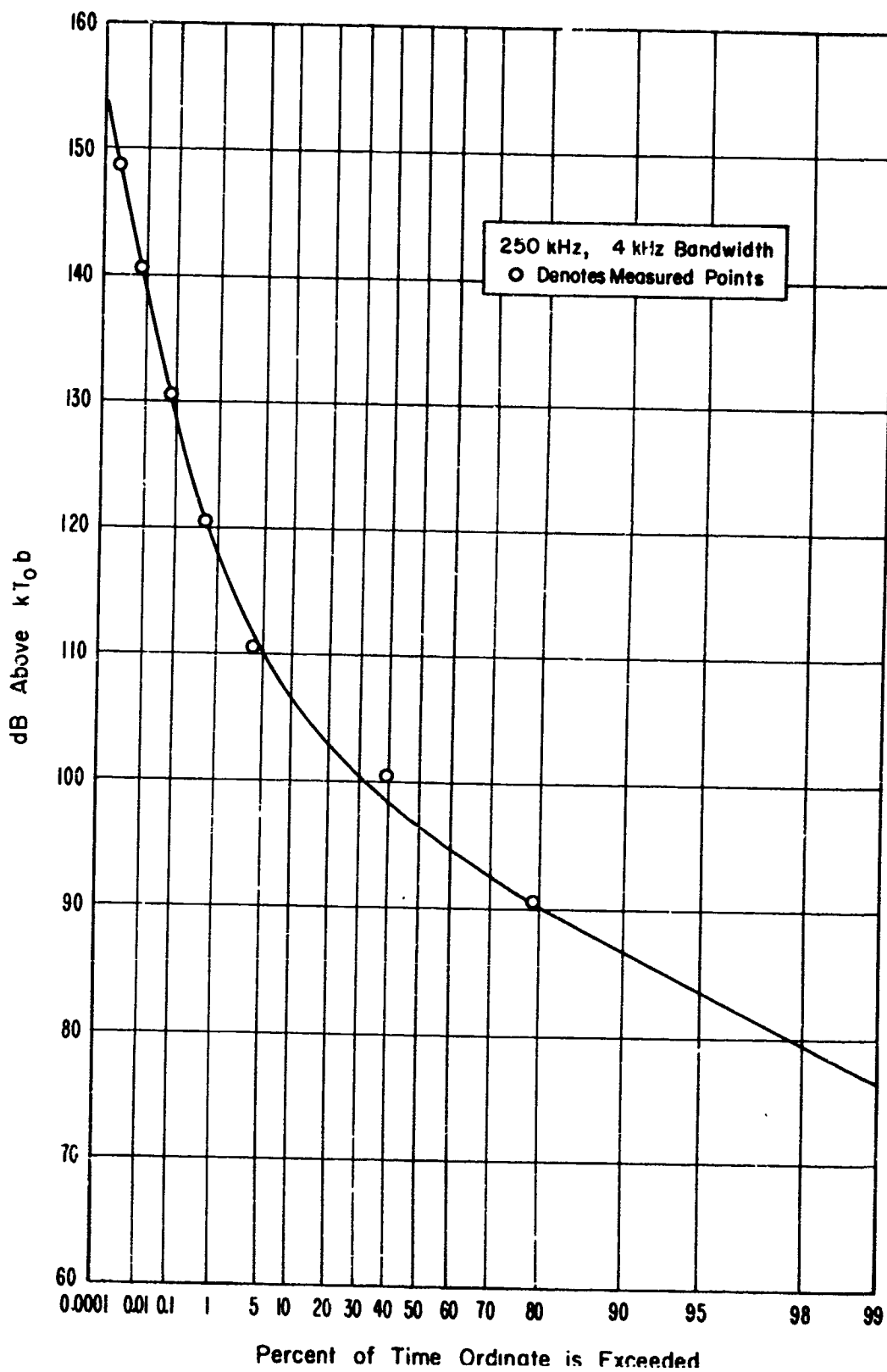
Figure 5.   Amplitude probability distribution of atmospheric radio noise
recorded at Eggleston Reservoir No. 1, Boulder, Colorado.
$F = 500$ kHz, $B_i = 4$ kHz, April 3, 1969, 0000-0400 hrs.

Figure 6. Pulse spacing distributions of atmospheric radio noise recorded at Eggleston Reservoir No. 4, Boulder, Colorado. F = 500 kHz, B_i = 4 kHz, April 3, 1969, 0000-0400 hrs.

Figure 7. Pulse duration distributions of atmospheric radio noise recorded at Eggleston Reservoir No. 4, Boulder, Colorado. $F = 500$ kHz, $B_i = 4$ kHz, April 3, 1969, 0000-0400 hrs.
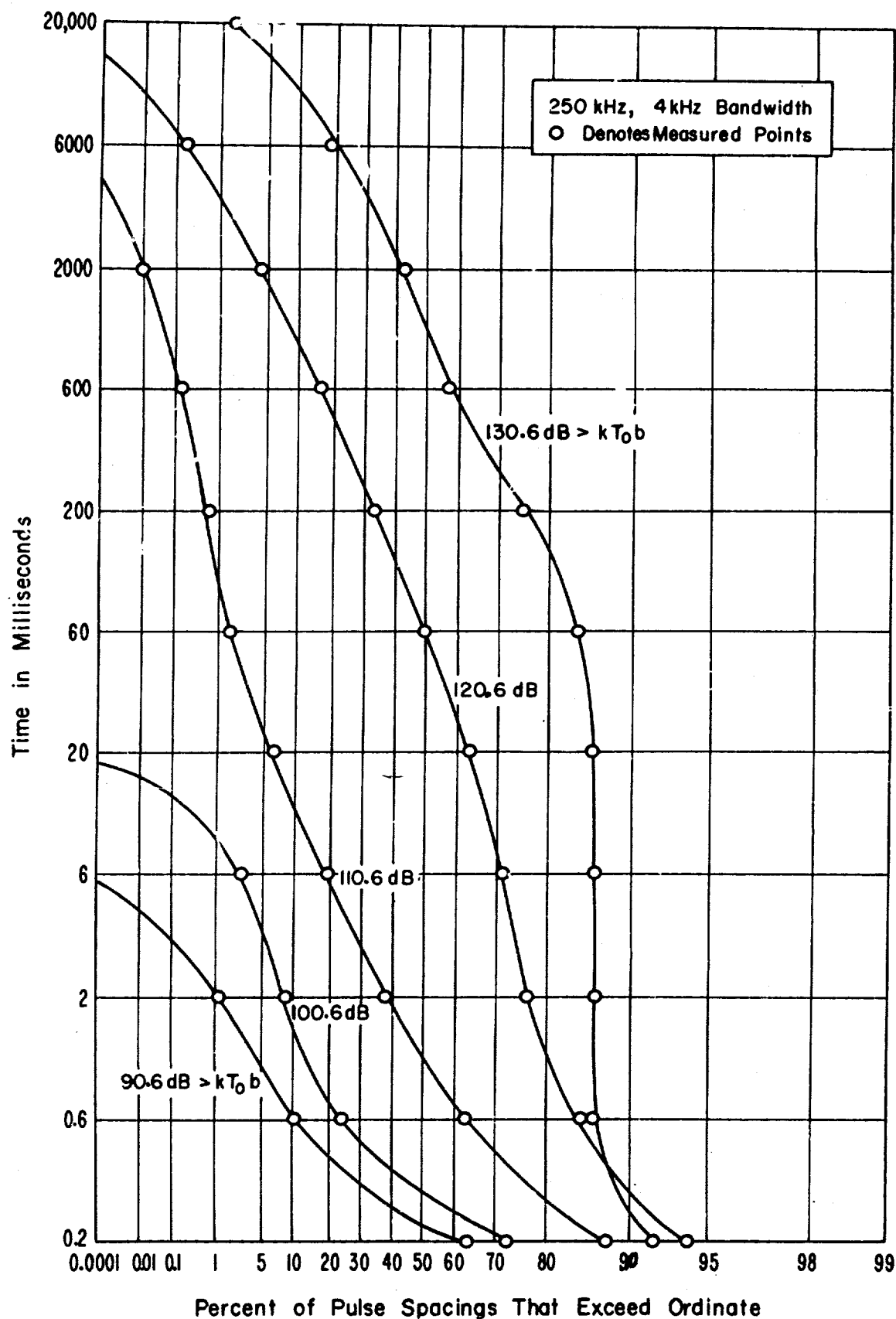
-41-

Figure 8. Average crossing rates of atmospheric radio noise recorded at Eggleston Reservoir No. 4, Boulder, Colorado. F = 500 kHz, B_i = 4 kHz, April 3, 1969, 0000-0400 hrs.

Figure 9. Amplitude probability distribution of atmospheric radio noise recorded at Eggleston Reservoir No. 4, Boulder, Colorado. $F = 250$ kHz, $B_i = 4$ kHz, April 5, 1969, 0000-0400 hrs.
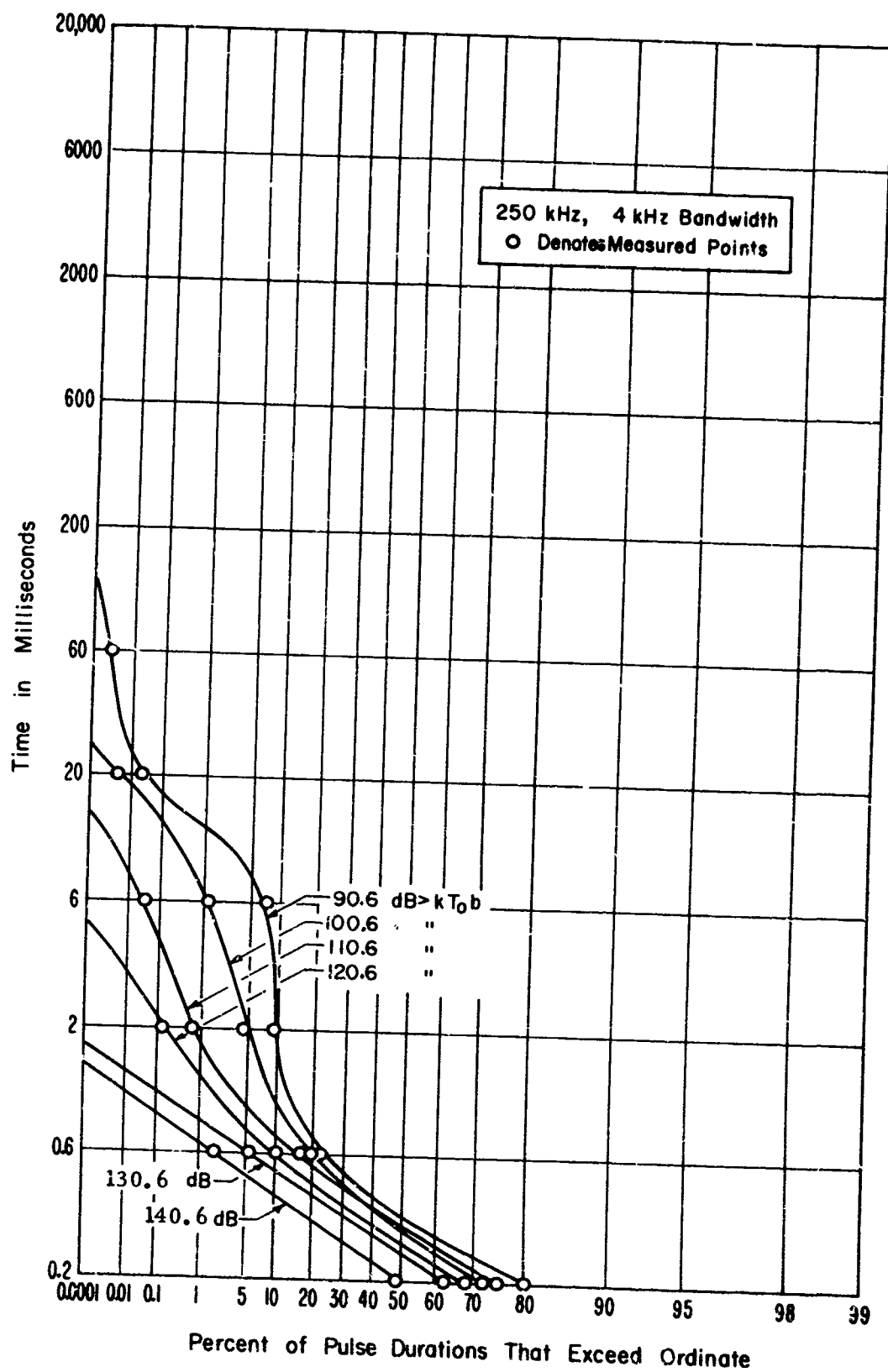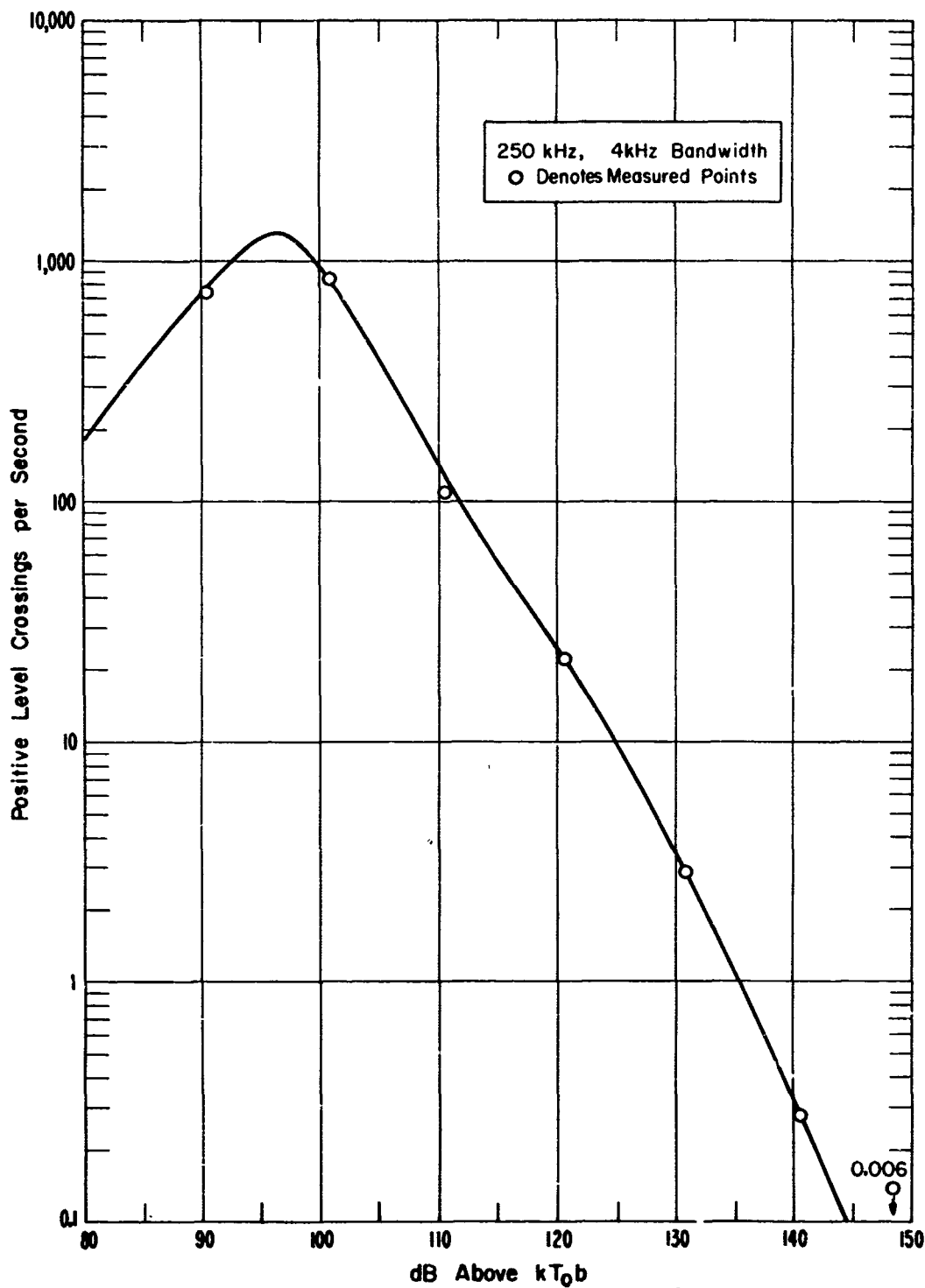
Figure 10. Pulse spacing distributions of atmospheric radio noise
recorded at Eggleston Reservoir No. 4, Boulder, Colorado.
F = 250 kHz, B$_i$ = 4 kHz, April 5, 1969, 0000-0400 hrs.

Figure 11. Pulse duration distributions of atmospheric radio noise recorded at Eggleston Reservoir No. 4, Boulder, Colorado.
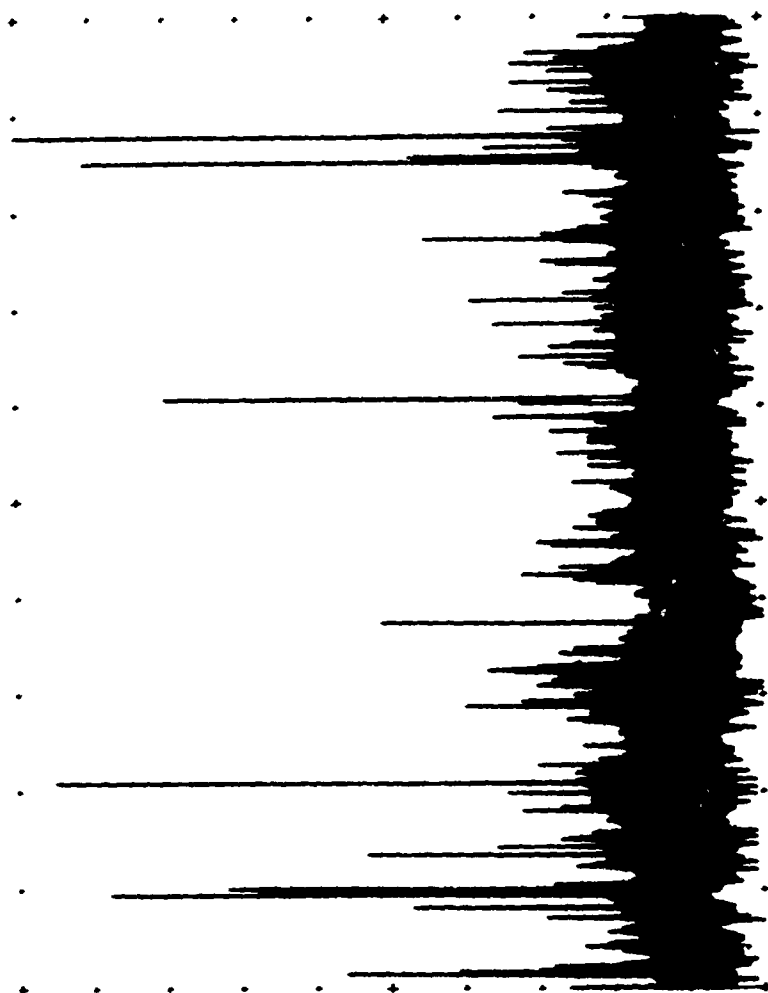F = 250 kHz, B_i = 4 kHz, April 5, 1969, 0000-0400 hrs.

Figure 12. Average crossing rates of atmospheric radio noise recorded at Eggleston Reservoir No. 4, Boulder, Colorado. F = 250 kHz, B_i = 4 kHz, April 5, 1969, 0000-0400 hrs.

03245201 INPUT DATA OF NOISE SAMPLE

	X – Min	Max	Y – Min	Max
Function	0.000+000	2.047+003	0.000+000	1.960+002
Graph	0.000+000	2.047+003	0.000+000	1.960+002

Run 17 Apr 1969 (107) at 12:20:56 L1,L2= 1, 1 2048 Points, Frame 16

d-c level = 25.1 mV

Figure 13. Digitized envelope amplitudes of atmospheric radio noise from recording at Eggleston Reservoir No. 4, Boulder, Colorado. $F = 500$ kHz, $B_i = 4$ kHz, April 3, 1969. Sample 1.

-47-
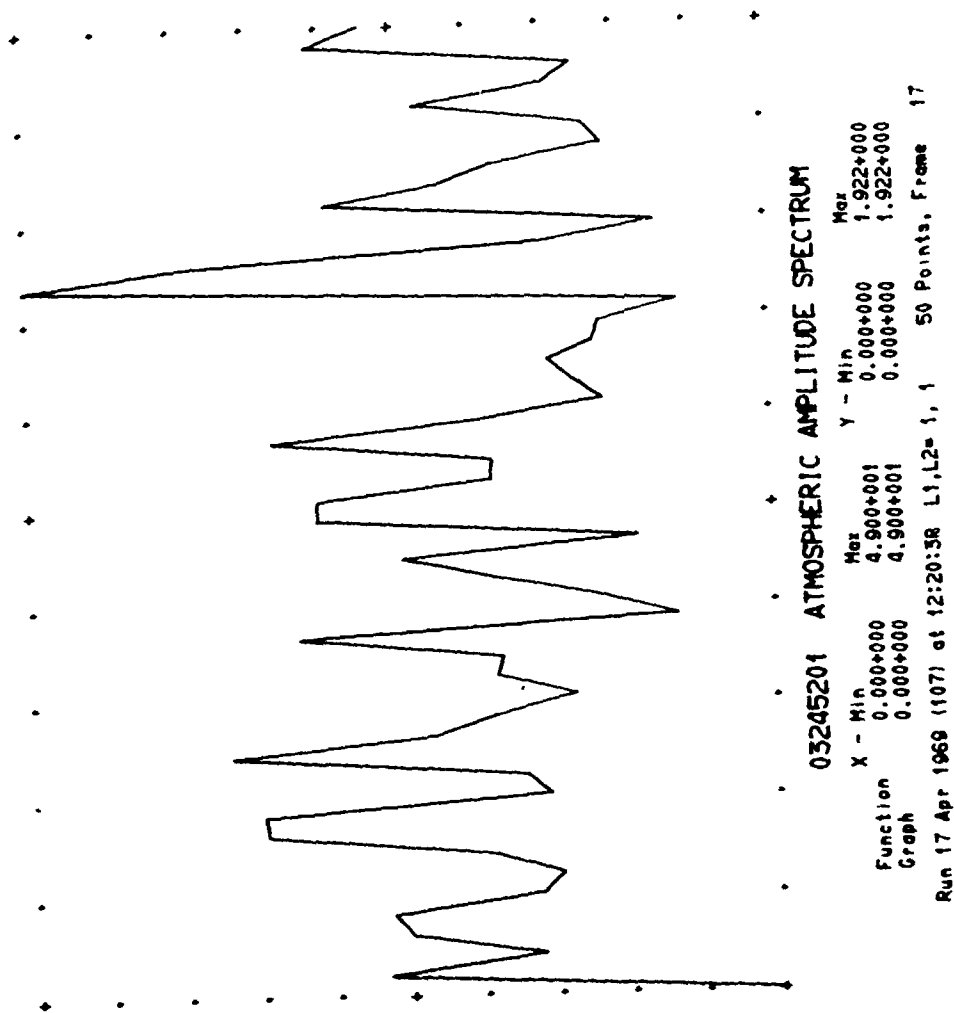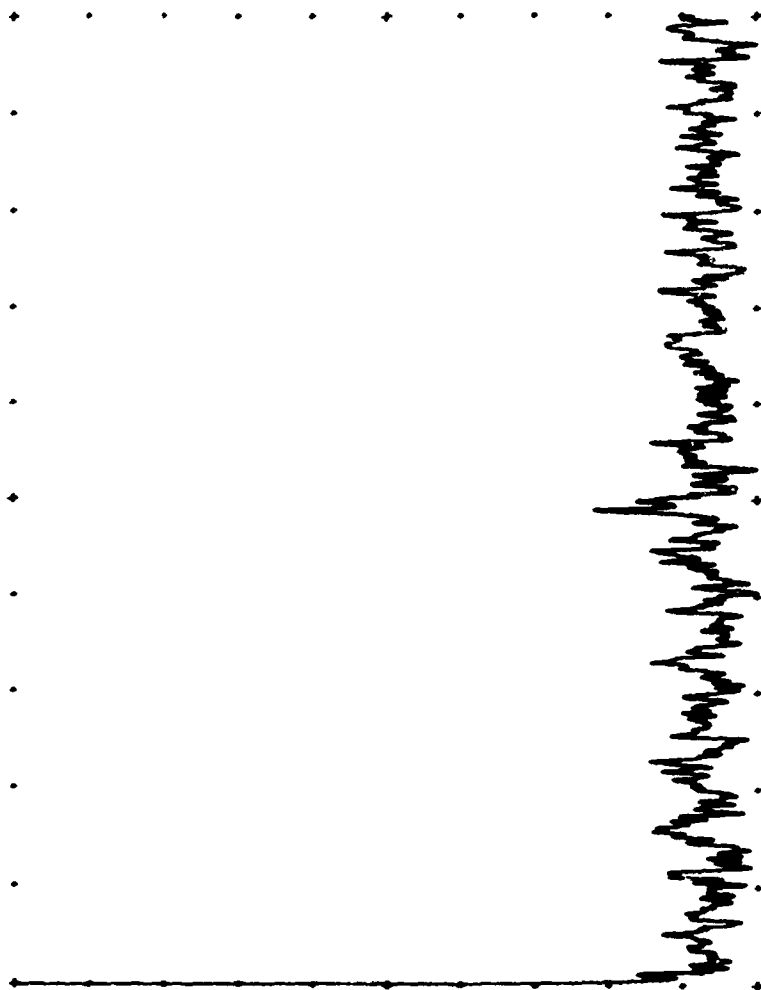
Figure 14. Spectrum of atmospheric radio noise from recording at Eggleston Reservoir No. 4, Boulder, Colorado. $F = 500$ kHz, $B_i = 4$ kHz, April 3, 1969, Sample 1.

-48-

Figure 15. Autocovariance of atmospheric radio noise from recording at Eggleston Reservoir No. 4, Boulder, Colorado. F = 500 kHz, B_1 = 4 kHz, April 3, 1969, Sample 1.
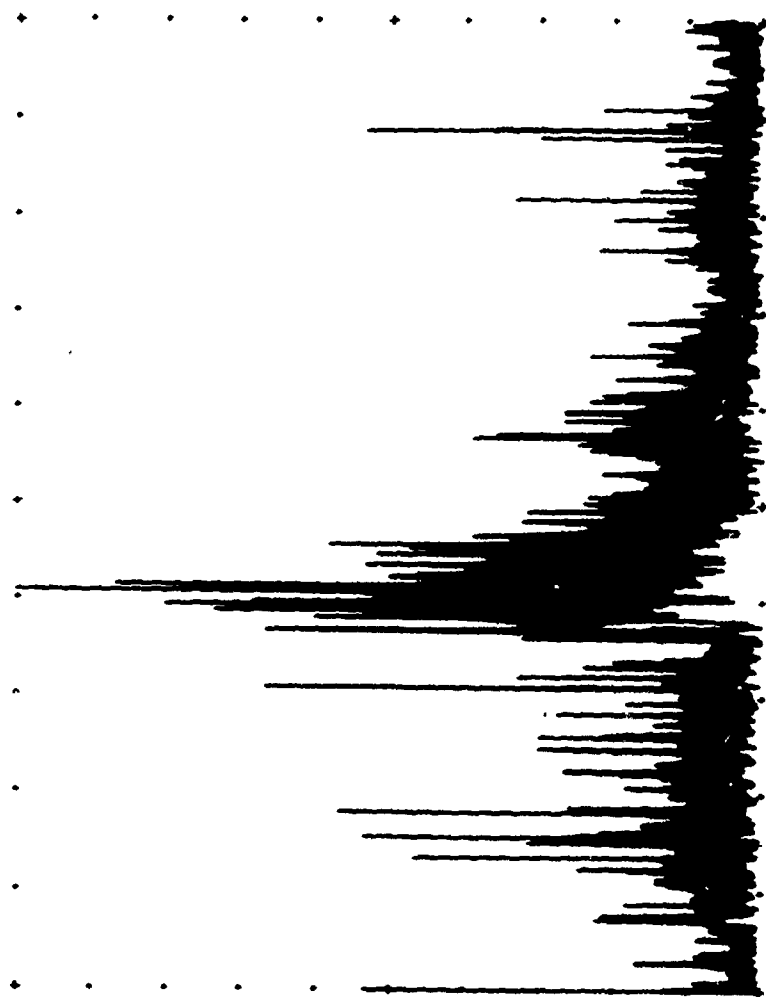
03245201 INPUT DATA OF NOISE SAMPLE

	X - Min	Max	Y - Min	Max
Function	0.000+000	2.047+003	0.000+000	9.370+002
Graph	0.000+000	2.047+003	0.000+000	9.370+002

Run 17 Apr 1969 (1107) at 12:20:02 L1,L2= 1, 1 2048 Points, Frame 15

d-c level = 81.9 mV

Figure 16. Digitized envelope amplitudes of atmospheric radio noise from recording at Eggleston Reservoir No. 4, Boulder, Colorado. F = 500 kHz, B_i = 4 kHz, April 3, 1969, Sample 2.

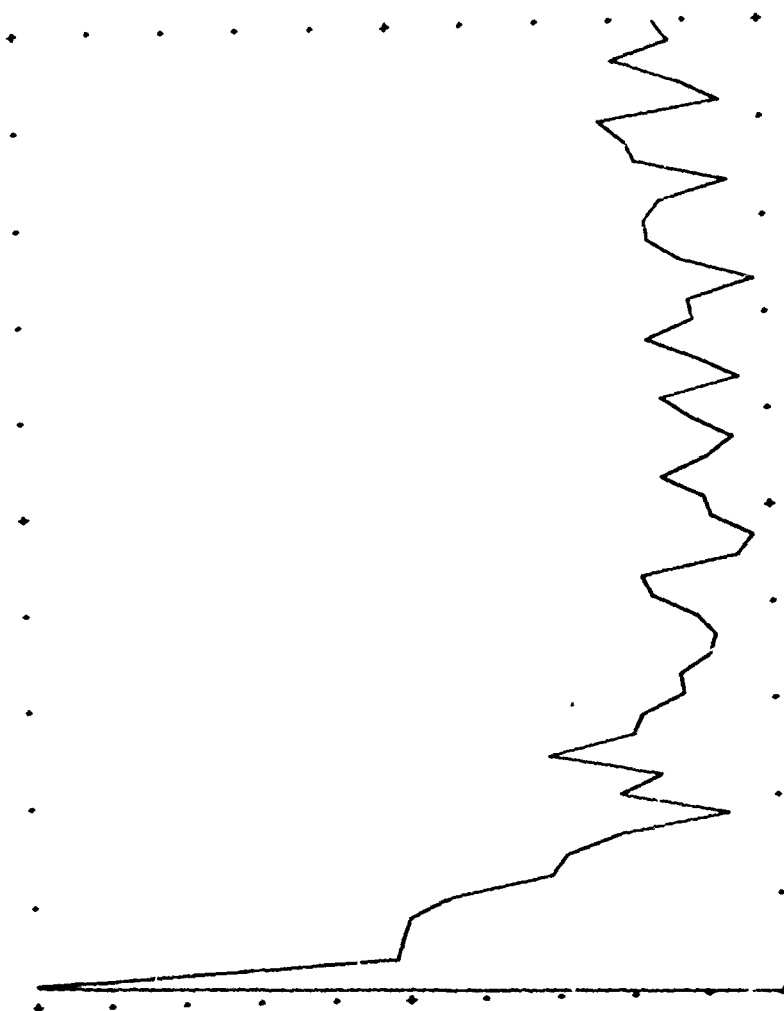-50-

03245201 ATMOSPHERIC AMPLITUDE SPECTRUM

	X - Min	Max	Y - Min	Max
Function	0.000+000	4.900+001	0.000+000	2.818+001
Graph	0.000+000	4.900+001	0.000+000	2.818+001

Run 17 Apr 1969 (107) at 12:20:04 L1,L2= 1, 1   50 Points, Frame 14

Figure 17. Spectrum of atmospheric radio noise from recording at
Eggleston Reservoir No. 4, Boulder, Colorado.
$F = 500$ kHz, $B = 4$ kHz, April 3, 1969, Sample 2.

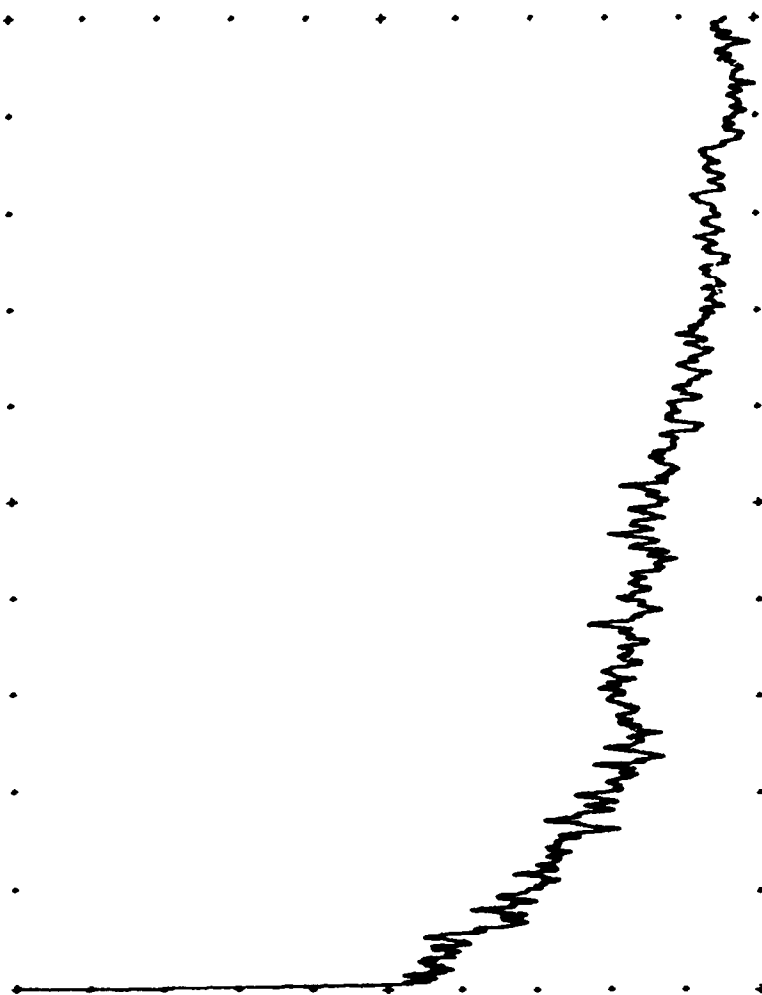03245201 AUTOCOVARIANCE OF ATMOSPHERICS

	X - Min	Max	Y - Min	Max
Function	0.000+000	1.023+003	-1.761+003	9.801+005
Graph	0.000+000	1.023+003	-1.761+003	9.801+005

Run 17 Apr 1969 (1107) at 12:20:05 L1,L2= 1, 1 1024 Points, Frame 15

Figure 18. Autocovariance of atmospheric radio noise from recording at Eggleston Reservoir No. 4, Boulder, Colorado. F = 500 kHz, B_1 = 4 kHz, April 3, 1969, Sample 2.

05575701 INPUT DATA OF NOISE SAMPLE
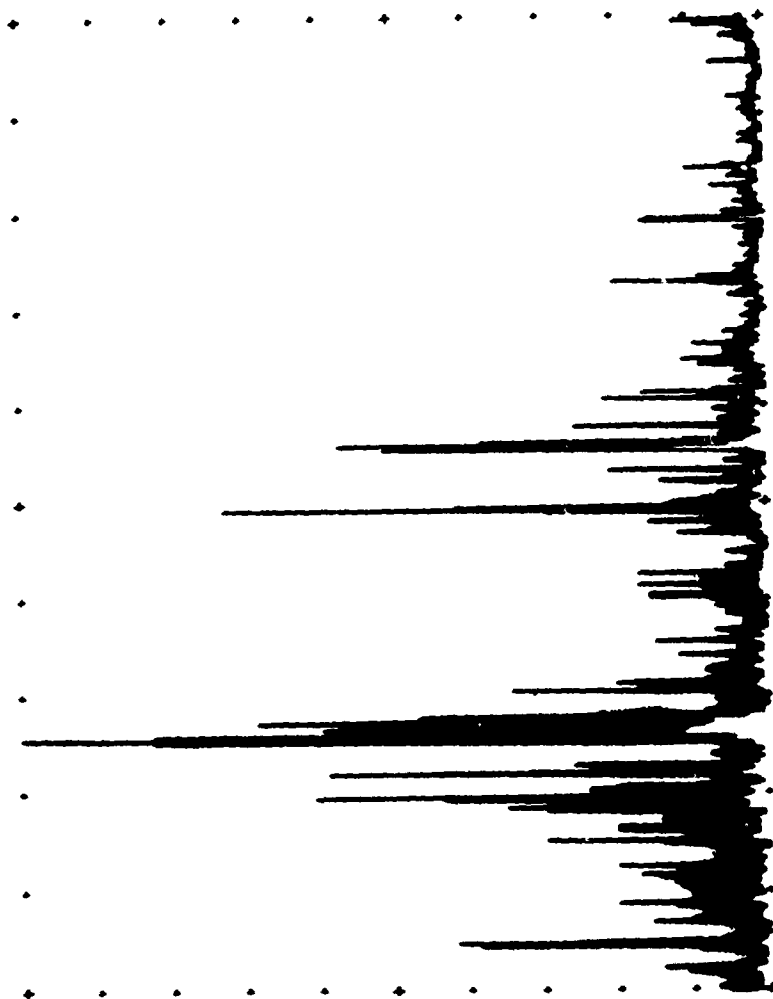
Function	X - Min	Max	Y - Min	Max
Graph	0.000+000	2.047+003	0.000+000	2.640+002
	0.000+000	2.047+003	0.000+000	2.640+002

Run 17 Apr 1969 (1107) at 11:21:07 L1,L2= 1, 1   2048 Points, Frame 7

d-c level = 14.1 mV

Figure 19. Digitized envelope amplitude of atmospheric radio noise from recording at Eggleston Reservoir No. 4, Boulder, Colorado. $F = 500$ kHz, $B_i = 4$ kHz, April 4, 1969.
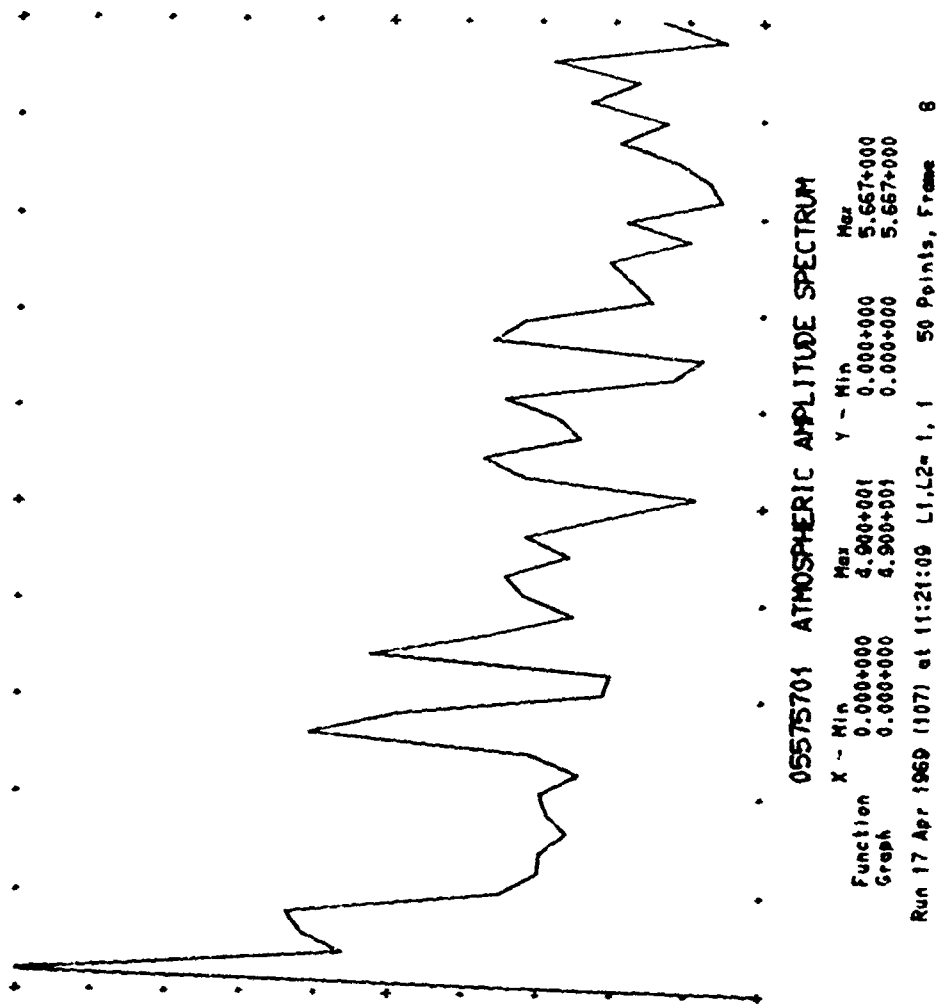
Figure 20. Spectrum of atmospheric radio noise from recording at Eggleston Reservoir No. 4, Boulder, Colorado. $F = 500$ kHz, $B_i = 4$ kHz, April 4, 1969.

Figure 21. Autocovariance of atmospheric radio noise from recording at Eggleston Reservoir No. 4, Boulder, Colorado. $F = 500$ kHz, $B_i = 4$ kHz, April 4, 1969.

Figure 22. Digitized envelope amplitude of atmospheric radio noise from recording at Eggleston Reservoir No. 4, Boulder, Colorado. $F = 2.5$ MHz, $B_i = 4$ kHz, April 4, 1969.

05245801 ATMOSPHERIC AMPLITUDE SPECTRUM

	X - Min	Max	Y - Min	Max
Function	0.000+000	4.900+001	0.000+000	9.870+000
Graph	0.000+000	4.900+001	0.000+000	9.870+000

Run 17 Apr 1969 (107) at 11:23:02 L1,L2= 1, 1   50 Points, Frame 17

Figure 23. Spectrum of atmospheric radio noise from recording at
Eggleston Reservoir No. 4, Boulder, Colorado.
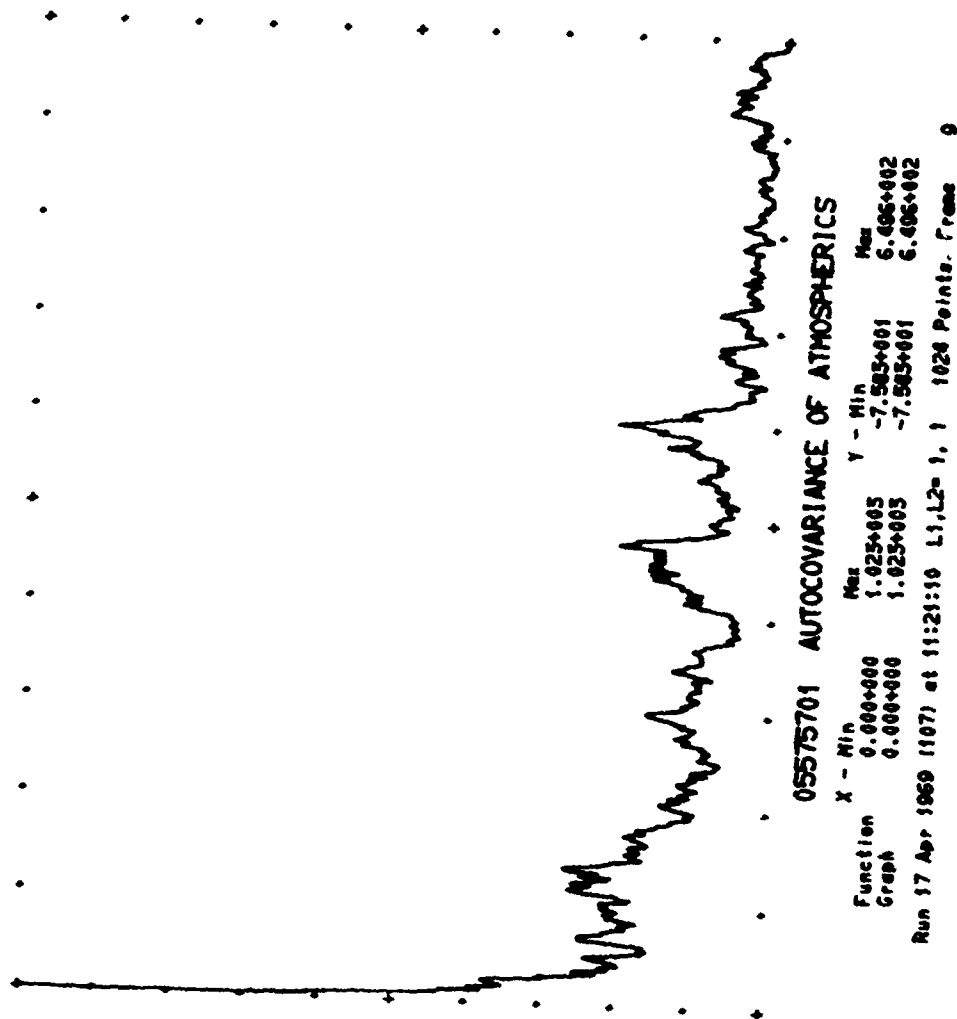F = 2.5 MHz, B_i = 4 kHz, April 4, 1969.

-57-
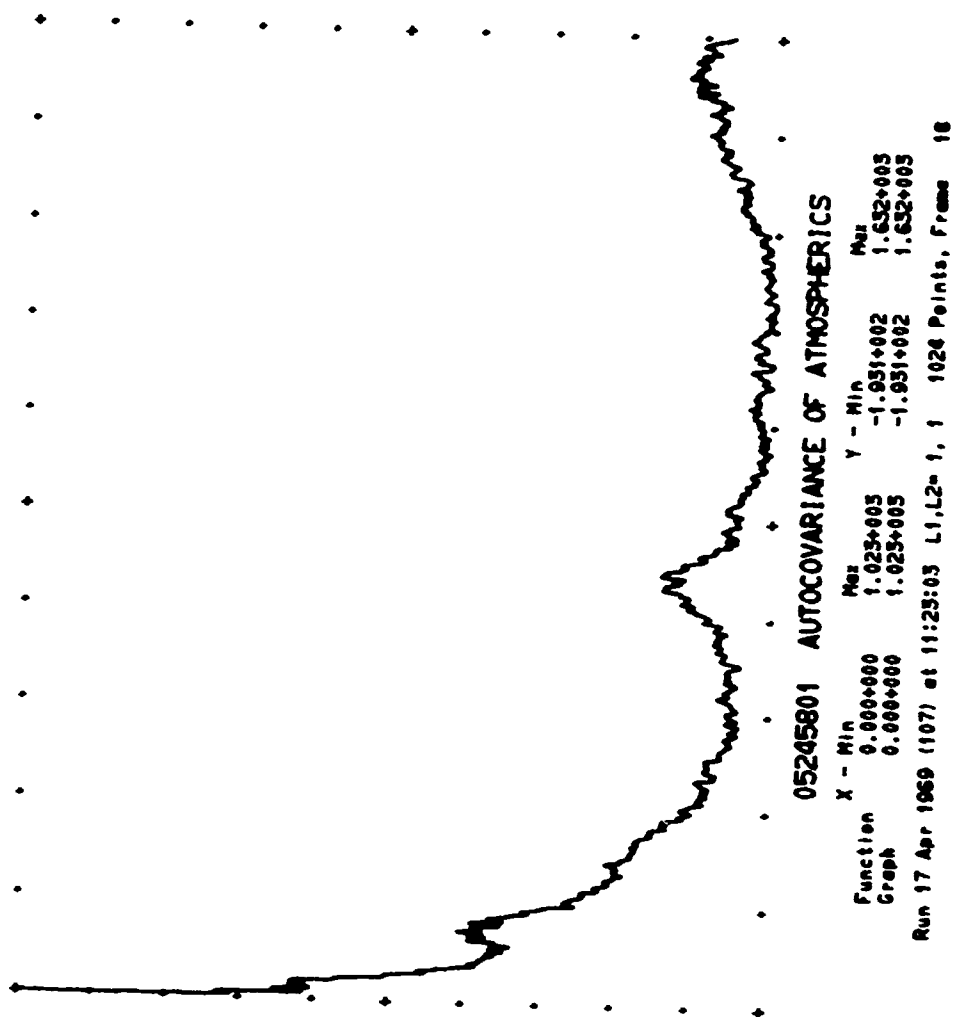
Figure 24. Autocovariance of atmospheric radio noise from recording at Eggleston Reservoir No. 4, Boulder, Colorado. $F = 2.5$ MHz, $B_i = 4$ kHz, April 4, 1969.
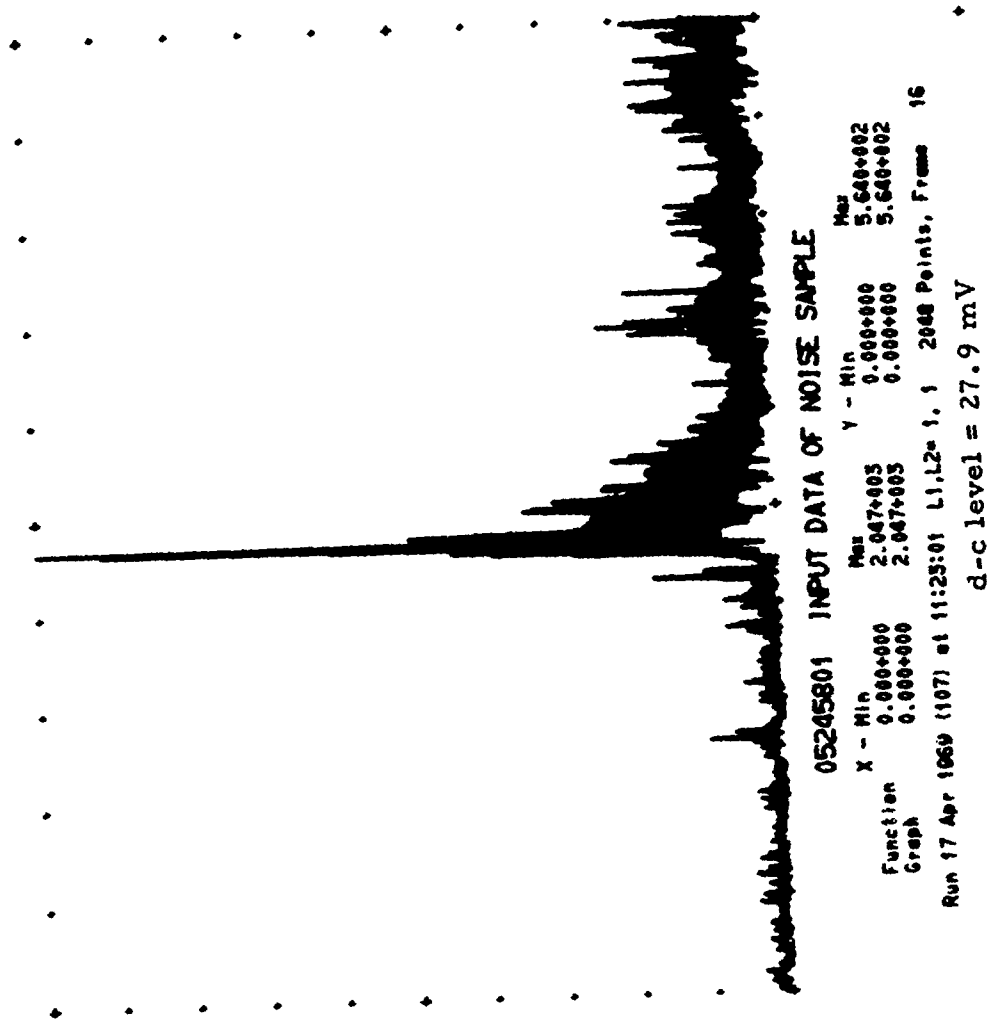
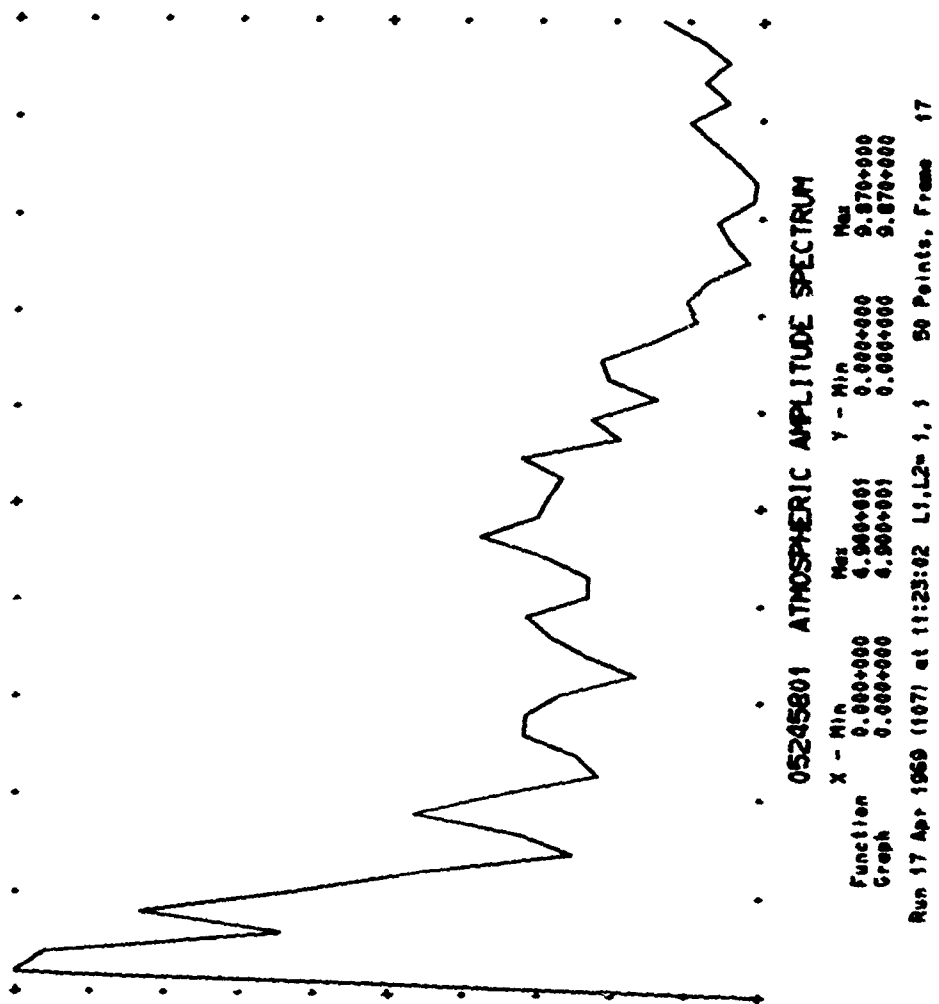Figure 25. Comparison of measured amplitude probability distribution with that calculated from the Hall model.

Figure 26. Comparison of measured average crossing rates with those calculated from the Hall model.

-60-
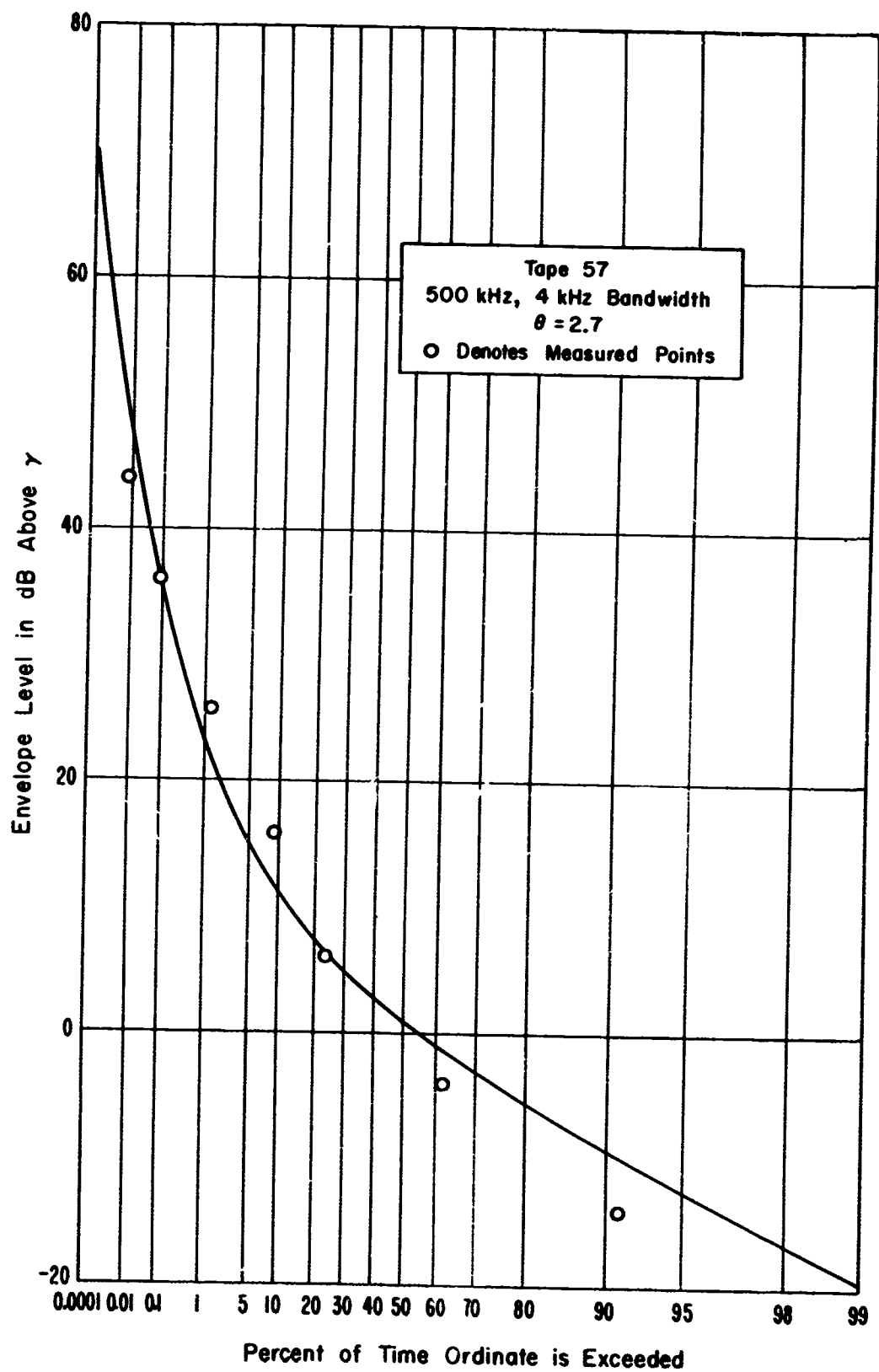
Figure 27. Comparison of measured amplitude probability distribution with that calculated from the Hall model.

-61-
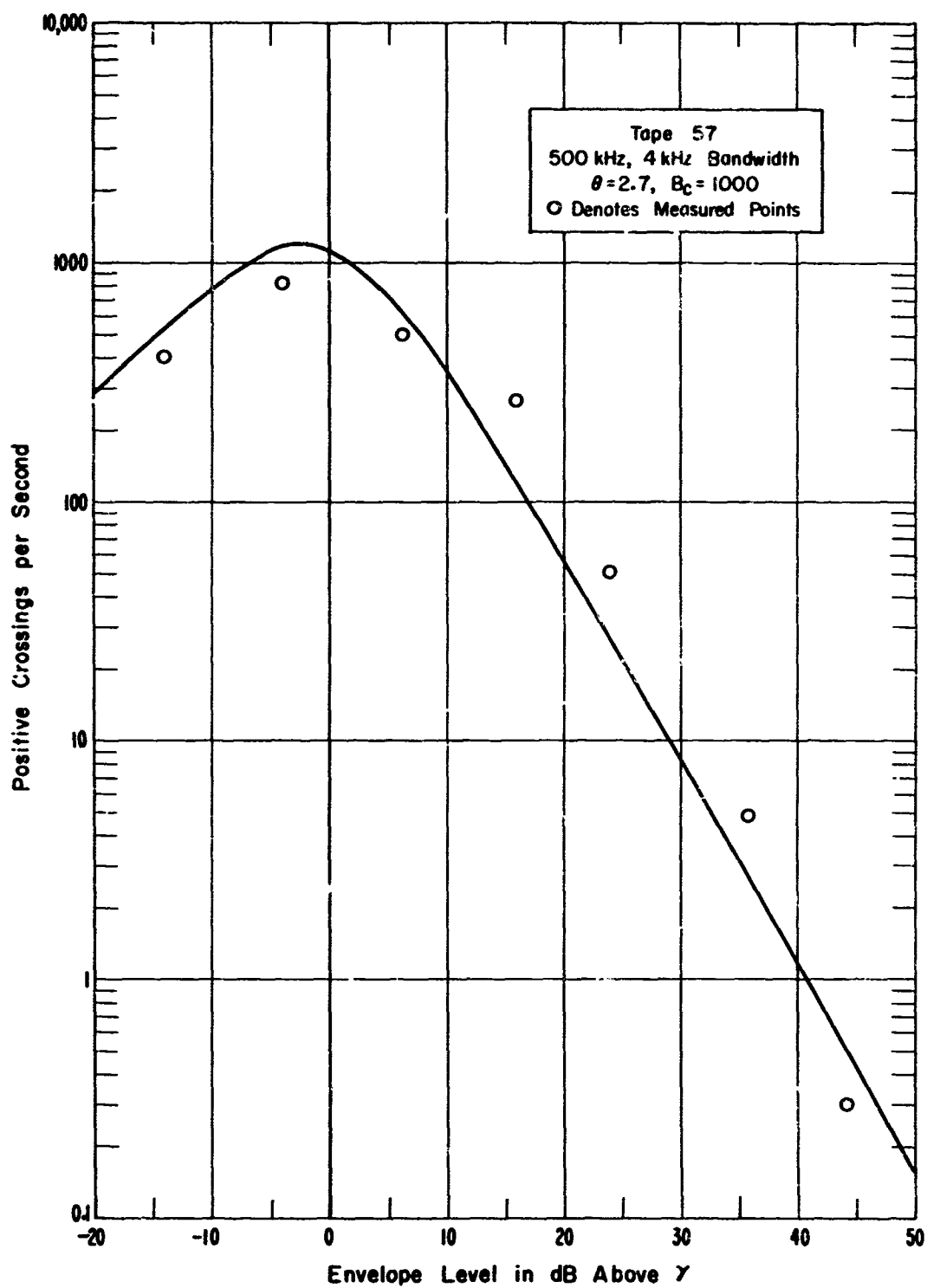
Figure 28. Comparison of measured average crossing rates with those
calculated from the Hall model.
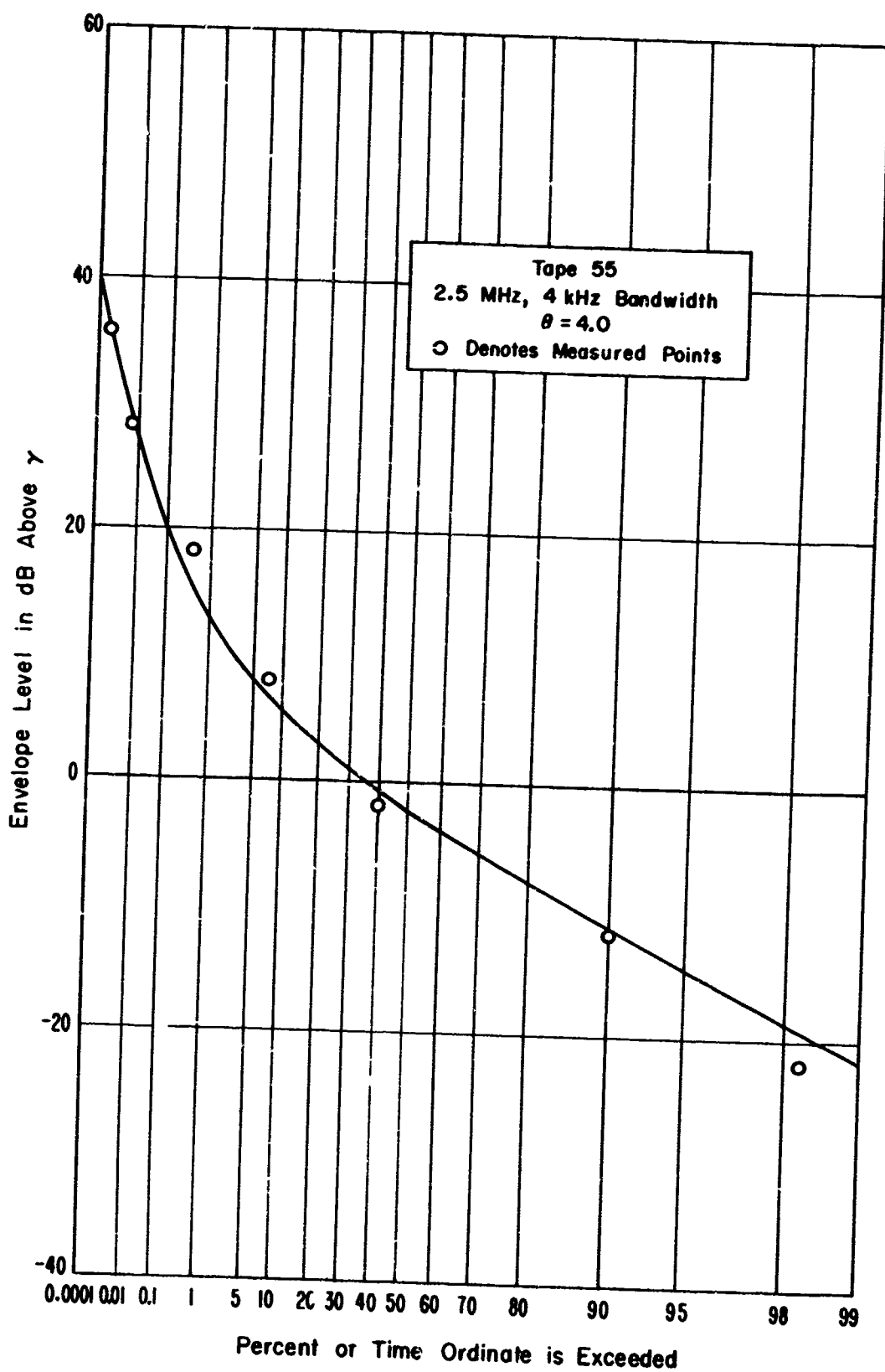
Figure 29. Comparison of measured amplitude probability distribution with that calculated from the Hall model.

-63-
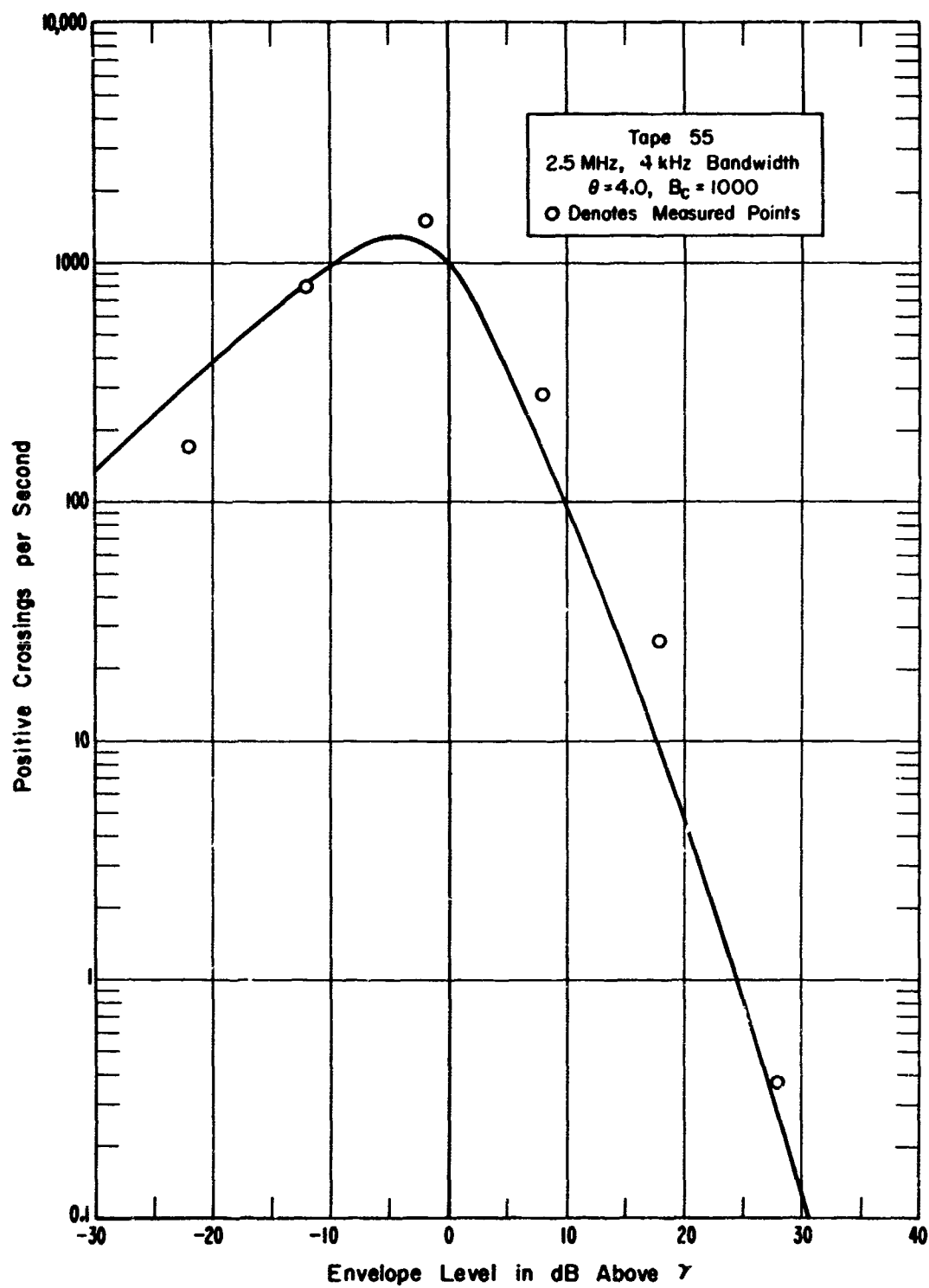
Figure 30. Comparison of measured average crossing rates with those calculated from the Hall model.
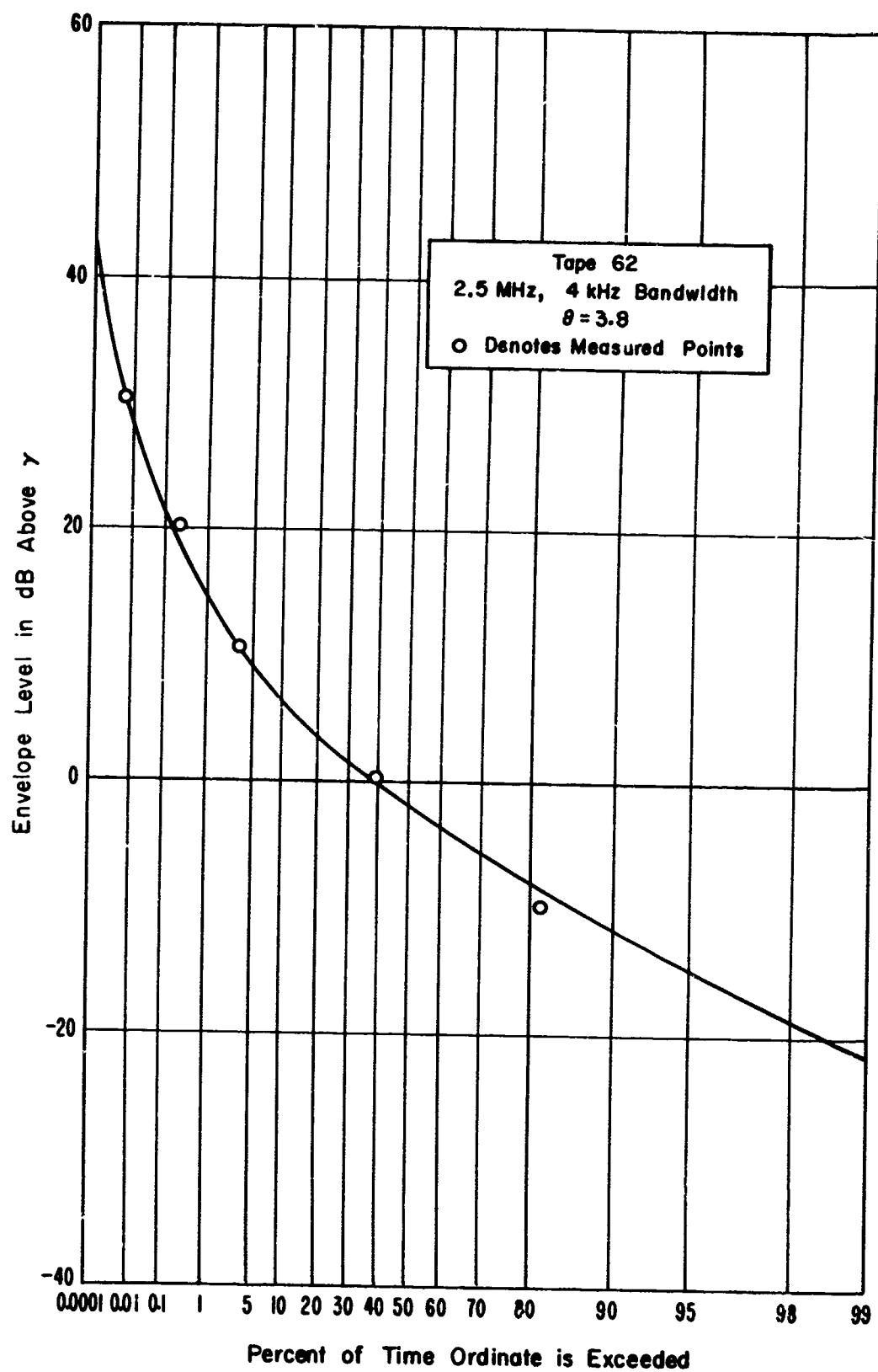
Figure 31. Comparison of measured amplitude probability distribution with that calculated from the Hall model.
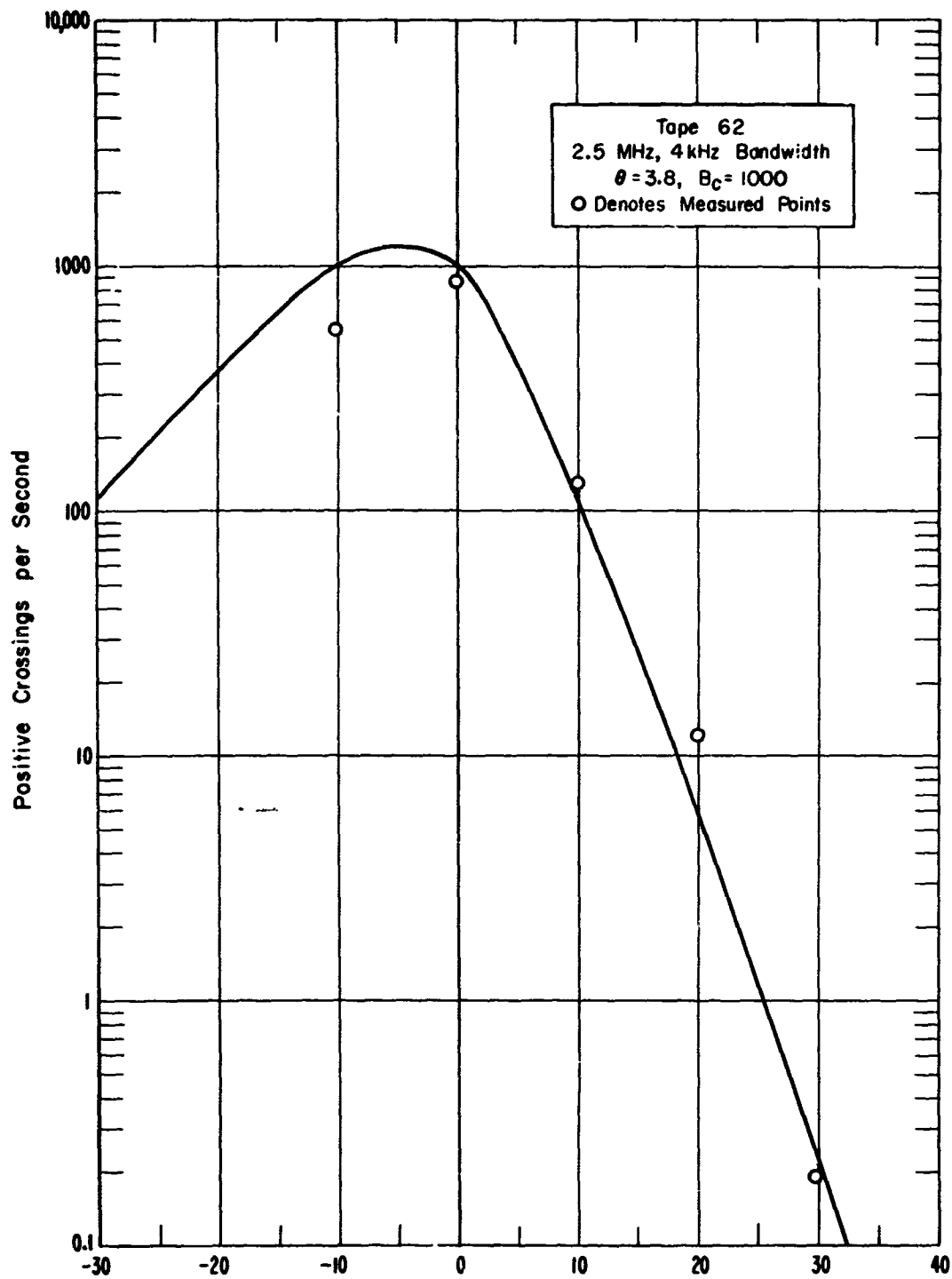
Figure 32. Comparison of measured average crossing rates with those calculated from the Hall model.
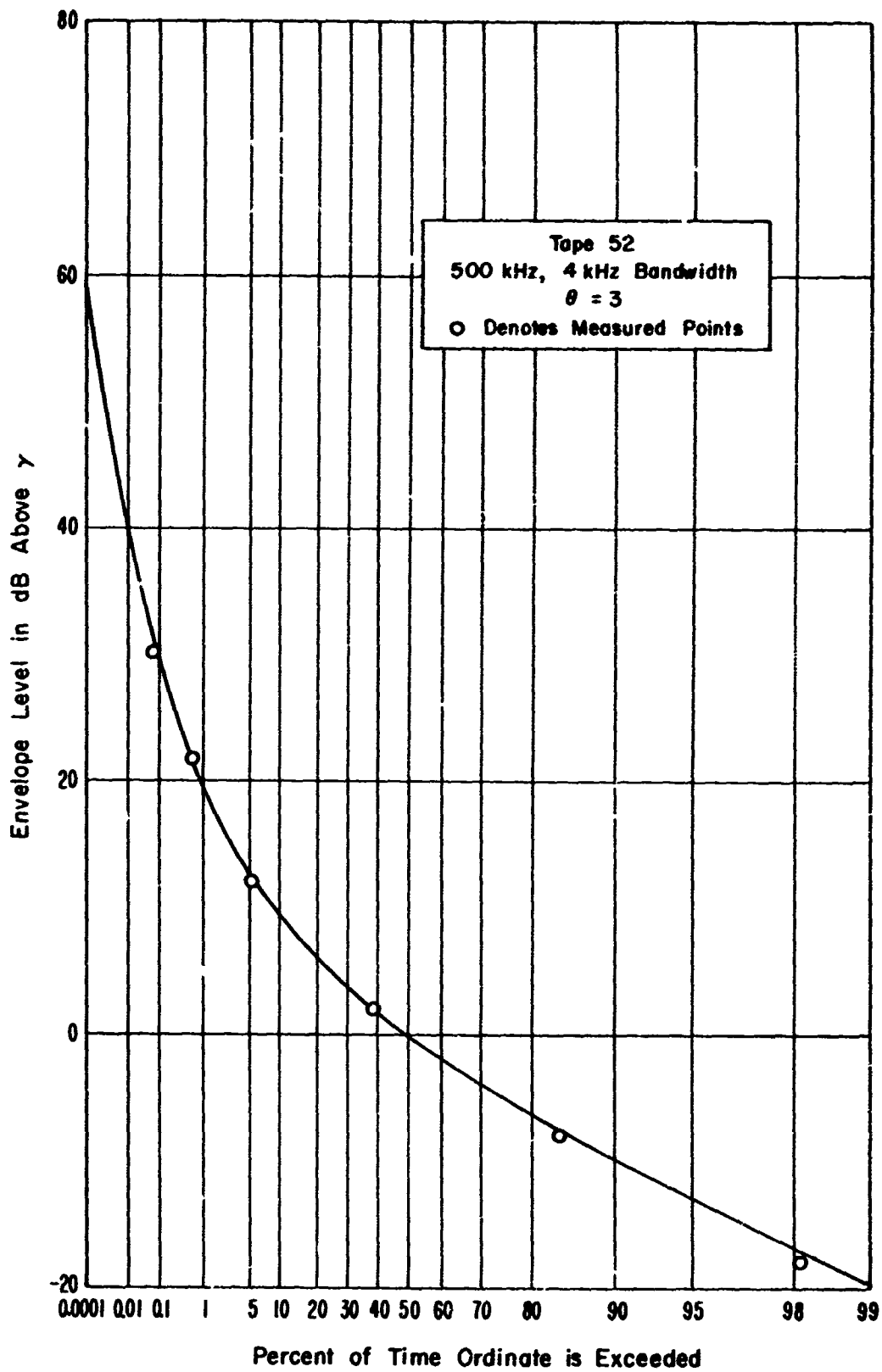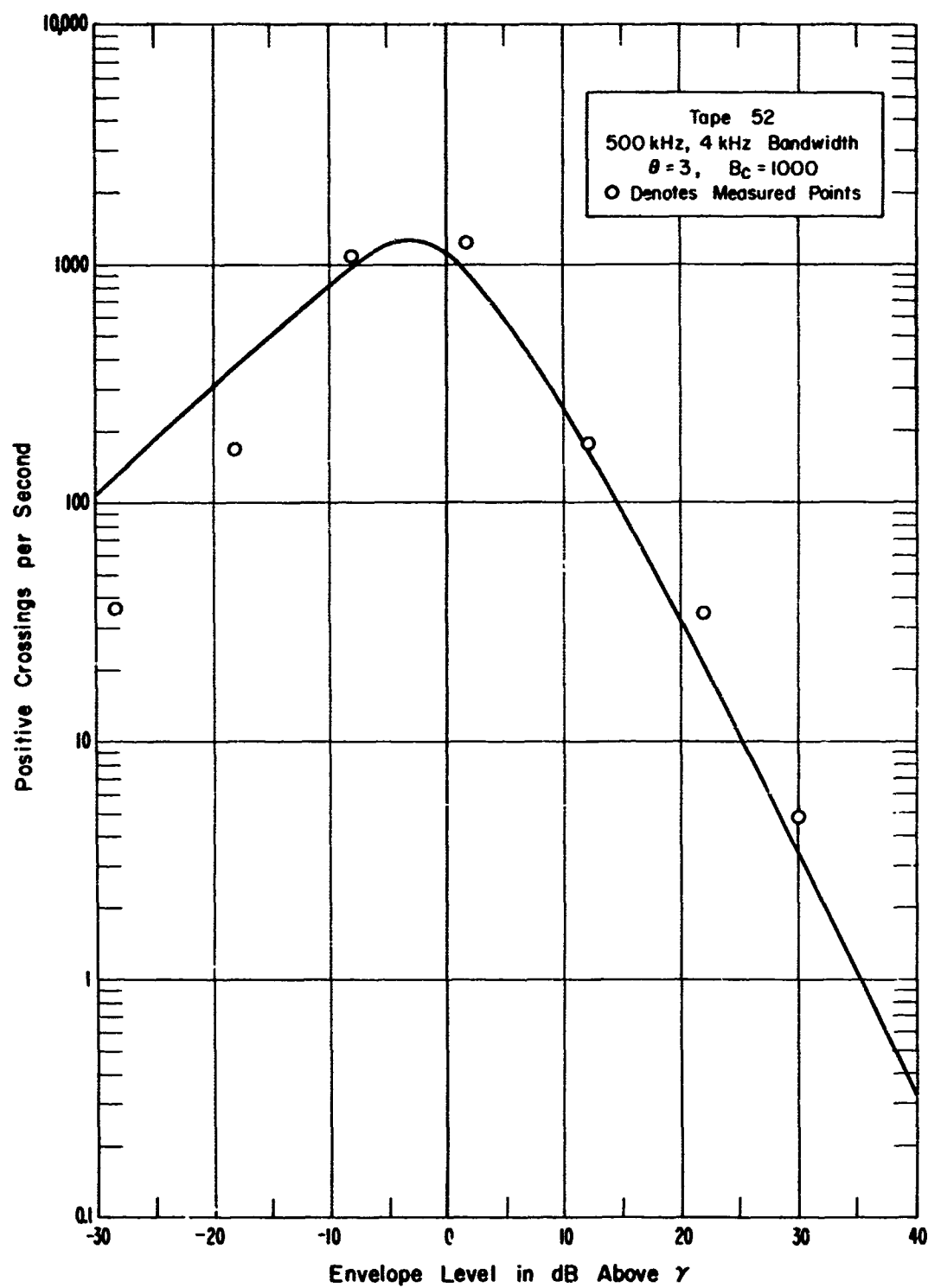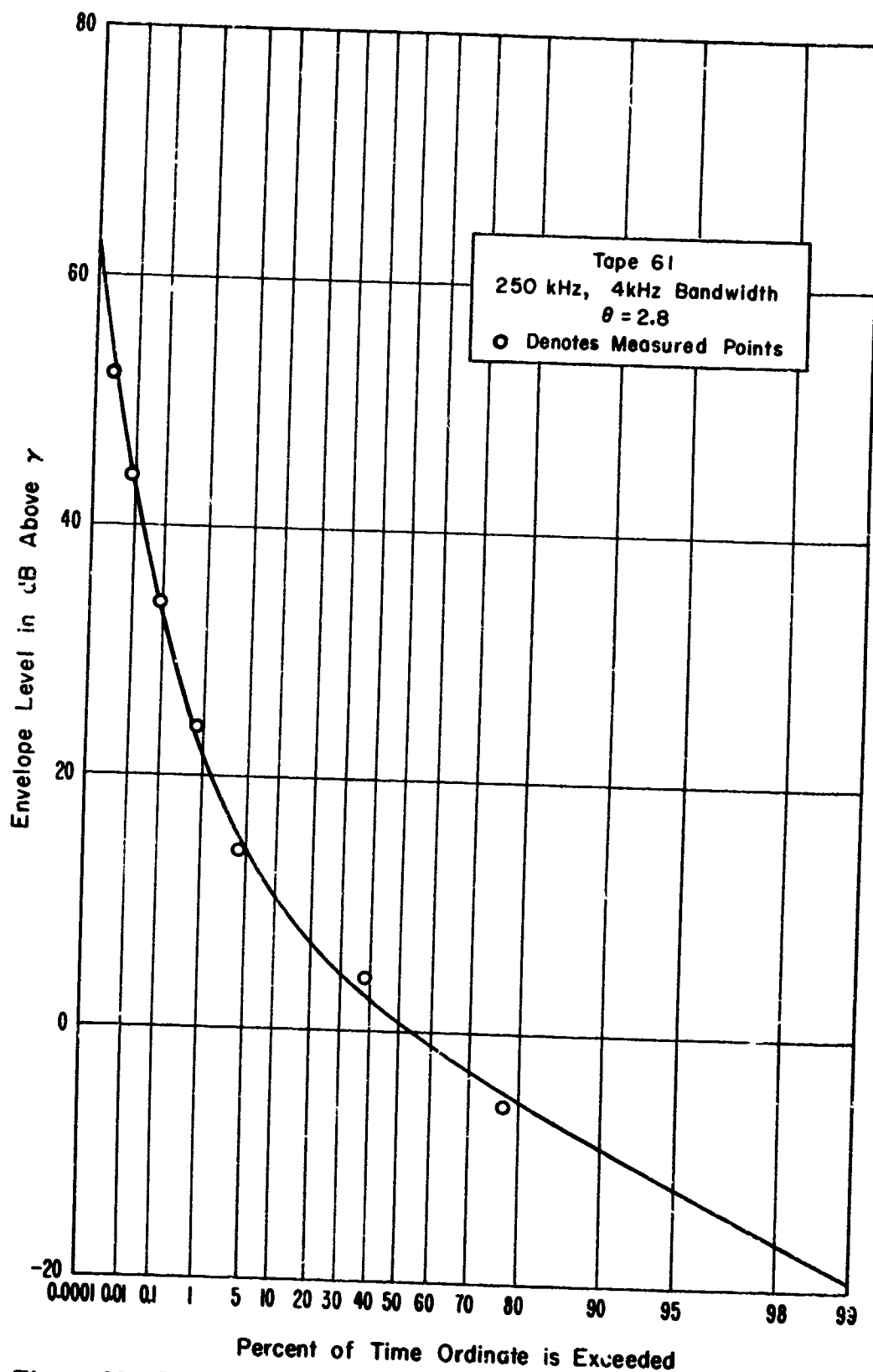
Figure 33. Comparison of measured amplitude probability distribution with that calculated from the Hall model.
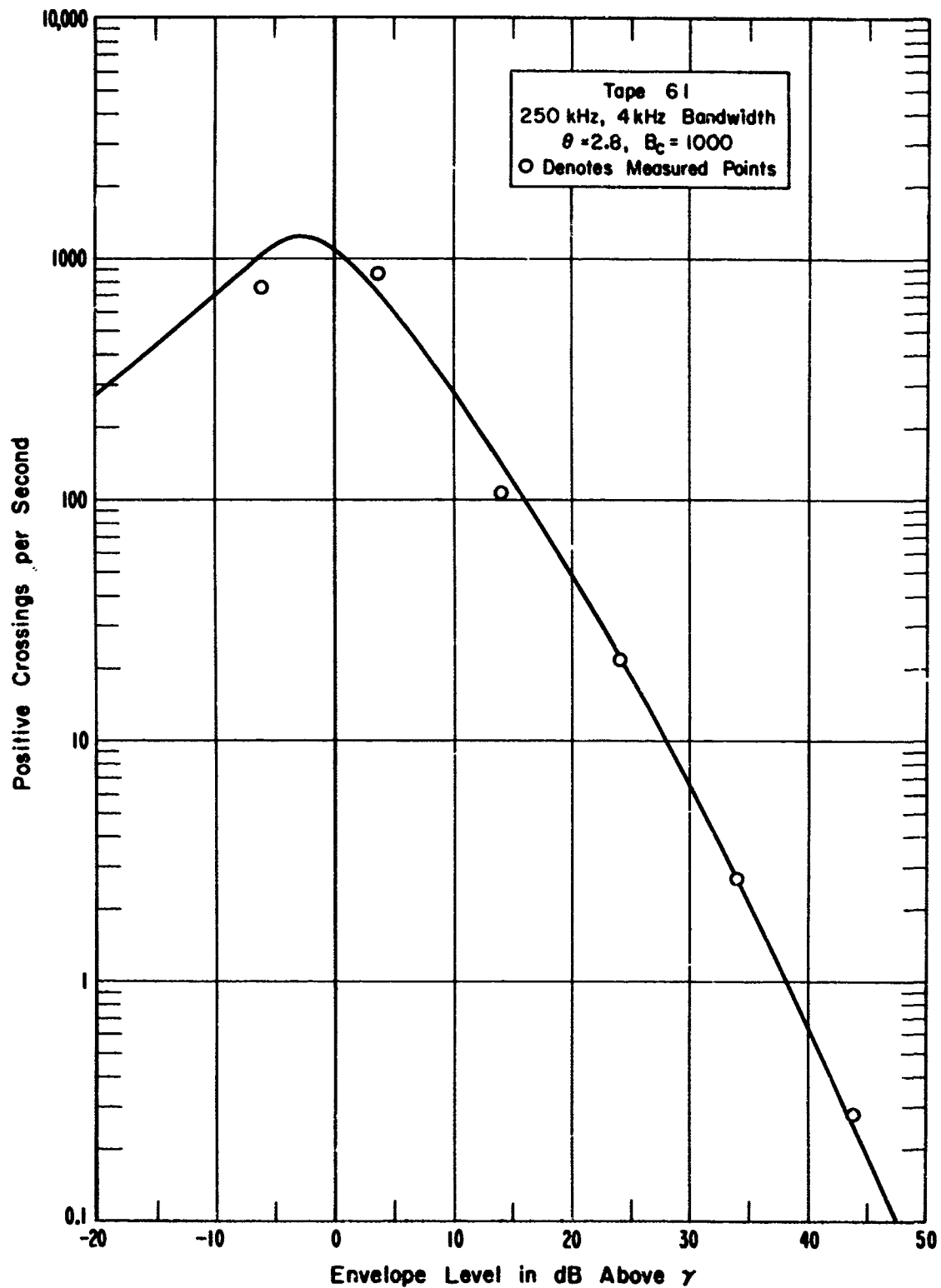
Figure 34. Comparison of measured average crossing rates with those calculated from the Hall model.

-68-
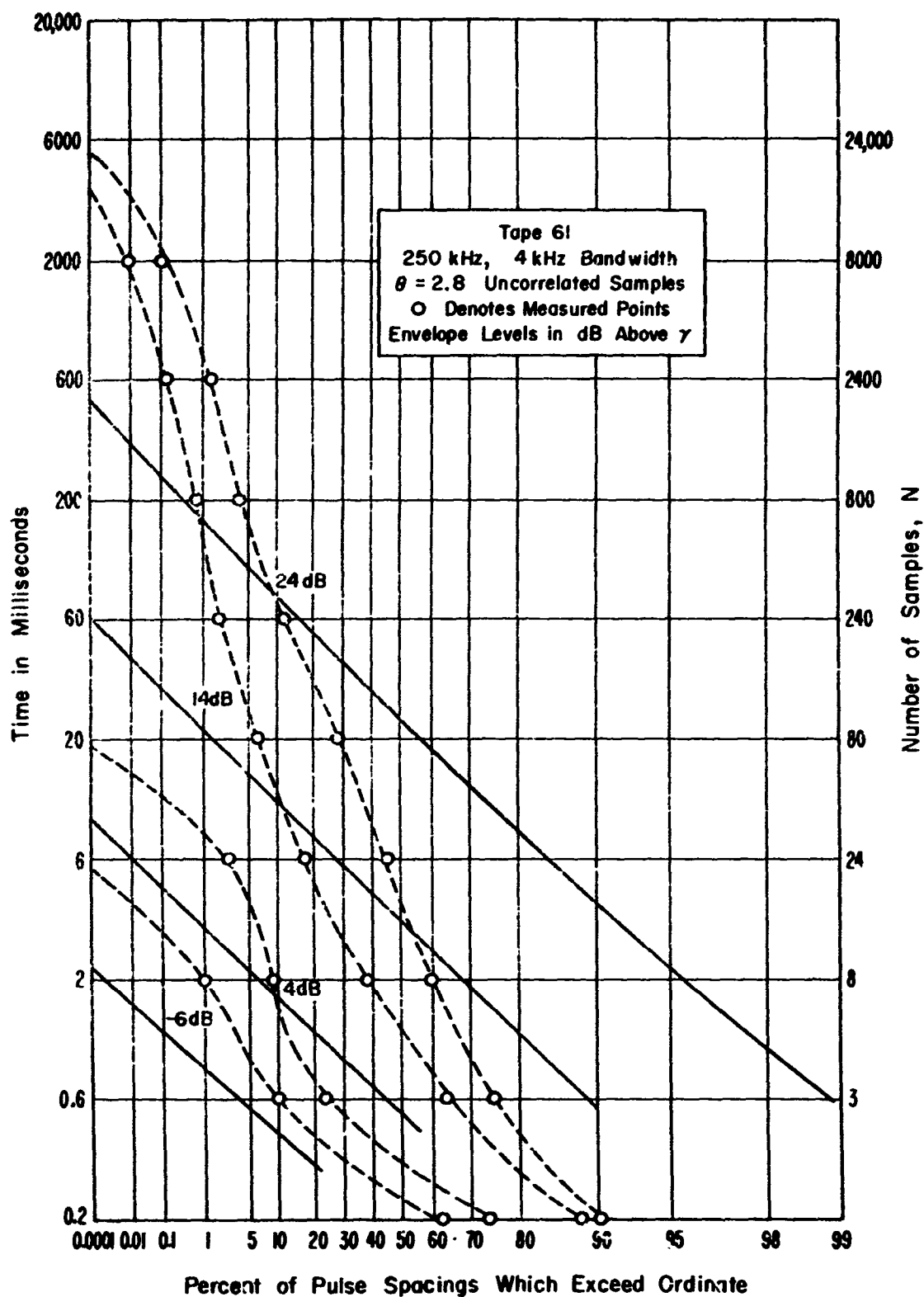
Figure 35.   Comparison of measured pulse spacing distributions with
distributions calculated from the Hall model (no correlation assumed).
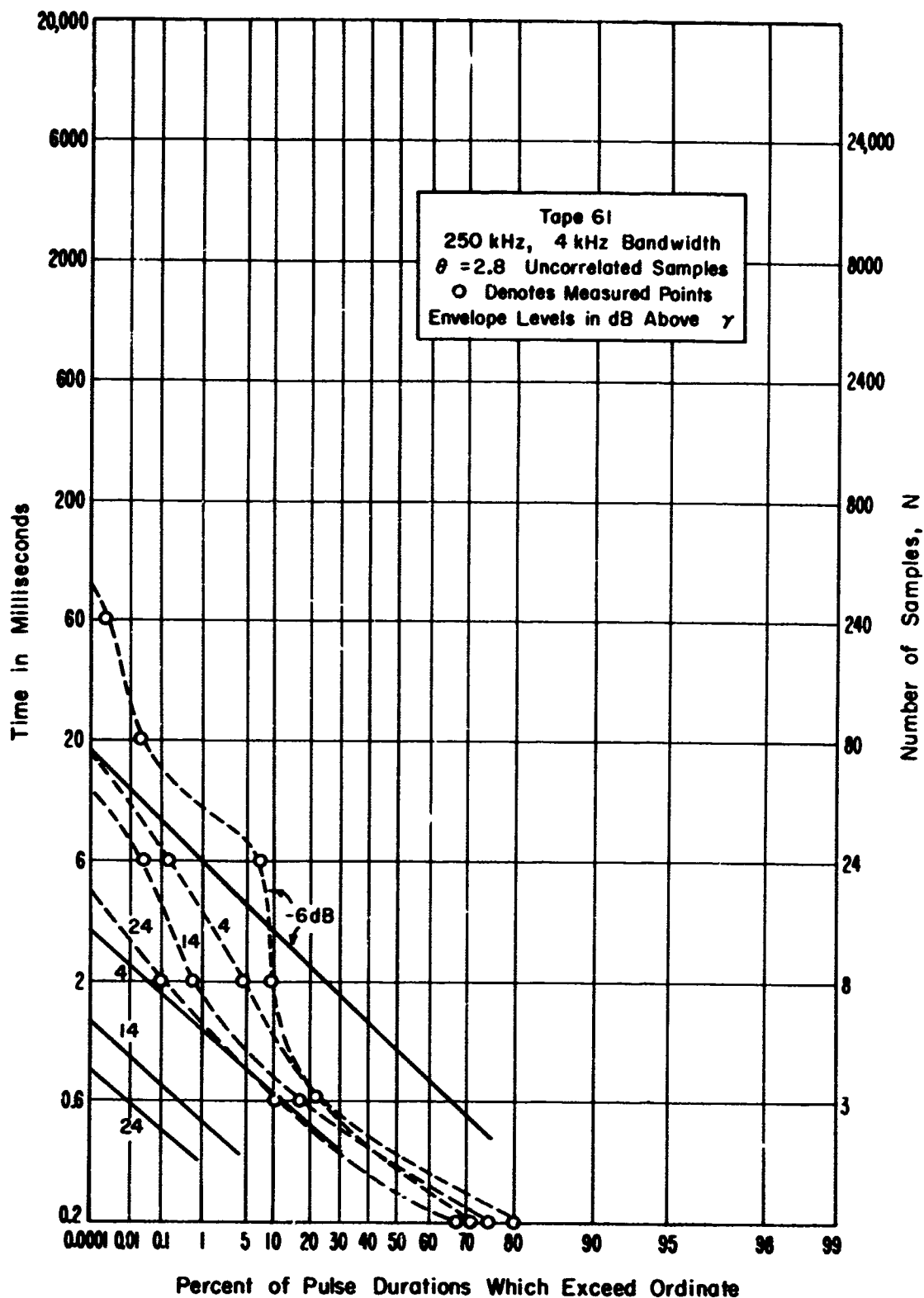
Figure 36. Comparison of measured pulse durations with distributions calculated from the Hall model (no correlation assumed).

-70-
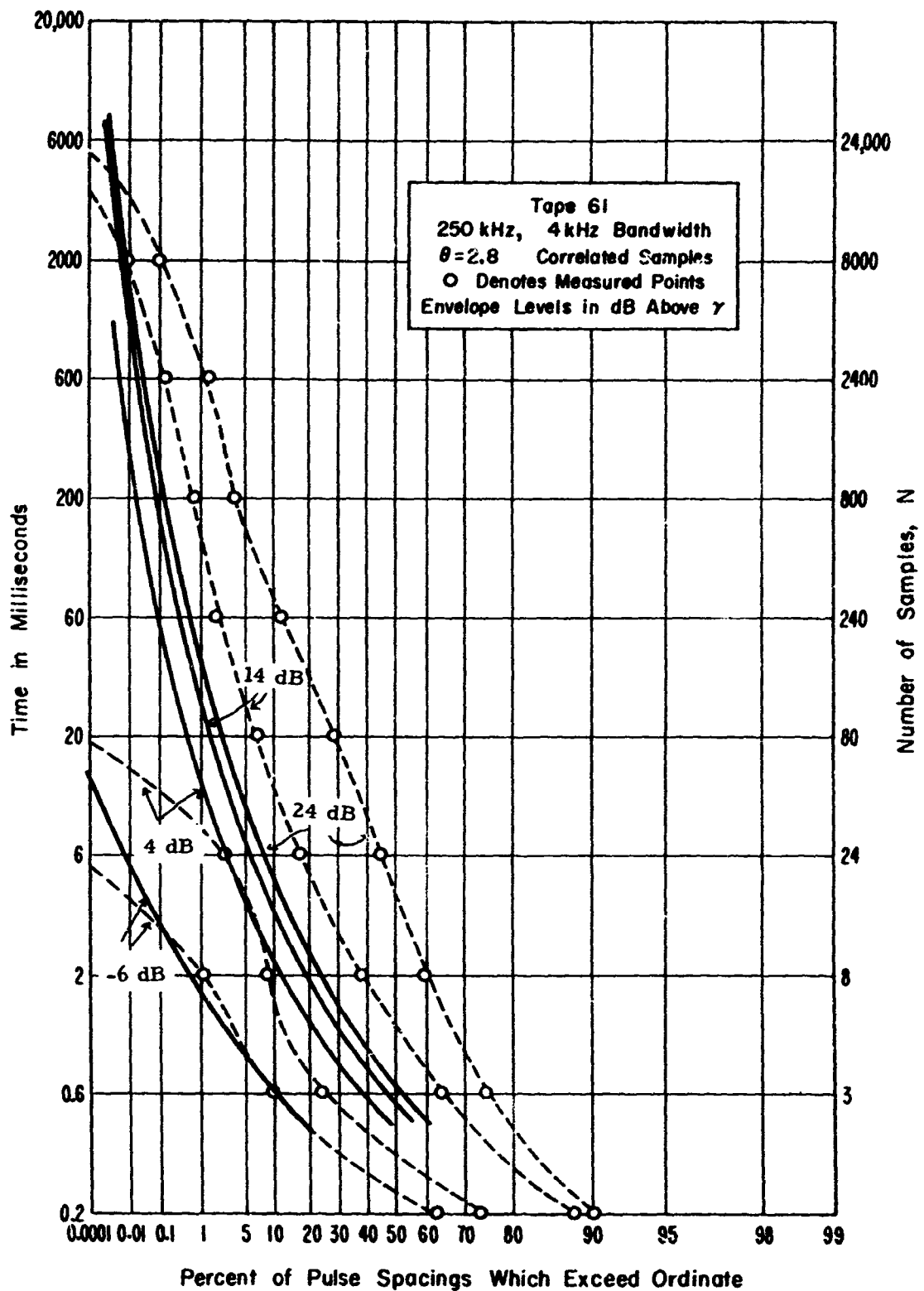
Figure 37.   Comparison of measured pulse spacing distribution with distributions calculated from the Hall model (some correlation assumed).
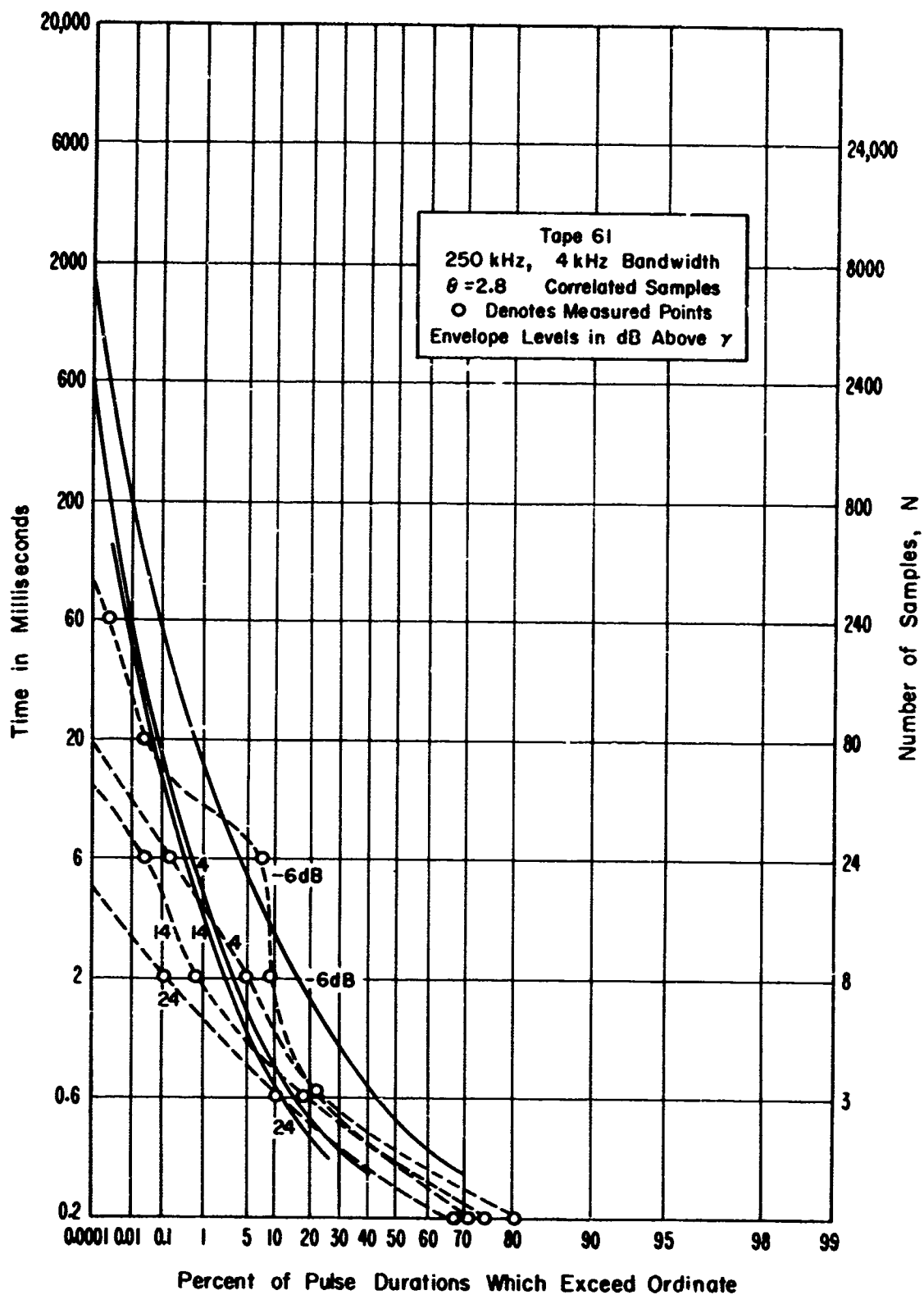
Figure 38. Comparison of measured pulse durations with distributions calculated from the Hall model (some correlation assumed).

Figure 39.   Comparison of measured amplitude probability distribution and
distribution calculated from the Hall model for m = 1.0 (V_d = 26.0 dB).
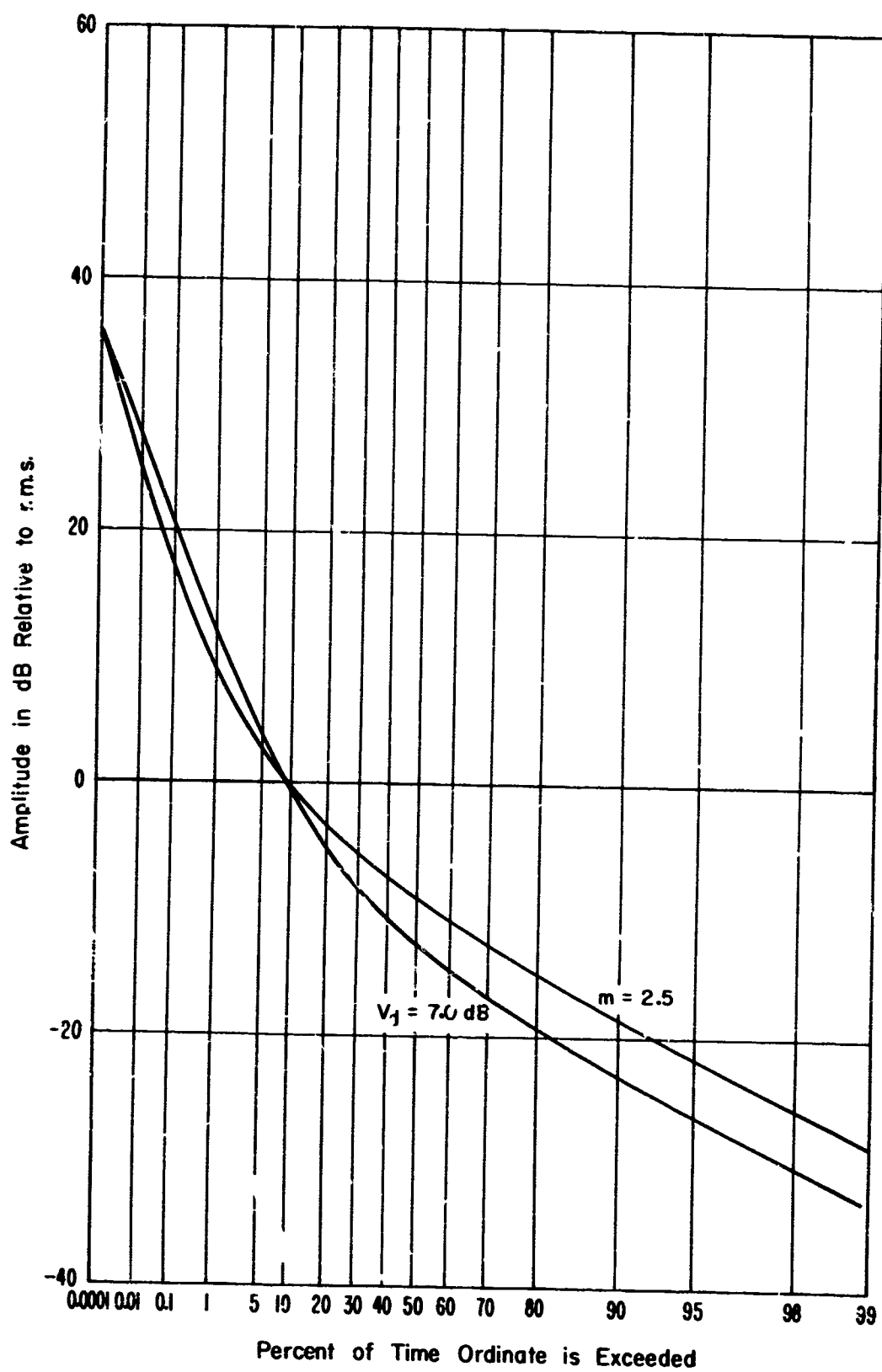
Figure 40.   Comparison of atmospheric radio noise amplitude probability
distribution for $V_d = 7$ dB, with distribution calculated from the
Hall model for m = 2.5.
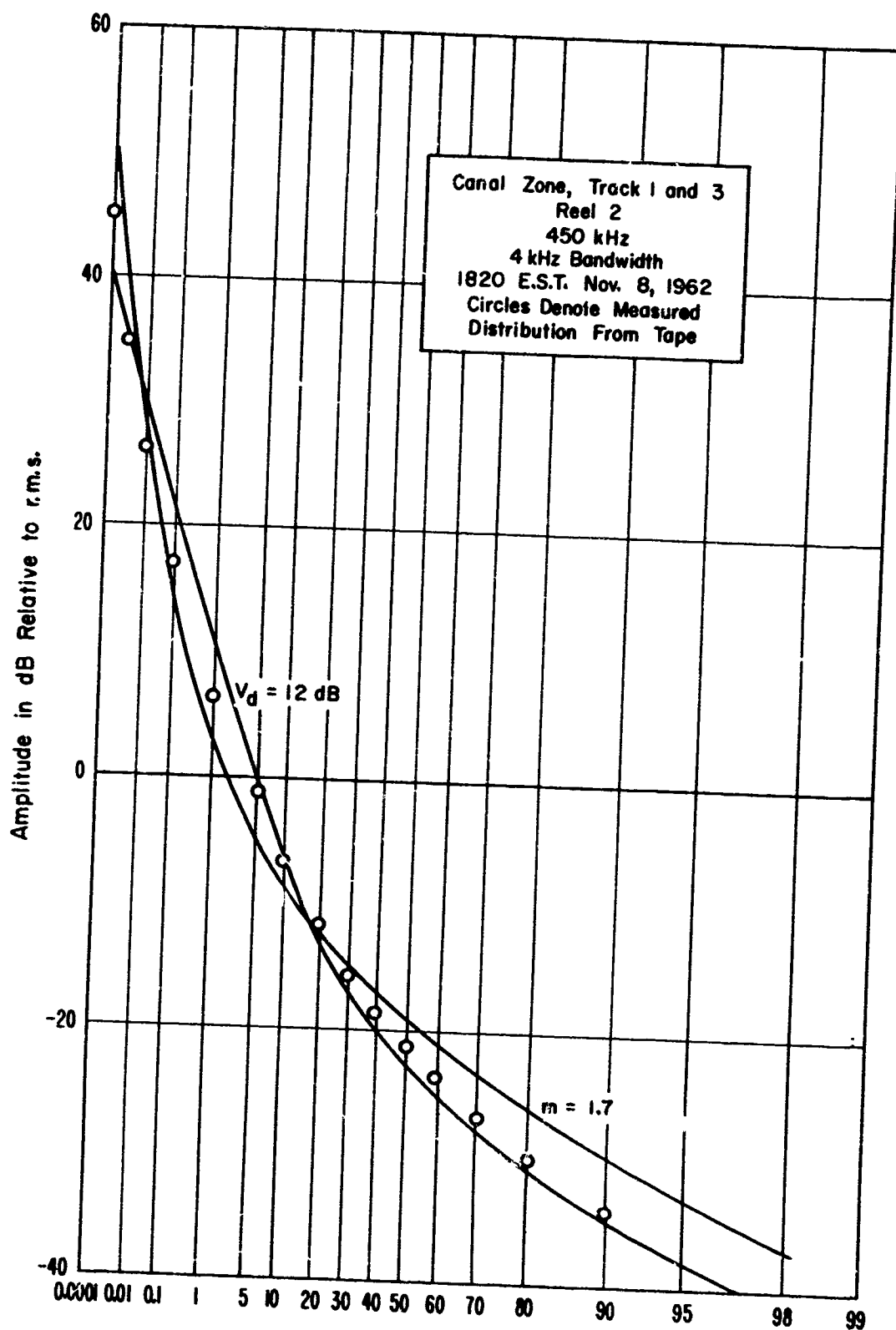
Figure 41. Comparison of atmospheric radio noise amplitude probability distributions for $V_d = 12$ dB and that calculated for the Hall model, m = 1.7 with the measured distribution.

-75-
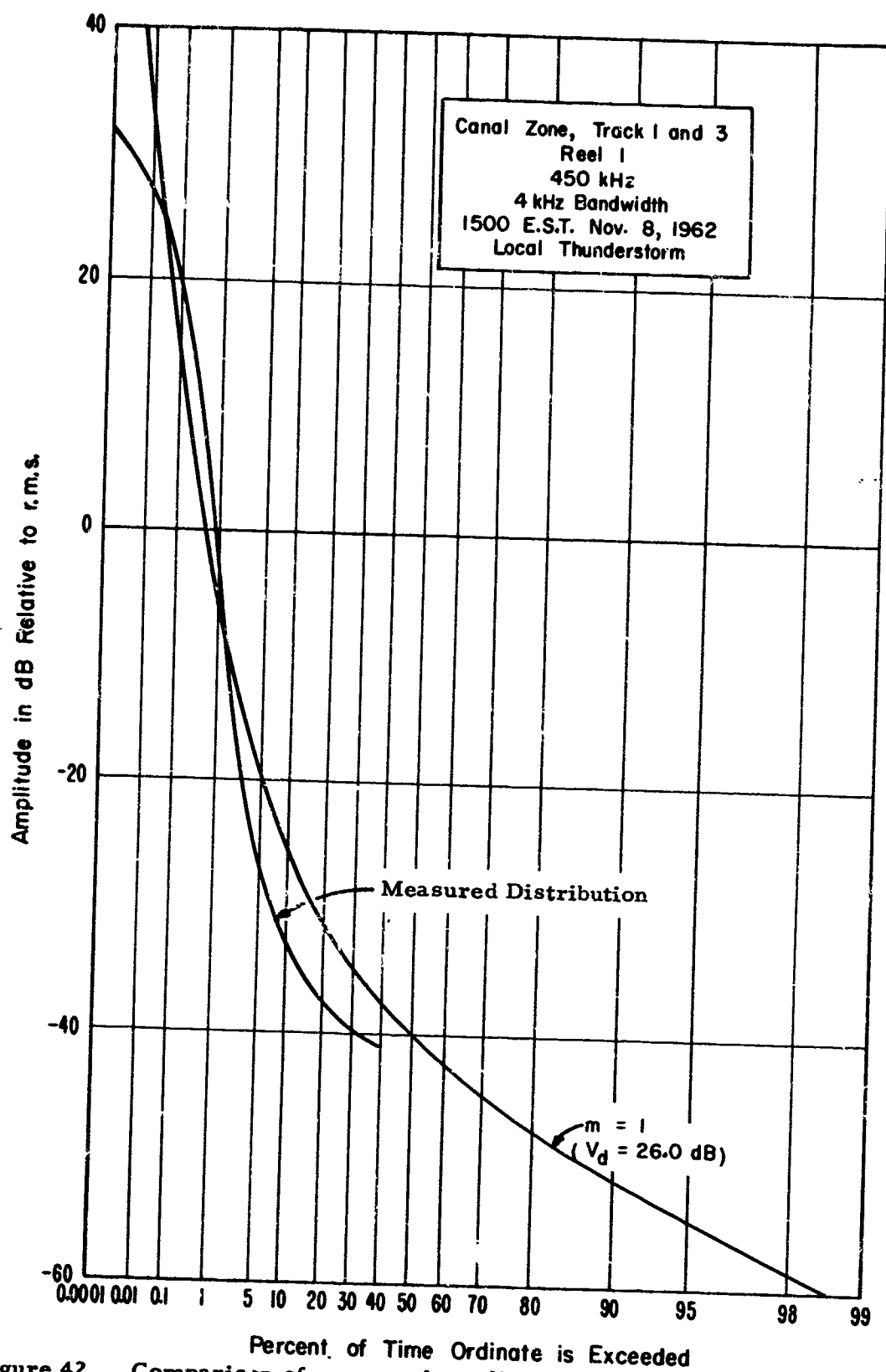
Figure 42.   Comparison of measured amplitude probability distribution and
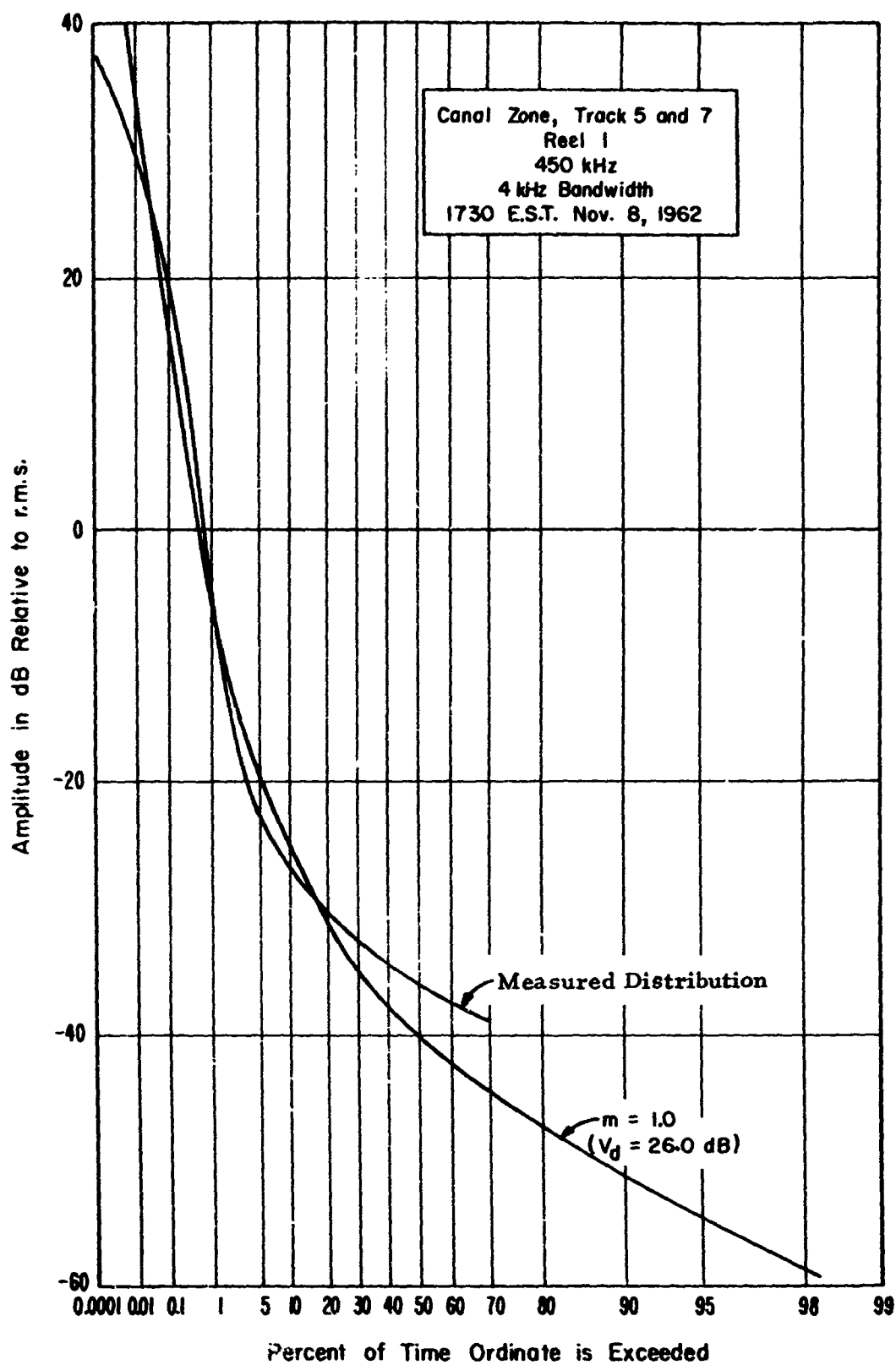distribution calculated from the Hall model for m = 1.0 (V_d = 26.0 dB).
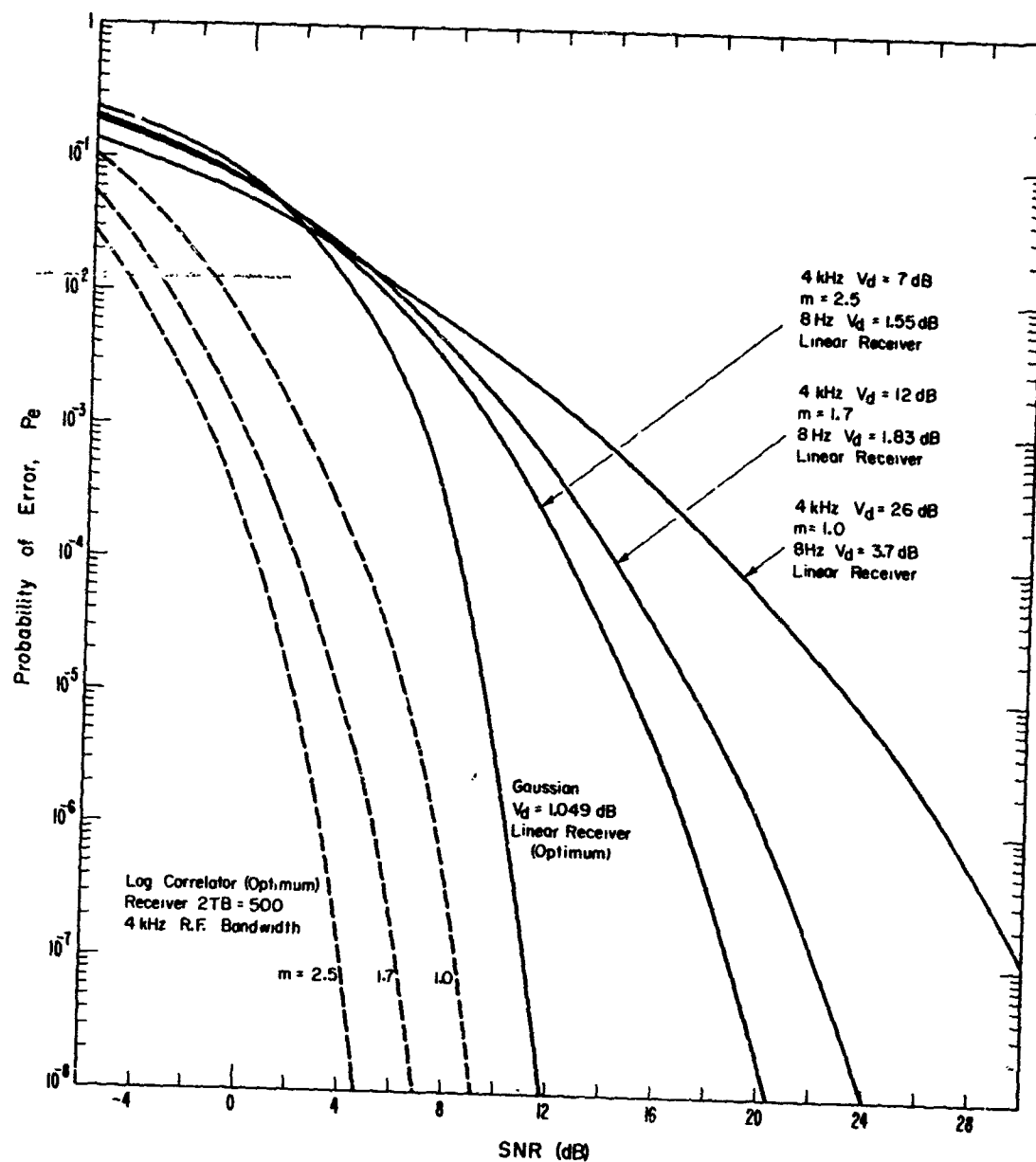
Figure 43.   Comparison of the performance of the optimum receiver with a matched filter linear receiver for a binary CPSK system.

-77-

APPENDIX A

A.1 Mathematical Modeling of the Noise Process

To be able to determine the performance of an optimum receiver subjected to man-made radio noise, a model for this narrow-band random noise process must be developed. Narrow-band noise processes result whenever the receiver bandwidth is substantially less than the receiver center frequency. The received waveform of the narrow-band process has an envelope and a phase. For determining the optimum receiver, more information about the noise is required than generally can be obtained from measurements. The problem is to develop a model for the noise that fits all the available measurements, that is physically meaningful when the nature of the noise sources are considered, and that still is simple enough that the required statistics can be obtained for solving signal detection problems.

Many attempts have been made to model narrow-band impulsive noise processes (Furutsu and Ishida, 1960; Middleton, 1961; Beckmann, 1964; Galejs, 1966). These models are essentially similar in that they take the received noise to be composed of a sum of filtered impulses whose amplitudes and occurrence in time follow various probability distributions. For example, the amplitudes of the impulse responses may be assumed to be log-normally distributed, while their times of occurrence may be assumed to be Poisson distributed.

Although the above forms are well-motivated physically and can be made to fit measured first-order statistics (amplitude probability distribution of the noise envelope, for example), they have several disadvantages as far as the signal detection problem is concerned:

(1) The models assume independence in the noise, while measurements indicate that this is not the case for either atmospheric noise or most forms of man-made noise. When one considers the correlation in the sources of man-made noise (automobile ignition systems resulting

-78-

in essentially periodic pulse trains, for example), the assumption of independence is obviously wrong.

(2) The resulting probability distributions are quite complicated and usually cannot even be put in closed form. For this reason no attempt has ever been made to apply these models to statistical detection problems at the receiver.

Various empirical models have been developed and related to measurements (Crichlow et al., 1960; Spaulding et al., 1962; Ibukun, 1966). These models do not represent the noise process but only the measured statistics of the process and, therefore, are not, in general, applicable in determining optimal receivers for the particular noise under consideration. They have been used to determine performance of various suboptimum linear receivers. The receivers now in use are designed to be optimum in Gaussian noise, and the performance of these receivers acting in impulsive noise has been determined (Akima, 1967; Bello, 1965; Conda, 1965; Halton and Spaulding, 1966; Lindenlaub and Chen, 1965; Shepelavey, 1963; Spaulding, 1964, 1966).

Here we are considering digital systems in which each signaling element is equally probable, and since the "cost" associated with making an error is the same for each type of possible error, "optimum" here simply means minimum probability of error. For example, in a binary system, by equal "costs " we mean making the error "decide signal one when signal two was sent" is just as bad as making the error "decide signal two when signal one was sent." Indications as to performance improvement by use of nonlinear elements (hole punchers, limiters, etc.) have also been given (ESSA, 1967; Linfield, 1965; Shchukin, 1946; Sisco, 1964; Sylvania, 1963).

Recently, Hall (1966) applied work on the applicability of a class of "self-similar" random processes as a model for certain intermittent

phenomena to signal detection problems considering LF atmospheric noise. The concept introduced is that of a random process controlled by one "regime" for the duration of observation, while this regime is itself a random process. This concept was introduced by Mandelbrot (1964) in the study of turbulence.

Hall (1966) has shown that the model to be specified in the next section fits the measured statistics of LF atmospheric noise. Other work at ITS has indicated that the model may be modified to fit HF atmospherics and man-made noise.

In the following section we will specify the model and possible modifications, determine the optimum receiver for some examples of LF atmospheric noise, considering frequencies around 500 kHz, obtain estimates of this optimum receiver's performance, and show how this performance compares with the performance of typical linear (matched filter or correlation) receivers.

As expected, the optimum receiver is nonlinear and its performance therefore depends on more than just the signal-to-noise ratio. We will see that, in general, performance will depend on the actual noise power, the actual signal energy, the signal shape, bandwidth, and time duration of the signals. We will analyze our optimum receiver's performance for the following situations:

(a) 1000 Hz bandwidth, binary system, signaling rate of 100 bps, with the highest atmospheric noise levels, as predicted by CCIR (1964) for the northwest U.S.

(b) Same as (a), but with a signaling rate of 50 bps.

For comparison with current receivers, case (a) would correspond to a receiver that tries to fight the noise by limiting in a 1000 Hz bandwidth and then uses approximately a 10-to-1 bandwidth reduction to limit the noise.

A.2 Specification of the Hall Model

The model proposed for received impulsive noise is one that takes the received noise to be a narrow-band Gaussian process multiplied by a weighting factor that varies with time. We will consider the narrow-band noise process $y(t)$, to be of the form

$$y(t) = a(t) \cdot n(t) , \qquad (A-1)$$

where $n(t)$ is a zero-mean narrow-band Gaussian process centered on the frequency of interest, ω_o, with covariance function, $R_n(\tau)$, and $a(t)$, the "regime" process, is stationary and independent of $n(t)$. The statistics of $a(t)$ must be chosen so that $y(t)$ is an accurate description of the received noise. We will further make the reasonable assumption that the modulating process, $a(t)$, is slowly varying (compared with $n(t)$) so that the spectrum of $a(t)$ has negligible overlap with the spectrum of $n(t)$. That is, $n(t)$ is a bandpass process, while $a(t)$ is a lowpass process. The details and arguments as to why this is a reasonable model for physical, as well as mathematical reasons, are given by Hall (1966).

An appropriate choice for $a(t)$ turns out to be a process with a probability density function given by

$$p_a(x) = \frac{(\frac{m}{2})^{\frac{m}{2}}}{\sigma^m \Gamma(\frac{m}{2})} \frac{1}{|x|^{m+1}} \exp\left[-\frac{m}{2\sigma^2} \frac{1}{x^2} \right] , \quad -\infty < x < \infty, \qquad (A-2)$$

where m and σ are parameters defining a two-sided chi distribution, $\chi_2(m, \sigma)$. The zero mean Gaussian process, $n(t)$, is completely described by its covariance function, $R_n(\tau)$, and its probability density is given by

$$p_n(x) = \frac{1}{\sqrt{2\pi \sigma_1^2}} \exp\left[-\frac{x^2}{2\sigma_1^2} \right] , \quad -\infty < x < \infty , \qquad (A-3)$$

-81-

where $R_n(0) = \sigma_1^2$, the variance of $n(t)$. Since $n(t)$ and $a(t)$ are assumed to be statistically independent,

$$P_y(x) = \int_{-\infty}^{\infty} \frac{dz}{|z|} \, P_a(\frac{x}{z}) \, P_n(z) \ . \tag{A-4}$$

If we let $\gamma = m^{\frac{1}{2}} \sigma_1 / \sigma$ and $\Theta = m + 1 > 1$, then

$$P_y(x) = \frac{\Gamma(\frac{\Theta}{2})}{\Gamma(\frac{\Theta-1}{2})} \, \frac{\gamma^{\Theta-1}}{\sqrt{\pi}} \, \frac{1}{\left[x^2 + \gamma^2\right]^{\Theta/2}} \ , \quad -\infty < x < \infty \ . \tag{A-5}$$

For this model Hall has computed the distribution of the noise envelope, the average number of level crossings of the noise envelope, and the distribution of level crossings (i.e., time between bursts) and has shown that by proper choice of the parameters, Θ and γ, the proposed model fits quite well these measured statistics for LF atmospheric noise. Even so, there are some problems. First, when Θ is in the range $2 < \Theta \leq 3$, $y(t)$ has infinite variance (i.e., infinite energy) and therefore cannot be a model for physical noise, even though it is found to fit the measurements. The problem arises in the tails of the distribution of $y(t)$ being such that $y(t)$ is either barely convergent or barely divergent, depending on the parameter Θ. This in turn arises from allowing the modulating process, which represents the statistics of the noise sources, to have an infinite range. Note that γ and Θ can be related to the two parameters commonly used to define the distribution of the noise envelope for atmospheric noise, V_d and the rms level, F_a (Spaulding et al., 1962). As we shall see, the problem of infinite variance will not bother us, because we will simply normalize our analysis to the point on the envelope distribution that corresponds to the actual rms level measured. That is, instead of normalizing to the (sometimes nonexistent) rms level of the

model, we will use a level that corresponds to the rms level of the actual measured atmospheric noise.

If we are interested in HF atmospheric or man-made noise, we can modify the above model as follows: since HF atmospheric noise and man-made noise generally exhibit a much smaller dynamic range than LF atmospherics, the modulation process, $a(t)$, can be allowed to have only a finite range, $-\beta < a < \beta$. While this introduces another parameter, β, and complicates the mathematics, this not only results in finite energy for $y(t)$ (for all choices of Θ), but should make it possible to model man-made noise quite closely by proper specification of covariance functions for $a(t)$ and $n(t)$. That is, we will use for the distribution of the process $a(t)$,

$$P_a(x) = \frac{k}{|x|^{m+1}} \; \exp\left(-\frac{m}{2\sigma^2} \frac{1}{x^2}\right), \; -\beta \le x \le \beta \; . \quad (A-6)$$

where k is chosen so that

$$\int_{-\beta}^{\beta} P_a(x)\,dx = 1 \; .$$

Figure 1 shows the APD's (envelope distributions) for a range of values, Θ, and a value of γ that corresponds to the expected APD's in 1000 Hz bandwidth in the northwest United States. Figure 2 shows the kind of modification that results in the envelope distribution ($\Theta = 3$) when various values of β are used. The expressions for the envelope distributions have been derived by Hall (1966) and are given in appendix B. The APD's shown in figures 1 and 2 were calculated by computer.

A. 3 Signal Representation and Determination of the Optimum Receiver

In this section we will derive the optimum receiver for noise and signal situations pertinent to the present problem. As shown by Hall, to gain any advantage over linear matched filter receivers, the

-83-

time duration of the signals must be many times the reciprocal of the receiver RF bandwidth. In fact, Hall has shown that the linear matched filter receiver is optimum when the signal duration is on the same order as the receiver reciprocal bandwidth. This is analogous to current noise-limiting techniques, in which large bandwidths (compared with signal duration) are required. Typically, we may use a signal length of 0.01 sec (100 bps)/sec with an RF bandwidth of 1000 Hz, so that the signal length is 10 times the reciprocal bandwidth.

Let us consider the problem of deciding which signal from among a set of two signals, $s_1(t)$ and $s_2(t)$, is represented by some received waveform, $x(t)$. We want to develop a decision scheme that will minimize the average "risk." The "risk" involved in making an error is defined as the probability of making that error times the "cost" of making that error. The problem is how to choose between two hypotheses, H_1 and H_2, where

$$H_1 \; : \; x(t) = s_1(t) + a(t) \, n(t)$$
$$H_2 \; : \; x(t) = s_2(t) + a(t) \, n(t) \quad .$$

$$(A-7)$$

We denote the "cost" associated with H_1 by C_1 (the cost to the observer if he decides H_2 is true when, in fact, H_1 is true minus the cost to the observer if he decides H_1 is true when, indeed, it is true) and the cost associated with H_2 by C_2. If the probability of occurrence of s_1 is q_1, and the probability of occurrence of s_2 is q_2, we have the threshold, Q, where

$$Q = \frac{q_1 C_1}{q_2 C_2} \quad . \qquad (A-8)$$

-84-

Let $L[x(t)]$ denote the likelihood ratio, given by

$$L[x(t)] = \frac{p(x(t)|H_1)}{p(x(t)|H_2)} \quad . \tag{A-9}$$

The minimum average risk is achieved then by choosing H_1 when

$$L[x(t)] > Q \quad , \tag{A-10}$$

and choosing H_2 otherwise.

The probability of making the error, "decide s_1 when s_2 was sent," is then

$$P_e = \text{prob} \{ L[x(t)] > Q | s_2 \} \quad , \tag{A-11}$$

so that the probability density of the likelihood ratio is required.

In the completely general case given by (A-7), the probabilities in the likelihood ratio are extremely difficult (if not impossible) to compute. In the situations of interest here, in which the receiver bandwidth is substantially less than the band center frequency, the hypotheses (A-7) can be formulated in terms of the complex envelope of $x(t)$ (Helstron, 1960). Without loss of generality, we can let $Q = 1$ (equal probabilities of occurrence and equal costs associated with s_1 and s_2), and we will further let $s_2(t) = 0$. Hall has evaluated the likelihood ratio for the case $m = 1$. We will follow Hall's procedure but will carry the calculations through for arbitrary m. Our two hypotheses can now be given in the following form:

$$H_1 : \chi(t) = \mu(t) + \eta(t)$$
$$0 \le t \le T \quad , \tag{A-12}$$
$$H_2 : \chi(t) = \eta(t)$$

Where T is the time duration of the signal, $\mu(t)$ denotes the complex envelope of the signal, $\eta(t)$ denotes the complex envelope of the additive

noise process, $y(t)$, and $x(t)$ denotes the complex envelope of the received narrowband waveform, e.g.,

$$x(t) = x_c(t) \cos \omega_o t - x_s(t) \sin \omega_o t$$
$$= R_e \left\{ \chi(t) e^{i\omega_o t} \right\} ,$$

and

$$\chi(t) = x_c(t) + i x_s(t) .$$

Let the signal, $\mu(t)$, be represented by a N dimensional vector, $\underline{\mu}$, i.e., $\underline{\mu} = \{\mu_1, \mu_2, \ldots, \mu_N\}$, where the μ_i are complex numbers and are samples from the waveform $\mu(t)$. We will now assume that the bandwidth of the signal is substantially less than the receiver bandwidth, $2B$. The signal may then be represented by $2BT$ samples. We break the interval, $[0, T]$, into N subintervals, Δt_i and $\mu_i = \mu(t_i)$, where t_i denotes some time in the interval, Δt_i. The waveform, $\mu(t)$, can be represented exactly in this manner.

Let the complex noise process, $\eta(t)$, be also represented by N samples, so that $\eta_i = \eta(t_i)(\Delta t_i)^{\frac{1}{2}}$. The η_i are now complex random variables, and the process, $\eta(t)$, is represented by the random vector $\underline{\eta} = \{\eta_1, \eta_2, \ldots, \eta_N\}$. (For the problems involved in representing a random waveform by a finite dimensional random vector and the connection between the processing of random vectors and the processing of continuous random waveforms, see Hannock and Wintz (1966, app. B).

Because of the above constraint on the signal, we may assume that the various η_i are independent (which corresponds to the atmospheric noise being white prior to detection).

Our two hypotheses are now given in vector form:

$$H_1 : \underline{x} = \underline{\mu} + \underline{\eta}$$

$$H_2 : \underline{x} = \underline{\eta} \qquad , \tag{A-13}$$

and we must now compute $p(\underline{x} | H_1)$ and $p(\underline{x} | H_2)$.

Now

$$p(\underline{x} \mid H_1) = p_{\underline{\eta}}(\underline{x} - \underline{\mu}) \ , \tag{A-14}$$

so that $p_{\eta}(\underline{\eta})$ is required. Recalling that the noise process, $y(t)$, is given by $\overline{a}(t)n(t)$, we can write

$$\eta_i = a_i v_i \ , \tag{A-15}$$

where $a_i = a(t_i)$ and $v_i = v(t_i)(\Delta t_i)^{\frac{1}{2}}$, in which $v(t)$ is the complex envelope of $n(t)$. Since $n(t)$ is a Gaussian process, $v(t)$ is a complex Gaussian process. Thus the probability density function, $p_{\underline{v}}(\underline{v})$, of the vector, $\underline{v}$, can be written in the form

$$P_{\underline{v}}(\underline{v}) = \frac{1}{\pi^N |\Phi|} \exp\left[-\underline{v}^*_T \Phi^{-1} \underline{v}\right] \ , \tag{A-16}$$

where $\underline{v}^*$ denotes the conjugate of $\underline{v}$, and $\underline{v}_T$ denotes the transpose of the vector, $\underline{v}$; Φ is the N by N covariance matrix of $v(t)$, i.e.,
$\Phi = \{E(v_i^* v_j)\}$, $1 \le i, j \le N$, where

$$E(v_i^* v_j) = E[v^*(t_i) v(t_j)] (\Delta t_i \Delta t_j)^{\frac{1}{2}} \ , \tag{A-17}$$

where E denotes the expectation operator.

Our assumption of impedance states that

$$E[v^*(t_i) v(t_j)] = \sigma_1^2 \delta_{ij}, \quad i, j = 1, 2, \ldots, N \ , \tag{A-18}$$

where δ_{ij} is Kronecker's delta, i.e., $\delta_{ij} = 0$ for $i \ne j$, and $\delta_{ij} = 1$, $i = j$. Letting $\Delta t_i = \Delta t$ for all i, we obtain then

$$P_{\underline{v}}(\underline{v}) = \frac{1}{\pi^N (\sigma_1^2 \Delta t)^N} \exp\left[-\frac{1}{\sigma_1^2 \Delta t} \underline{v}^*_T \underline{v}\right] \ . \tag{A-19}$$

To compute $p_{\eta}(\underline{\eta})$ we will make the transformation $b = 1/a$, where now, since the distribution of a is given by (A-2), the distribution for b is

$$P_b(b) = \frac{(\frac{m}{2})^{m/2}}{\sigma^m \Gamma(\frac{m}{2})} |b|^{m-1} \exp\left[-\frac{m}{2\sigma^2} b^2\right] \ . \tag{A-20}$$

and then

$$P_{\underline{\eta}}(\underline{\eta}) = \int P_{\underline{\eta}}(\underline{\eta}|\underline{b}) \ P_{\underline{b}}(\underline{b}) \ d\underline{b} \quad , \qquad (A-21)$$

where $\underline{b}$ is the vector $\{b_1, b_2, \ldots b_n\}$, and $b_i = 1/a_i$. Our assumption of independence makes the b_i's independent, i.e.,

$$E\left[b(t_i) \ b(t_j) \right] = \sigma^2 \delta_{ij} \quad . \qquad (A-22)$$

Therefore the distribution of the vector, $\underline{b}$, based on (A-20)

$$P_{\underline{b}}(\underline{b}) = \frac{\frac{m}{2}^{m/2}}{\sigma^m \Gamma(\frac{m}{2})} \prod_{i=1}^{N} |b_i|^{m-1} \exp\left[-\frac{m}{2\sigma^2} \ \underline{b}_T \underline{b} \right] \quad . \qquad (A-23)$$

Now, since $\eta_i = \nu_i/b_i$, η and ν complex, the Jacobian of the transformation $\nu_i \to \eta_i$ is b_i^2. This means, then,

$$P_{\underline{\eta}}(\underline{\eta}|\underline{b}) = \left(\prod_{i=1}^{N} b_i^2 \right) P_{\underline{\nu}}(\nu_i = b_i\eta_i, \ i = 1, 2, \ldots, N) \quad .$$

Therefore from (A-19),

$$P_{\underline{\eta}}(\underline{\eta}|\underline{b}) = \left(\prod_{i=1}^{N} b_i^2 \right) \frac{1}{\pi^N (\sigma_1^2 \Delta t)^N} \ \exp\left[-\frac{1}{\sigma_1^2 \Delta t} \sum_{i=1}^{N} b_i^2 |\eta_i|^2 \right] \cdot (A-24)$$

Substituting into (A-21)

$$P_{\underline{\eta}}(\underline{\eta}) = K \int_{-\infty}^{\infty} db_1 \ldots \int_{-\infty}^{\infty} db_N \prod_{i=1}^{N} |b_i|^{m+1} \cdot \exp\left[-\sum_{i=1}^{N} \left(\frac{m b_i^2}{2\sigma^2} + \frac{b_i^2 |\eta_i|^2}{\sigma_1^2 \Delta t} \right) \right] \cdot (A-25)$$

where

$$K = \frac{(\frac{m}{2})^{m/2}}{\sigma^m \Gamma^{(\frac{m}{2})} \pi^N (\sigma_1^2 \Delta t)^N} \quad . \qquad (A-26)$$

Evaluating (A-25), we obtain

$$P_{\underline{\eta}}(\underline{\eta}) = K \prod_{i=1}^{N} \Gamma\left(\frac{m+2}{2} \right) \left(\frac{|\eta_i|^2}{\sigma_1^2 \Delta t} + \frac{m}{2\sigma^2} \right)^{-\frac{m+2}{2}} \quad , \qquad (A-27)$$

-88-

$$P_{\underline{\eta}}(\underline{\eta}) = K \Gamma\left(\frac{m+2}{2}\right)\left(\sigma_1^2 \Delta t\right)^{\frac{m+2}{2}} \prod_{i=1}^{N}\left(|\eta_i|^2 + \frac{m\sigma_1^2 \Delta t}{2\sigma^2}\right) \quad . \tag{A-28}$$

From (A-14), our likelihood ratio, $L[\underline{x}]$, becomes

$$L[\underline{x}] = \frac{\displaystyle\prod_{i=1}^{N}\left[|x_i|^2 + \frac{m\sigma_1^2 \Delta t}{2\sigma^2}\right]^{\frac{m+2}{2}}}{\displaystyle\prod_{i=1}^{N}\left[|x_i - \mu_i|^2 + \frac{m\sigma_1^2 \Delta t}{2\sigma_2}\right]^{\frac{m+2}{2}}} \tag{A-29}$$

Our optimum decision rule (A-4) becomes "choose H_1, if

$$\prod_{i=1}^{N}\left[|x_i|^2 + \frac{m\sigma_1^2 \Delta t}{2\sigma^2}\right] \geq \prod_{i=1}^{N}\left[|x_i - \mu_i|^2 + \frac{m\sigma_1^2 \Delta t}{2\sigma^2}\right]." \tag{A-30}$$

This is equivalent to the rule

$$\sum_{i=1}^{N} \ln\left[|x_i|^2 + \frac{m\sigma_1^2}{2\sigma^2}\right] \geq \sum_{i=1}^{N} \ln\left[|x_i - \mu_i|^2 + \frac{m\sigma_1^2}{2\sigma^2}\right] \quad , \tag{A-31}$$

and in terms of the time functions available to the receiver, the rule (A-31) becomes

$$\int_0^T \ln\left[|x(t)|^2 + \frac{m\sigma_1^2}{2\sigma^2}\right] dt \geq \int_0^T \ln\left[|x(t) - \mu(t)|^2 + \frac{m\sigma_1^2}{2\sigma^2}\right] dt. \tag{A-32}$$

There are many physical realizations of (A-32) (see, for example, Hall, 1966). The receiver consists of two branches, one to compute each side of the inequality (A-32). Each branch could contain an envelope detector, followed by a square law device (which gives $|x(t)|^2$, for example), followed by a log amplifier biased by $m\sigma_1^2/2\sigma^2$ (a bias proportional to the

actual expected noise power), followed by an integrator. Threshold logic

circuitry would then compare the thus computed quantities and announce

a decision. This receiver can, therefore, be easily constructed. Any

digital receiver is simply a box for computing some quantity from the

received waveform and for comparing this quantity with a threshold.

Figure 3 (from Hall, 1966) shows a block diagram of one receiver structure

which implements the decision rule. It now remains to analyze the per-

formance (compute the error rate) of our receiver.

A.4   Calculation of Probability of Error

The probability of error expression (A-11) is

$$P_e = \text{prob} \left\{ L(\underline{x}) \geq 1 \mid H_2 \text{ is true} \right\} , \tag{A-33}$$

or, from (A-29), since H_2 being true implies $|x(t)| = |\eta(t)|$,

$$P_e = \text{prob} \left\{ \prod_{i=1}^{N} \left[\frac{|\eta_i|^2 + \dfrac{m\sigma_1^2 \Delta t}{2\sigma^2}}{|\eta_i - \mu_i|^2 + \dfrac{m\sigma_1^2 \Delta t}{2\sigma^2}} \right] \geq 1 \right\} . \tag{A-34}$$

Putting (A-34) in a more manageable form, we have

$$P_e = \text{prob} \left\{ \sum_{i=1}^{N} \ln z_i \geq 0 \right\} , \tag{A-35}$$

where

$$z_i = \frac{|\eta_i|^2 + \dfrac{m\sigma_1^2 \Delta t}{2\sigma^2}}{|\eta_i - \mu_i|^2 + \dfrac{m\sigma_1^2 \Delta t}{2\sigma^2}} . \tag{A-36}$$

Now, it is not possible to compute P_e directly, since we cannot

obtain the probability density for $\sum_{i=1}^{N} \ln z_i$, and we must be satisfied with

good estimates for p_e. Since p_e is given in terms of a sum of random variables, the characteristic functions for the random variables, $\ell n z_i$, should be useful. We will use characteristic functions to obtain the appropriate Chernoff bound on p_e (Van Trees, 1968).

Let $\phi(s)$ denote the characteristic function for our likelihood ratio L, under hypothesis H_2, that is,

$$\phi(s) = \int_{-\infty}^{\infty} e^{sL} \, p(L|H_2) \, dL \quad . \tag{A-37}$$

Now define

$$\rho(s) = \ell n \phi(s) \quad . \tag{A-38}$$

We then have the Chernoff upper bound

$$P_e \leq e^{\rho(s) - s\dot{\rho}(s)}, \quad s \geq 0 \quad , \tag{A-39}$$

and the minimum upper bound is obtained by evaluating (A-39) for the value of s, s_o, which makes $\dot{\rho}(s) = 0$. We can now apply the central limit theorem to the above to obtain the approximation (Van Trees, 1968)

$$P_e \simeq \{ \exp [\rho(s) - s\dot{\rho}(s) + \frac{s^2}{2} \ddot{\rho}(s)] \} \, \text{erfc} [s \sqrt{\ddot{\rho}(s)} \quad , \tag{A-40}$$

where erfc denotes the complimentary error function. For values of $s\sqrt{\ddot{\rho}(s)} > 3$, we can approximate the erfc term to obtain

$$P_e \overset{\sim}{=} \frac{1}{\sqrt{2\pi \, s^2 \ddot{\rho}(s)}} \, \exp [\rho(s) - s\dot{\rho}(s)] \quad . \tag{A-41}$$

It turns out that for the range of p_e of interest to us (10^{-3} and less) the factor $1/\sqrt{2\pi s^2 \ddot{\rho}(s)}$ will not appreciably change the results, and besides, as we shall see, it is extremely difficult to evaluate $\ddot{\rho}(s_o)$.

In our case, then, if $g_i(s)$ denotes the characteristic functions for the independent random variables $\ell n z_i$,

$$\rho(s) = \ell n \prod_{i=1}^{N} g_i(s) \quad , \tag{A-42}$$

-91 -

so that the approximation we will use is given by

$$P_e \leq \prod_{i=1}^{N} g_i(s_o) \quad . \tag{A-43}$$

It follows that (Hall, 1966)

$$g_i(s) = E[\exp(s \ln z_i)]$$

$$= \frac{\Gamma(\frac{m+2}{2})}{\Gamma(\frac{m}{2})} \frac{\xi^m}{\pi} \int_{-\infty}^{\infty} dn_{ic} \int_{-\infty}^{\infty} dn_{is} \frac{[|\eta_i|^2 + \xi^2]^{(2s-m-2)/2}}{[|\eta_i - \mu_i|^2 + \xi^2]^s} \quad , \tag{A-44}$$

where $\xi^2 = \dfrac{m\sigma_1^2 \Delta t}{2\sigma^2}$, and η_{ic}, η_{is} denote the real and imaginary parts

of the complex number η_i. Equation (A-43) states that the performance is

dependent on the actual noise power (which is proportional to ξ^2) and on

the actual signal shape and energy (i.e., depends on the 2TB samples,

μ_i, of the signal complex envelope). To simplify things, let the

imaginary part of $\mu_i = 0$, for all i. An example of such a signal would be

$$s_1(t) = r(t) \cos \omega_o t \quad .$$

The samples, μ_i, are now real numbers, and our integral (A-44) reduces to

$$g_i(s) = \frac{\Gamma(\frac{m+2}{2})}{\Gamma(\frac{m}{2})} \frac{\xi^m}{\pi} \int_{-\infty}^{\infty} dx \int_{-\infty}^{\infty} dy \frac{(x^2 + y^2 + \xi^2)^{\frac{2s-m-2}{2}}}{[(x-\mu_i)^2 + y^2 + \xi^2]^s} \quad . \tag{A-45}$$

As one might expect, and as Hall (1966) has shown, the best signal design

is a signal whose energy is uniformly distributed in the signaling interval.

This means that the μ_i can be considered equal, resulting in needing

to evaluate only one $g_i(s)$. Our estimate now becomes

$$P_e \leq \prod_{i=1}^{N} g_i(s_o) = [g(s_o)]^{2BT} \quad . \qquad \text{(A-46)}$$

In terms of the total energy per received bit, and the noise power density, (A-45) becomes

$$g(s) = \frac{\Gamma(\frac{m+2}{2})}{\pi \Gamma(\frac{m}{2})} \int_{-\infty}^{\infty} dx \int_{-\infty}^{\infty} dy \frac{(x^2 + y^2 + 1)^{\frac{2s-m-2}{2}}}{(x^2 + y^2 - 2ax + a^2 + 1)^s} \qquad \text{(A-47)}$$

where the parameter, a, is given by

$$a = \frac{\mu_i}{\xi} = \frac{\sqrt{2E}}{\sqrt{TBN}} \quad , \qquad \text{(A-48)}$$

where E denotes the signal energy (joules) and N denotes the noise power density (watts/hertz). The integral (A-41) must be evaluated for $s_\cup s_o$, where, from (A-42), s_o is the solution to

$$\frac{\int_{-\infty}^{\infty} dx \int_{-\infty}^{\infty} dy \frac{(x^2 + y^2 + 1)^{2s-m-2)/2}}{(x^2 + y^2 - 2ax + a^2 + 1)^s} \ln\left(\frac{x^2 + y^2 + 1}{x^2 + y^2 - 2ax + a^2 + 2}\right)}{\int_{-\infty}^{\infty} dx \int_{-\infty}^{\infty} dy \frac{(x^2 + y^2 + 1)^{(2s-m-2)/2}}{(x^2 + y^2 - 2ax + a^2 + 1)^s}} = 0 \quad . \qquad \text{(A-49)}$$

For each a of interest, (A-49) must be solved for s_o and then evaluated for this value of s. Quite fortunately it can be shown that (A-49) is uniquely solved, for all a, by

$$\qquad \text{(A-50)}$$

$$s_o = \frac{m+2}{4} \quad .$$

The integral (A-47) must now be evaluated for this s_o, and computer techniques have been developed and programs written to do this.

The case, $\Theta = 3$ (m = 2), is a special case. For m = 2, (A-49) is uniquely solved for all a by s = 1, and for s = 1, the integral (A-47) can be evaluated in closed form by first performing the x integration and then the y integration. The result is

$$g(1) = \frac{2}{a\sqrt{a^2+4}} \, \ell n \left(\frac{\sqrt{a^2+4}+a}{\sqrt{a^2+4}-a} \right) . \qquad (A-51)$$

From (A-46), we see that we can make the probability of error arbitrarily small by making 2BT large enough. Of course, it is well known that by signaling slowly enough (i.e., making T large), the probability of error can be made as small as desired.

We will now consider the following example: summer nighttime, Washington state area, $\omega_o = 500$ kHz, 1000 Hz bandwidth, and 100(2TB = 10) and 50 (2TB = 20) bps. From CCIR (1964) we have F_{am} F_{am}(500 kHz) = 133 dB, and V_{dm}(1 kHz bandwidth) = 14 dB, i.e., dynamic range of the envelope distribution for probabilities from 10^{-6} to .99 is about 88 dB. This corresponds to $\Theta \cong 3$. F_{am} = 133 dB gives us that the noise power density is 7.95×10^{-8} W/Hz. This number is required to determine the value of γ to use in specifying the envelope distribution and the amount of bias required on the log amplifiers of our optimum receiver.

Figure 4 shows the performance of the optimum receiver. It also shows the performance of a binary matched filter, differentially coherent phase shift keying receiver for both Gaussian noise and atmospheric noise ($\Theta = 3$).

If we now tried to improve our estimate by using (A-40) or (A-41), we would need to evaluate $\ddot{\rho}(s)$ for $s = 1$, $m = 2$. This is

$$\tilde{\rho}(1) = \frac{2TB \int\limits_{-\infty}^{\infty} dx \int\limits_{-\infty}^{\infty} dy \; \frac{(x^2+y^2+1)^{-1}}{(x-a)^2+y^2+1} \left[\ln \frac{x^2+y^2+1}{(x-a)^2+y^2+1} \right]^2}{\int\limits_{-\infty}^{\infty} dx \int\limits_{-\infty}^{\infty} dy \; \frac{(x^2+y^2+1)^{-1}}{(x-a)^2+y^2+1}} . \qquad \text{(A-52)}$$

However, instead of trying to evaluate the above, we note from figure 4 that, if the factor $1/\sqrt{2\pi s^2 \ddot{\rho}(s)}$ were on the order of 0.1, this would change our estimate by less than 1 dB, and even if $1/\sqrt{2\pi s^2 \ddot{\rho}(s)}$ were on the order of 0.01, a change of less than 2 dB would result. That is, for a given probability of error, the required SNR would be not more than 2 dB less. This indicates that, while the curve shown is an upper bound on the true probability of error characteristic, it is a very tight upper bound. Estimates of (A-52) indicate that the factor $1/\sqrt{2\pi s^2 \ddot{\rho}(s)}$ is somewhere between 0.1 and 0.25.

Figure 5 shows the performance of the optimum receiver for a range of values of Θ for $2\,TB = 10$, and figure 6 shows the same for $2TB = 20$.

If we try to carry out the above calculations with a modified Hall model (to fit HF atmospherics or man-made noise), we find that, besides being much more difficult, the optimum receiver is different for each value of β we might use. Studies like this with a modified model remain to be done.

For completeness, we have included figures 7, 8, and 9, which summarize the performance of typical linear receivers in noise of atmospheric type. Figure 7 shows the relationship between the probability of error and the signal-to-noise ratio, parametric in V_d, for

binary differentially coherent phase shift keying (DCPSK). These curves were obtained by the method described by Halton and Spaulding (1966) and also are applicable to noncoherent frequency shift keying (NCFSK), if we add 3 dB to the abscissa value.

Figure 8 shows the probability of element error for a four-phase DCPSK system as a function of signal-to-noise ratio, parametric in V_d. As in figure 7, the signal is assumed to be steady. The binary error rate is approximately equal to one-half the element error rate at large signal-to-noise ratios.

Figure 9 shows probability of error characteristics for both two- and four-phase DCPSK systems when the signal is Rayleigh fading, as described by Halton and Spaulding (1966).
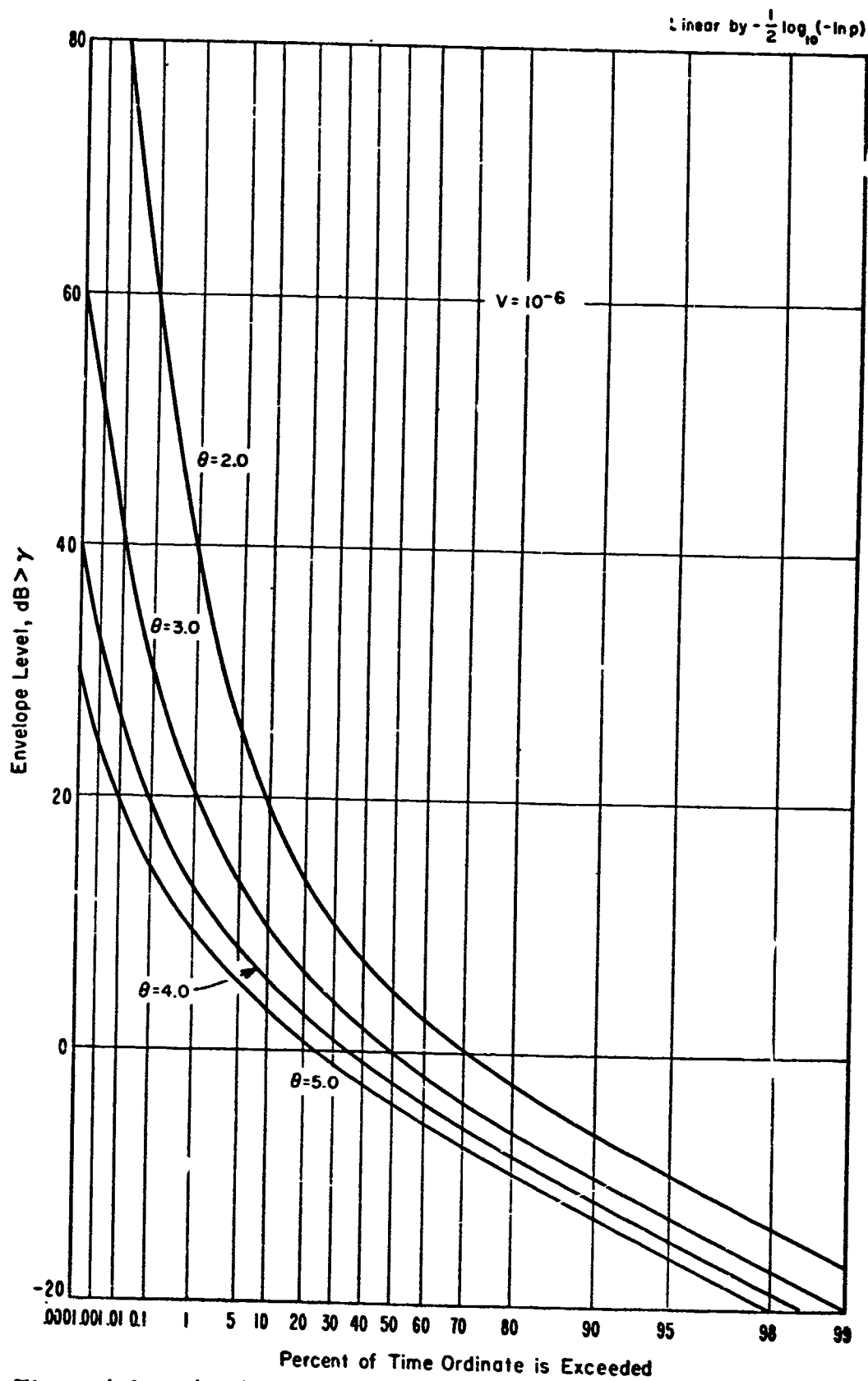
Figure A.1   Amplitude probability distributions of the noise envelope of the
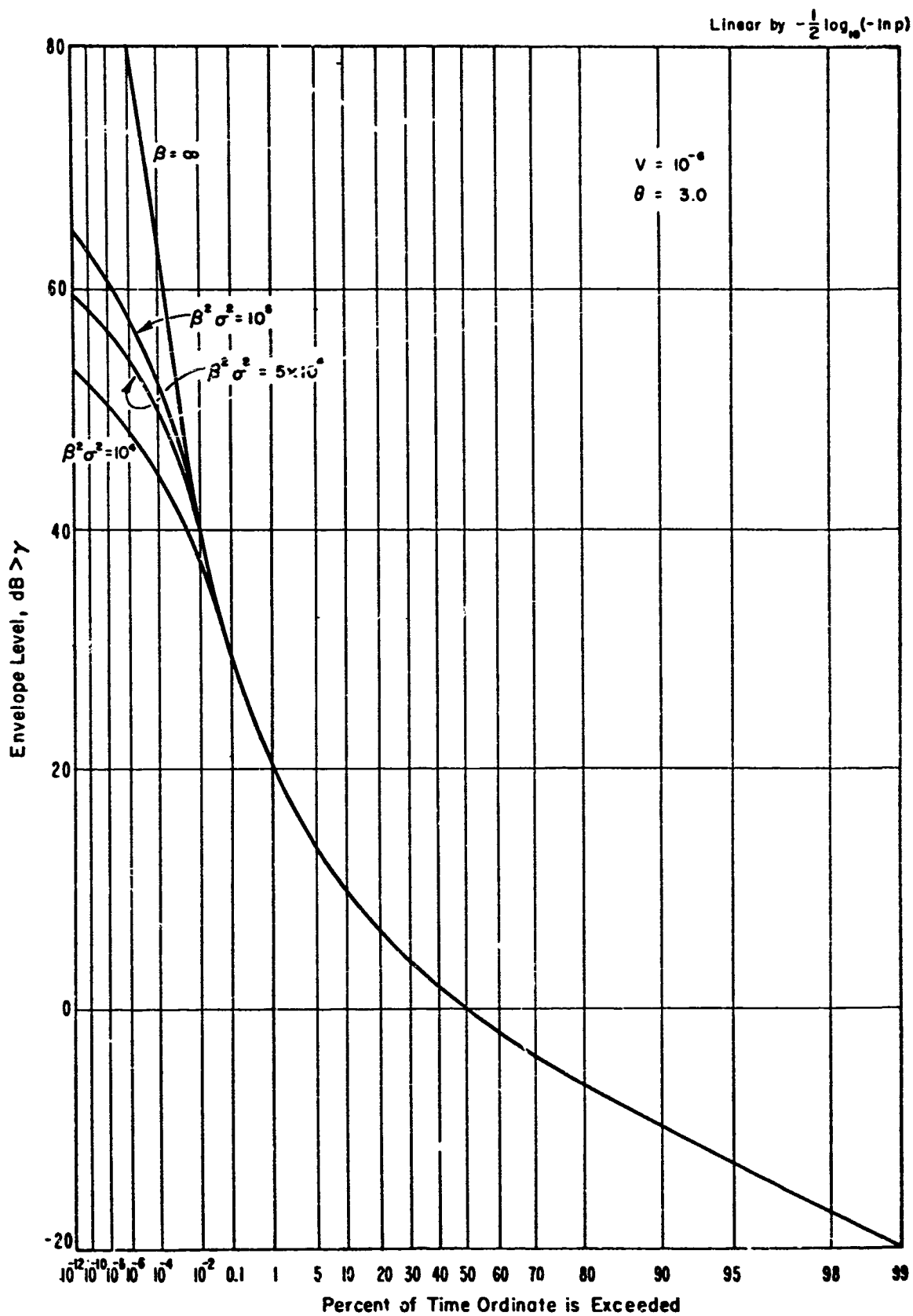Hall model for a range of values of the parameter Θ.

Figure A.2   Amplitude probability distributions of the noise envelope of the modified Hall model for a range of values of the parameter β.
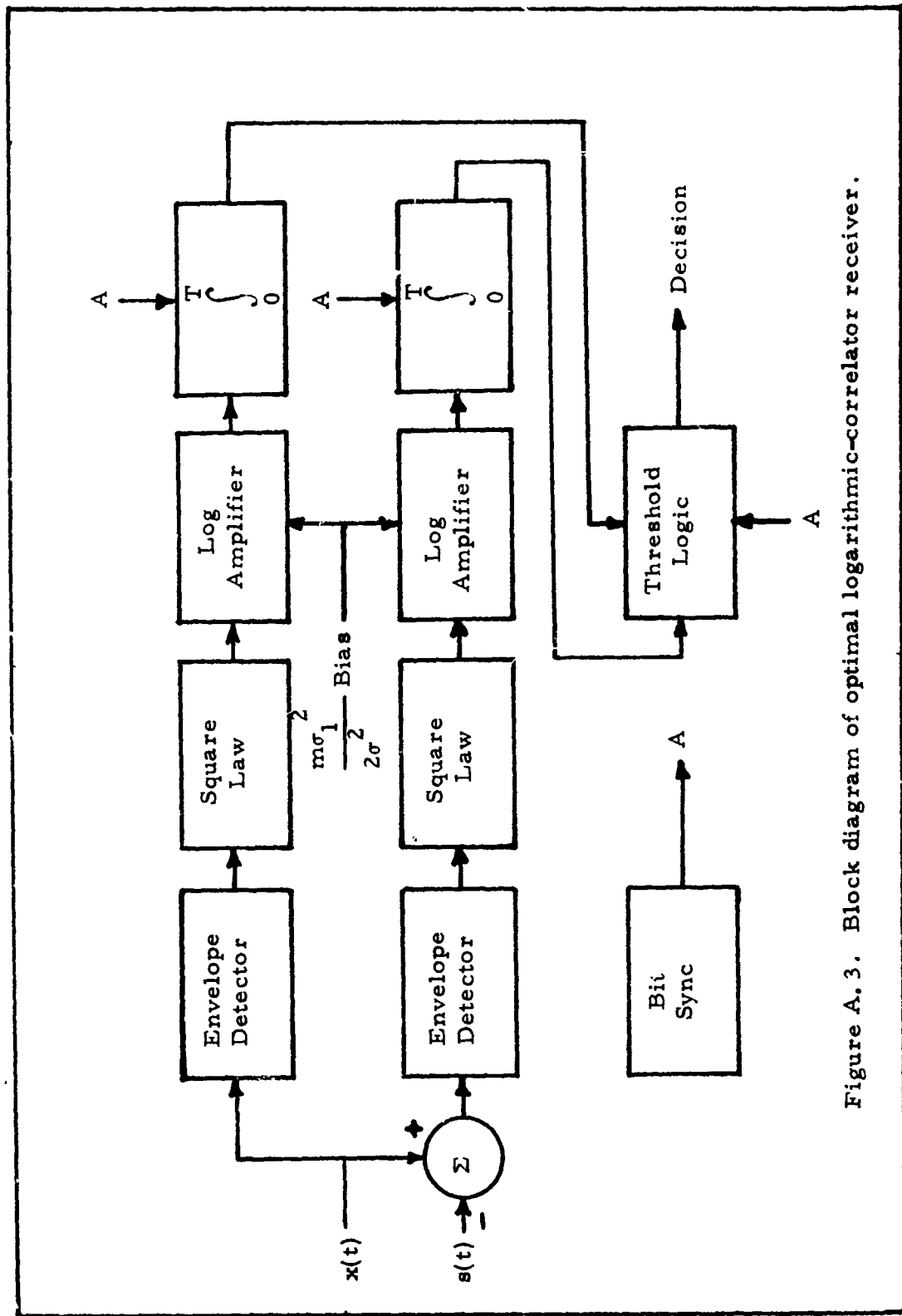
Figure A.3. Block diagram of optimal logarithmic-correlator receiver.

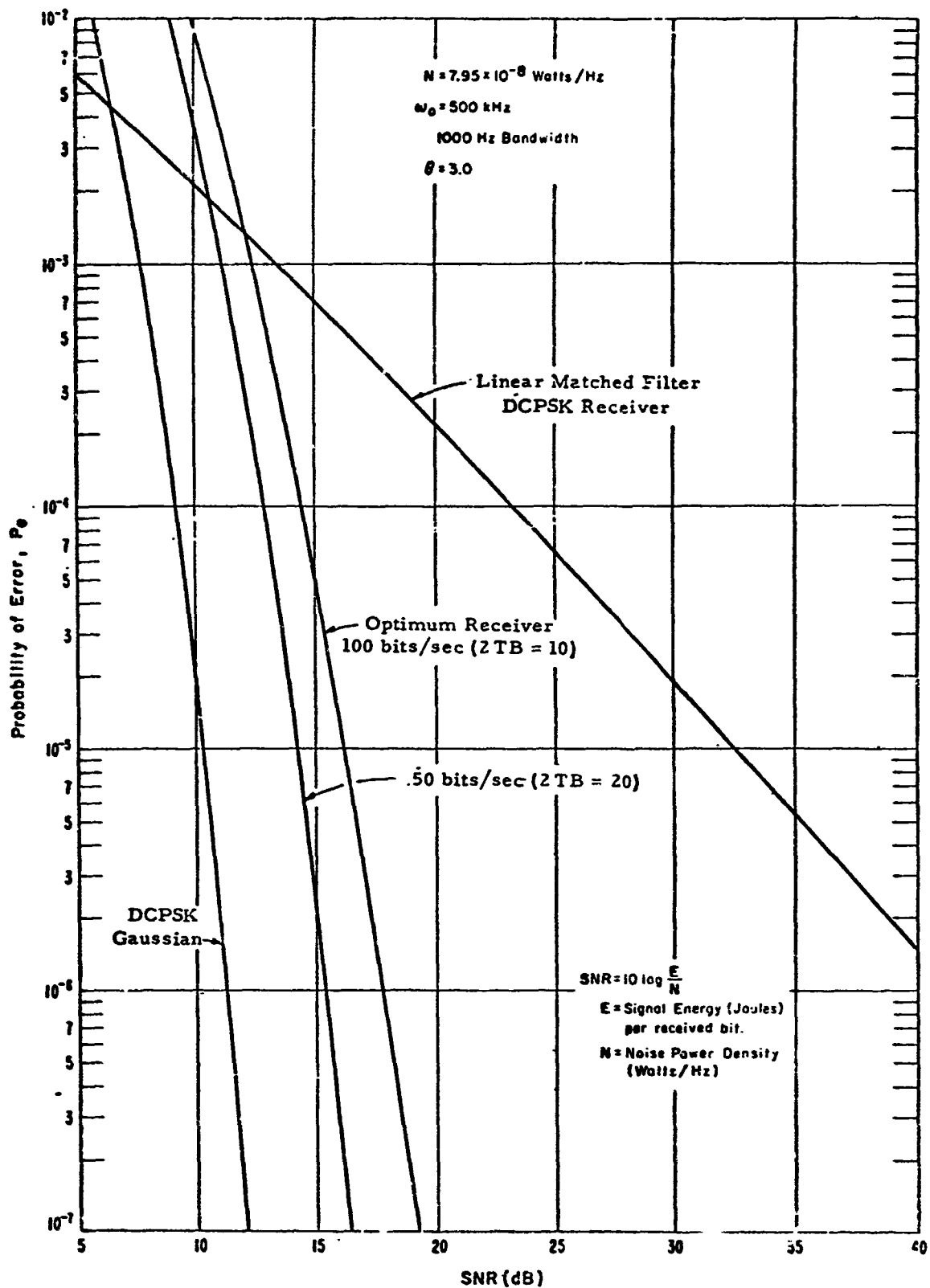Figure A.4. The performance of the optimum receiver ($\Theta = 3$) compared with the performance of a linear DCPSK receiver ($\Theta = 3$) and the performance of a linear DCPSK receiver in white Gaussian noise.
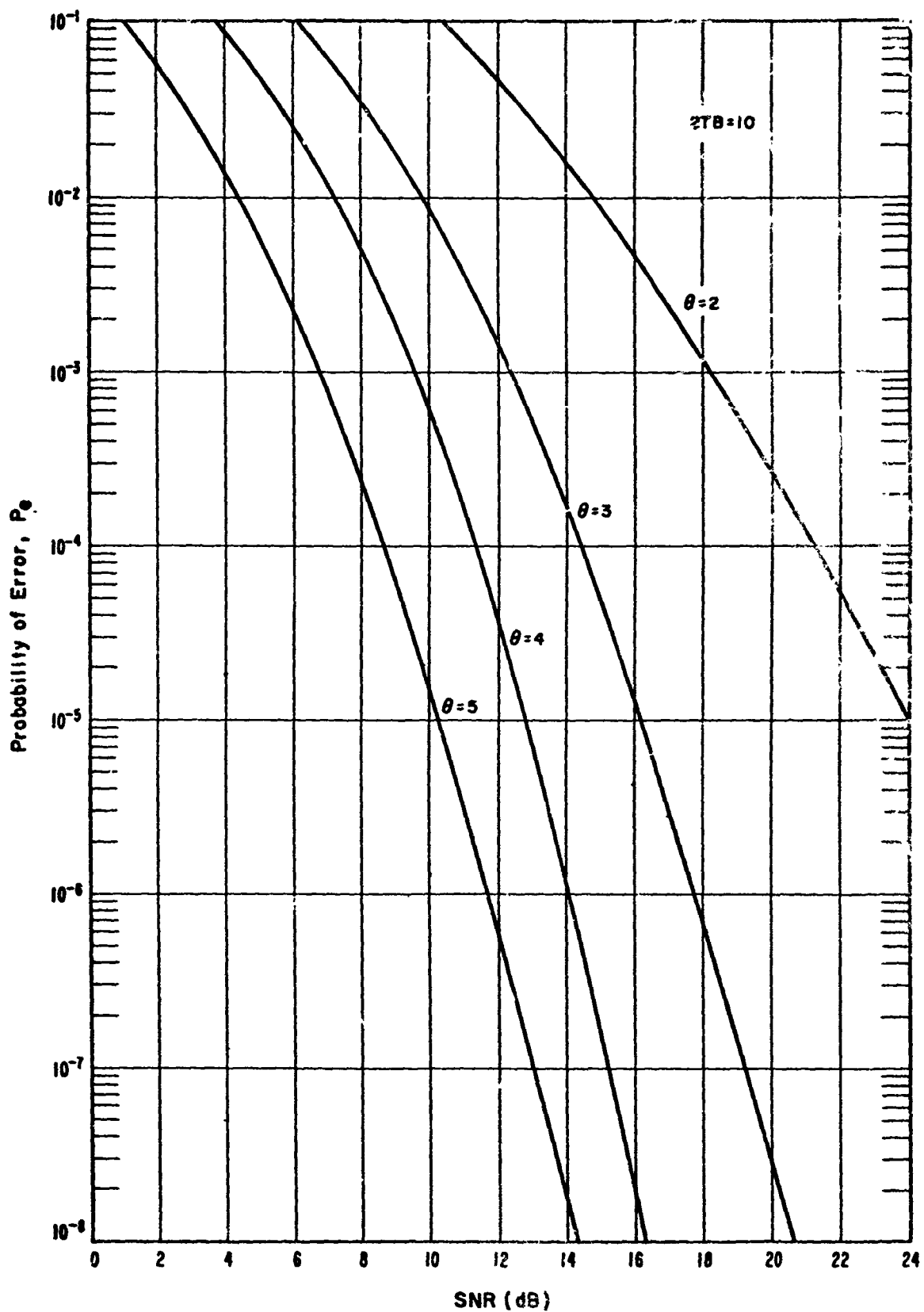
-100-

Figure A.5. The performance of the optimum receiver for a signal duration 10 times the reciprocal receiver bandwidth for a range of values of the parameter θ.
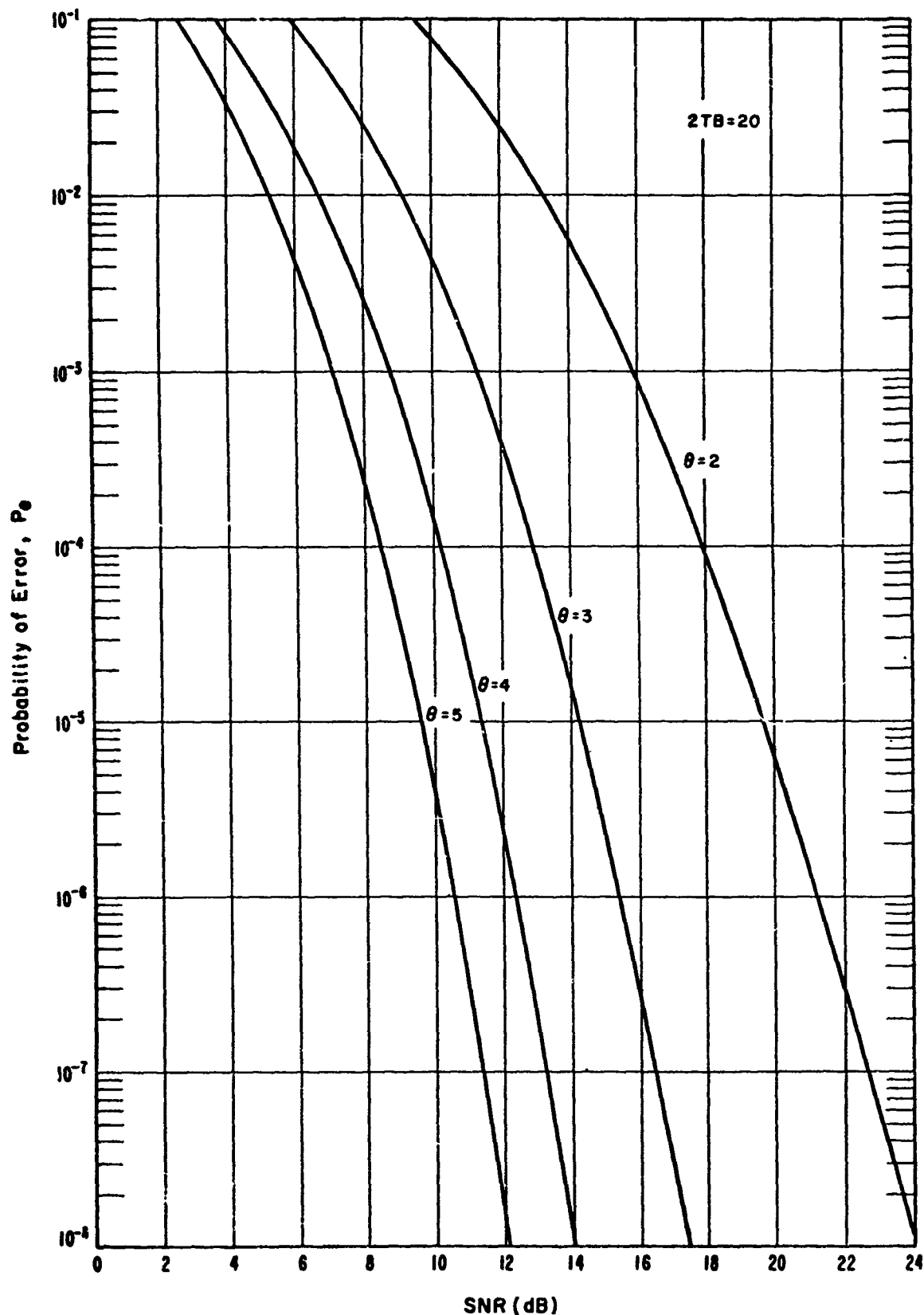
Figure A.6.   The performance of the optimum receiver for a signal duration
              20 times the reciprocal receiver bandwidth for a range of value of
              the parameter Θ.

-102-
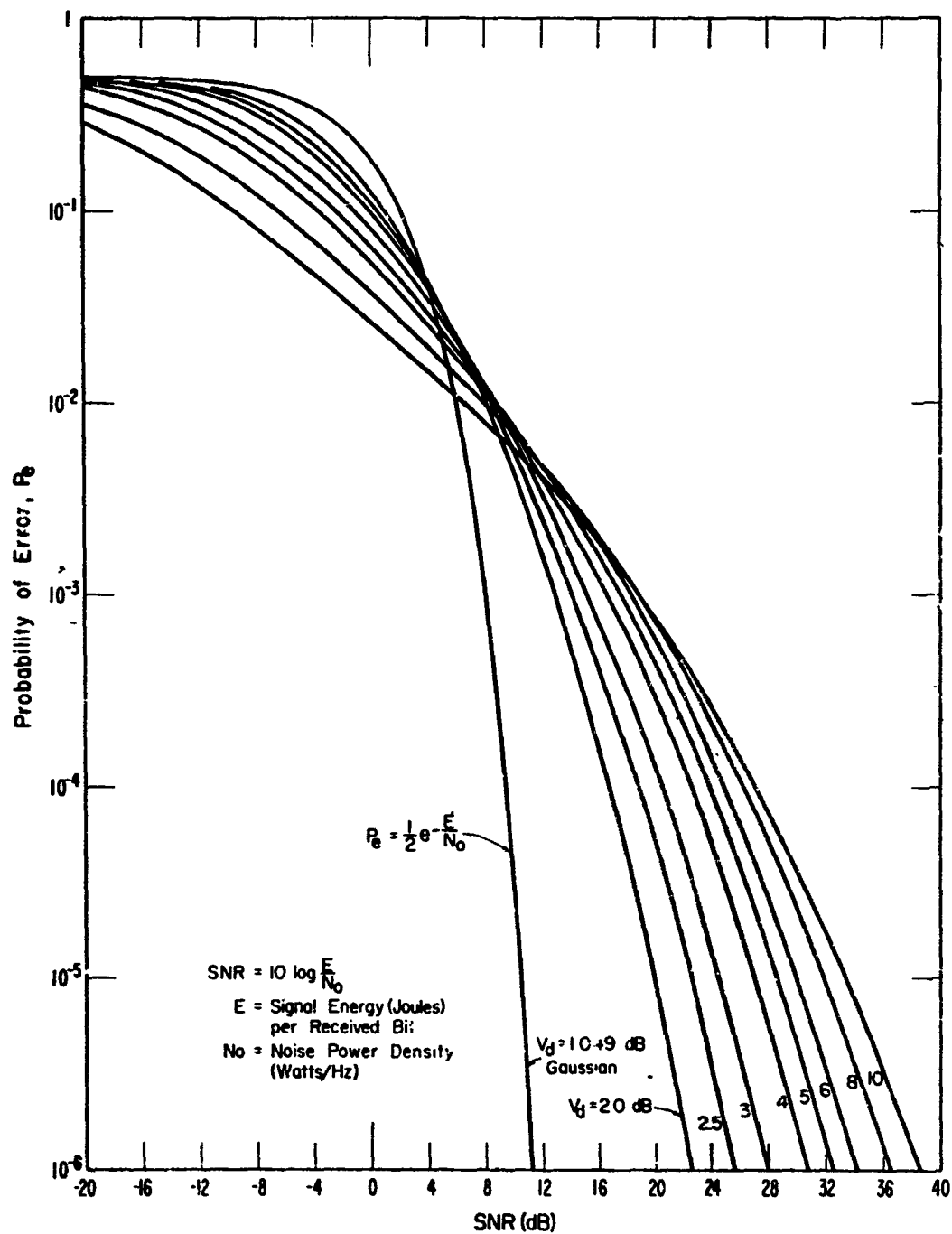
Figure A.7. Probability of error for a binary DCPSK system, constant signal.

-103-

Note For DCPSK 4 Phase
Composed of 2 Orthogonal Binary
Channels, Probability of Error for
Each Channel is for Large SNR
Given by $P_{SUB} \cong \frac{P_e}{2}$, and for All
SNR's We Have $P_{SUB} < P_e < 2P_{SUB}$

$V_d = 1.049$ dB
Gaussian

$V_d = 2.0$ dB
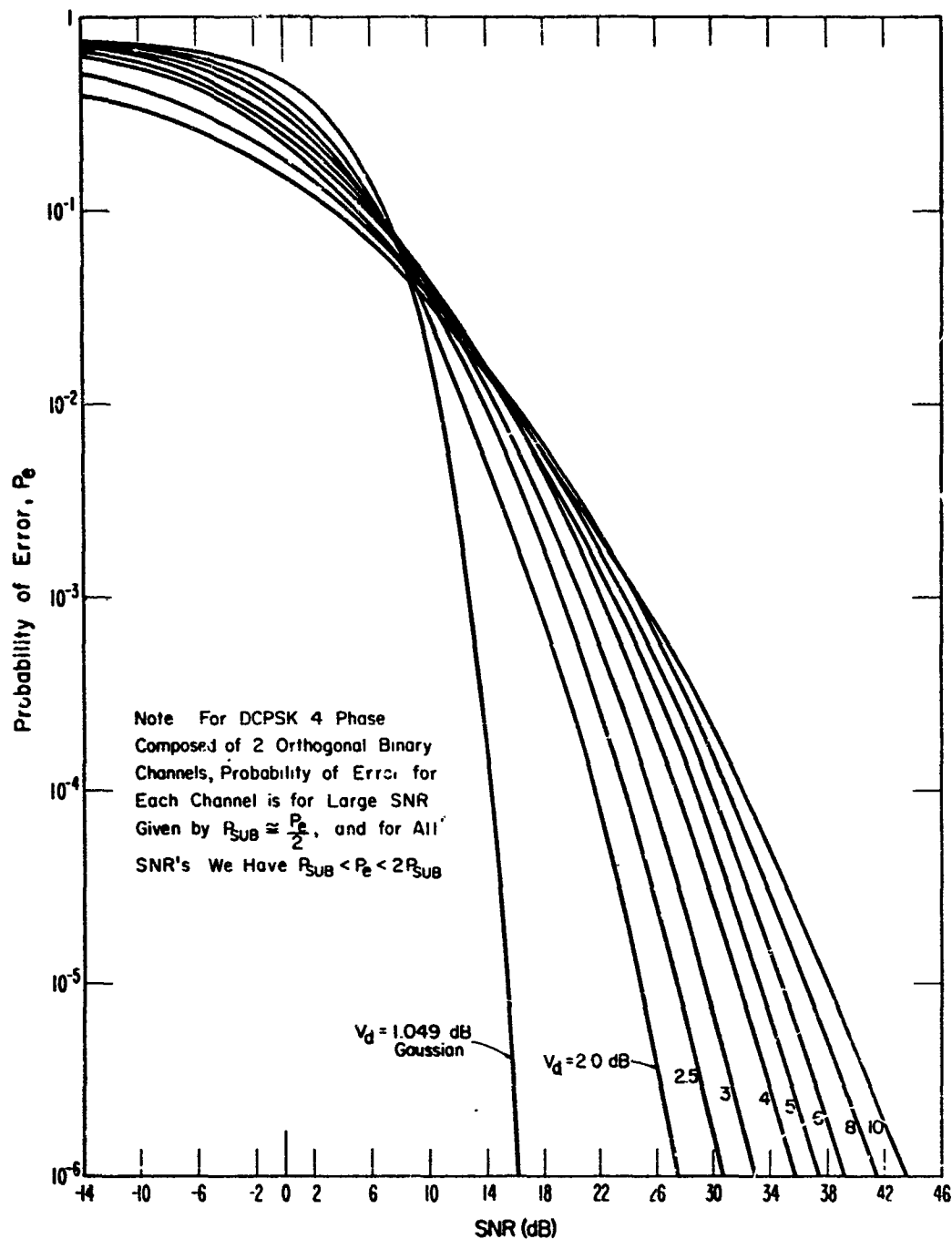
2.5   3   4   5   6   8 10

SNR (dB)

Figure A.8.   Probability of error for a four-phase DCPSK system, constant signal.
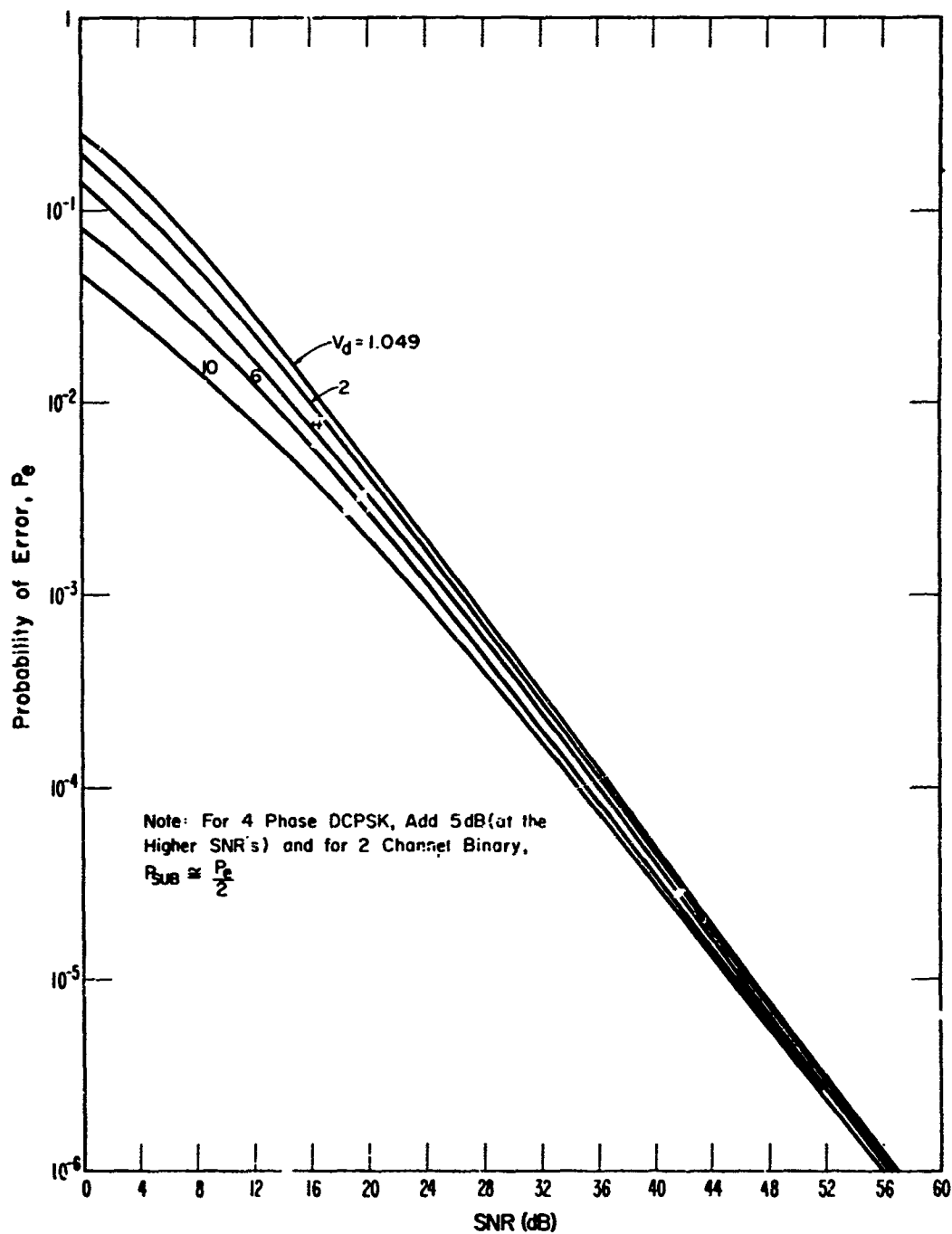
-104-

Figure A.9.   Probability of error for a binary DCPSK system, fading signal.

APPENDIX B

Distribution of the Envelope and Phase for the Hall Model

Our narrowband noise process is of the form

$$y(t) = a(t) n(t) \quad . \tag{B-1}$$

Since this is a narrowband process, it can be expressed as

$$y(t) = V(t) \cos\left[\omega_0 t + \phi(t)\right] \quad , \tag{B-2}$$

where $V(t)$ is the noise envelope process, and $\phi(t)$ is the phase process.

The joint probability density of V and ϕ is given by

$$p_{V,\phi}(V, \phi) = V p_{y, \tilde{y}} (V \cos\phi, \, V \sin\phi) \quad , \tag{B-3}$$

where $\tilde{y}$ denotes the Hilbert transform (quadrature component) of y.
That is, the envelope V is given by

$$V = (y^2 + \tilde{y}^2)^{\frac{1}{2}} \quad . \tag{B-4}$$

Now since the spectrum of $a(t)$ has negligible overlap with the spectrum of $n(t)$, we have

$$\tilde{y}(t) = a(t) \, \tilde{n}(t) \quad , \tag{B-5}$$

and since $n(t)$ is a Gaussian process, $\tilde{n}(t)$ is a Gaussian process, independent of $n(t)$, and identically distributed as $n(t)$.

Thus,

$$p_{y, \tilde{y}}(y, \tilde{y}) = p_{an, a\tilde{n}}(y, \tilde{y}) \tag{B-6}$$

$$= \int_{-\infty}^{\infty} \frac{dx}{x^2} \, p_{a, n, \tilde{n}}(x, \frac{y}{x}, \frac{\tilde{y}}{x})$$

$$= \int_{-\infty}^{\infty} \frac{dx}{x^2} \, p_a(x) \, p_n(\frac{y}{x}) \, p_{\tilde{n}}(\frac{\tilde{y}}{x}) \quad ,$$

and

$$p_n(x) = p_{\tilde{n}}(x) = \left(2\pi\,\sigma_1^2\right)^{-\frac{1}{2}} \exp\left(\frac{x^2}{2\sigma_1^2}\right) , \qquad (B-7)$$

and

$$p_a(x) = \frac{k}{|x|^{m+1}} \exp\left(-\frac{m}{2\sigma^2}\,\frac{1}{x^2}\right), \quad -\beta \le x \le \beta , \qquad (B-8)$$

where k is chosen to satisfy

$$\int_{-\beta}^{\beta} p_a(x)\,dx = 1 .$$

So, we have, substituting (B-7) and (B-8) into (B-6),

$$p_{y,\tilde{y}}(y,\tilde{y}) = \frac{k}{\pi\sigma_1^2} \int_0^\beta \frac{dx}{x^{m+3}} \exp\left(-\frac{m}{2\sigma^2 x^2} - \frac{y^2}{2\sigma_1^2 x^2} - \frac{\tilde{y}^2}{2\sigma_1^2 x^2}\right) . \; (B-9)$$

Substituting into (B-3) gives

$$(B-10)$$

$$p_{V,\phi}(V,\phi) = \frac{Vk}{\pi\sigma_1^2} \int_0^\beta \frac{dx}{x^{m+3}} \exp\left(-\frac{m}{2\sigma^2 x^2} - \frac{V^2\cos^2\phi}{2\sigma_1^2 x^2} - \frac{V^2\sin^2\phi}{2\sigma_1^2 x^2}\right)$$

$$= \frac{Vk}{\pi\sigma_1^2} \int_0^\beta \frac{dx}{x^{m+3}} \exp\left(-\frac{m}{2\sigma^2 x^2} - \frac{V^2}{2\sigma_1^2 x^2}\right) .$$

Let $z = \frac{1}{x^2}$, then

$$p_{V,\phi}(V,\phi) = \left(\frac{1}{2\pi}\right) \frac{Vk}{\sigma_1^2} \int_{1/\beta^2}^\infty z^{m/2} \exp\left[z\left(-\frac{m}{2\sigma^2} - \frac{V^2}{2\sigma_1^2}\right)\right] dz . \qquad (B-11)$$

So, we see that ϕ is uniformly distributed, i.e.,

$$p_\phi(\phi) = \frac{1}{2\pi} , \quad 0 \le \phi < 2\pi \qquad (B-12)$$

-107-

and

$$p_V(V) = \frac{Vk}{\sigma_1^2} \int_{1/\beta^2}^{\infty} z^{m/2} \exp\left[z\left(-\frac{m}{2\sigma^2} - \frac{V^2}{2\sigma_1^2}\right)\right] dz \quad . \tag{B-13}$$

The integral, $p_V(V)$ is easily evaluated in closed form for m even, and is easily evaluated numerically (by Gauss-Laquerre quadratures) for any m.

For $\beta = \infty$, we have

$$p_V(V) = \frac{\gamma^m V}{\left(V^2 + \gamma^2\right)^{\frac{m+2}{2}}} \quad , \tag{B-14}$$

and for the probability of the envelope exceeding the level V_0, that is, the APD,

$$P(V \geq V_0) = \int_{V_0}^{\infty} p_V(x) \, dx = \frac{1}{\left[\left(\frac{V_0}{\gamma}\right)^2 + 1\right]^{m/2}} \quad . \tag{B-15}$$

APPENDIX C

Average Rate of Envelope Level Crossings

Letting $N(V_o)$ denote the average number of crossings per second of the level V_o by the noise envelope, V, it is well known (Middleton, 1961, p. 427) that for a stationary random process, $V(t)$,

$$N(V_o) = \int_{-\infty}^{\infty} |\dot{V}| \left[p_{V,\dot{V}}(V, \dot{V}) \right]_{V = V_o} d\dot{V} \quad , \tag{C-1}$$

where $\dot{V}(t) = dV(t)/dt$.

As shown in appendix A, the assumption of negligible spectral overlap of $a(t)$ and $n(t)$ allows the envelope of the noise process to be given by

$$V(t) = |a(t)| E(t) \quad , \tag{C-2}$$

where $E(t)$ is the envelope of the narrow-band Gaussian process $n(t)$. Thus,

$$\frac{dV(t)}{dt} = |a(t)| \frac{dE(t)}{dt} + \frac{d|a(t)|}{dt} E(t) \tag{C-3}$$

If we are dealing with bandwidths that are a small fraction of our center frequency, ω_o, it is reasonable to assume that the modulating process, $a(t)$, is varying sufficiently slowly, so that

$$|a(t)| \frac{dE(t)}{dt} >> \frac{d|a(t)|}{dt} E(t) \quad , \tag{C-4}$$

which allows us to represent $\dot{V}(t)$, where

$$\dot{V}(t) = |a(t)| \dot{E}(t). \tag{C-5}$$

So,

$$p_{V,\dot{V}}(V, \dot{V}) = p_{|a|E, |a|\dot{E}}(V, \dot{V})$$

$$= \int_0^{\infty} \frac{dx}{x^2} p_{|a|}(x) p_{E,\dot{E}}\left(\frac{V}{x}, \frac{\dot{V}}{x}\right) \quad , \tag{C-6}$$

where, from appendix B,

$$P_{|a|}(x) = \frac{2k}{|x|^{m+1}} \exp\left(-\frac{m}{2\sigma^2 x^2}\right), \quad 0 \le x \le \beta . \tag{C-7}$$

The problem now reduces to finding $P_{E,\dot{E}}(E,\dot{E})$. Since $E(t)$ is the envelope of a narrow-band Gaussian process, it can be shown that, in general (Middleton, 1961, p. 420),

$$P_{E,\dot{E}}(E,\dot{E}) = \frac{E}{(2\pi\mu_{33})^{\frac{1}{2}}} \exp\left(\frac{-\mu_{33}\dot{E}^2}{2|\mu|}\right) \exp\left[\frac{-E^2(\mu_{11}\mu_{33}-\mu^2_{14})}{2\mu_{33}|\mu|}\right] , \tag{C-8}$$

where $|\mu| = (b_o b_2 - b_1^2)^2$, $\mu_{11} = b_2|\mu|^{\frac{1}{2}}$, $\mu_{33} = b_o|\mu|^{\frac{1}{2}}$, $\mu_{14} = b_1|\mu|^{\frac{1}{2}}$,

and the b_n are the frequency moments

$$b_n = \int_o^\infty S_n(f)(\omega - \omega_o)^n df , \tag{C-9}$$

where $S_n(f)$ denotes the spectral density of the process $n(t)$. Since $S_n(f)$ is the Fourier transform of the correlation function for $n(t)$, $R_n(\tau)$, these moments can also be computed from $R_n(\tau)$.

If the spectrum is symmetrical about ω_o, then (C-8) reduces to

$$P_{E,\dot{E}}(E,\dot{E}) = \frac{E}{b_o\sqrt{2\pi b_2}} \exp\left[-\frac{E^2}{2b_o} - \frac{\dot{E}^2}{2b_2}\right] . \tag{C-10}$$

Then, with $z = 1/x^2$,

$$P_{V,\dot{V}}(V,\dot{V}) = \frac{kV}{b_o\sqrt{2\pi b_2}} \int_{1/\beta^2}^\infty z^{\frac{m+1}{2}} \exp\left[-z\left(\frac{m}{2\sigma^2} + \frac{V^2}{2b_o} + \frac{\dot{V}^2}{2b_2}\right)\right] dz . \tag{C-11}$$

The frequency moments, b_n, are determined by the bandpass shape of the receiver, and once known, then $N(V_o)$ can be evaluated.

Now, if $R_n(\tau)$ has the typical form

$$R_n(\tau) = R_c(\tau) \cos \omega_0 \tau \quad , \tag{C-12}$$

and we define the rms bandwidth, B_c,

$$B_c = \left(\int_{-\infty}^{\infty} f^2 \frac{S_c(f)}{R_c(o)} \, df \right)^{\frac{1}{2}} \quad , \tag{C-13}$$

where $S_c(f)$ is the Fourier transform of $R_c(\tau)$, Hall(1966) has shown that, when $\beta = \infty$,

$$N(V_0) = \frac{\Gamma\left(\frac{\Theta + 2}{2}\right) 8 \pi^{\frac{1}{2}} \gamma^{\Theta - 1} B_c V_0}{\Gamma\left(\frac{\Theta - 1}{2}\right) \Theta \left(V_0^2 + \gamma^2\right)^{\Theta/2}} \quad , \tag{C-14}$$

where, as before, $\gamma = m^{1/2} \sigma_1/\sigma$ and $\Theta = m + 1 > 1.$